The Design and Effect of Power Electronics on Vibration-Based Energy Harvesting Methods

by

Aaron Llevret Farchaus Stein

A dissertation submitted in partial fulfillment
of the requirements for the degree of
Doctor of Philosophy
(Electrical Engineering-Systems)
in The University of Michigan
2016

Doctoral Committee:

Associate Professor Heath Hofmann, Chair
Professor Ian A. Hiskens
Assistant Professor Juan M. Rivas Davila
Associate Professor Jeffrey T. Scruggs
Associate Professor David D. Wentzloff

For my parents, with lots of love

ACKNOWLEDGEMENTS

Some might say the largest contributions of this dissertation exist in the field of energy harvesting, but to me its greatest contributions are the lessons it afforded me. This journey required dedication and perseverance, and is an experience I will use to guide me for the rest of my life. It would not have been possible without out so many great people in my life.

First, I would like to thank my advisor, Professor Heath Hofmann. Professor Hofmann is one the smartest people I know, and it was a privilege to have the opportunity to learn from him. His academic prowess does not detract from his ability as teacher, where he excels at providing intuitive explanations for difficult concepts. These skills made him an excellent mentor, and I am very grateful for all of his hard work. I certainly could not have completed this work with out his guidance.

Next, I would like to thank Professor Juan Rivas and Professor Ian Hiskens. Professor Rivas introduced me to the field of power electronics, and his unrivaled passion for the field fueled my interest in writing a dissertation on the subject. I am also indebted to him for his invaluable introductions to people in the power electronic community. Professor Ian Hiskens has been an indispensable advisor throughout my time at the University of Michigan. He has helped guide me through class selection, qualifying exams, and the difficult task of finding a post-doctoral position.

There are many staff members here at the University of Michigan that I owe a debt of gratitude, but three stand out in particular: Shelly Feldkamp, Becky Turanski, and Liz Zaenger. I appreciate their extraordinary efforts, each of them went out of their way to help and support me. Thank you.

I would like to extend a special thank you to my family. They have been a constant source of love and support throughout my life, and my time in graduate school was no different. My parents, Jeff and Karen Stein, who taught me so much about the research process, but also were there to celebrate my successes and support me through my setbacks. I will never forget the time we spent together each summer on Beaver Island! My sister, Sara Stein, for her unwavering support, sense of humor, and fantastic cooking! And Tony and Colleen who have been with me every step of

the way.

My girlfriend Tori Holden has been a loving partner, and our adventures together made the last few years the best of my life. Her many contributions to the field of micro-biology including [19], have made her great role model for success.

There are many friends (fishing buddies) I would like to thank: Ian Beil, Dimitris Assanis, Greg Ledva, Hayley Warsinske, Pat Belancourt, and Greg Handy. Thanks for all of the adventures and I am sorry if I ever put your life in danger in the pursuit of fish! I would like to thank Steve Martinez for teaching me so much over the past 5 years. I would also like to thank Dave Reed, Kan Zhou, Stephanie Crocker, Matt Prelee, Nick Asendorf, Abdi Zenyu, and Askhay Sarin. Thanks for making such a fun work environment, and for all of your academic support.

Last but not least, a huge thank you to Newton Alan Denard Stein. His unparalleled enthusiasm, dedication, and energy provided me great motivation over the past 3 years.

Go Blue!

TABLE OF CONTENTS

LIST OF FIGURES

Figure

LIST OF TABLES

Table

ABSTRACT

The Design and Effect of Power Electronics on Vibration-Based Energy Harvesting Methods

by

Aaron L F Stein

Chair: Heath Hofmann

Recent advancements in communication and low-power sensor nodes have led to innovative data acquisition systems for applications such as heart monitoring, forest-fire detection, and environmental controls for buildings. These sensor nodes play a vital role in human safety and comfort. Often these systems are in locations characterized by limited access to electrical power, yet they are in the presence of ambient mechanical vibrations. Therefore, energy harvesting from mechanical vibrations is proposed as a solution for powering these wireless sensor nodes. There are two devices that are commonly used for vibration-based energy harvesting: piezoelectric devices and electrostatic devices. This dissertation focuses on the power electronic interface between vibration energy harvesting devices and electrical energy storage elements. The power electronic interface is especially important for these devices when active energy harvesting methods are used because active methods utilize bidirectional power-flow, which increases the energy flow through the electronic interface.

By including power electronic efficiency as a parameter in the analysis of variable-capacitance energy harvesting, new fundamental properties of these devices are derived: a threshold efficiency necessary for energy harvesting, analytical solutions for optimal harvesting conditions, a comparison of energy harvesting methods at practical power electronic efficiencies, and a comparison of energy harvesting capabilities of various device architectures. Case studies are presented to illustrate practical applications of the theory presented in this work. The first case study demonstrates the advantage of using the Charge Pump Method for MEMs applications, and illustrates the use of these new fundamental properties to aid power electronic architecture selec-

tion. Ultimately, the analysis-aided design produces more than twice as much power as previous implementations on the same device. A second case study elucidates the energy harvesting benefit of selecting a gap-closing device architecture. Implementing the Constant Charge Method on a gap-closing device maximizes the energy harvested from variable-capacitance devices at practical power electronic efficiencies; however, challenges arise due to large voltages. This case study leads to the proposal of a new energy harvesting method which constrains the maximum charge and maximum voltage on the energy harvesting device.

Recently, the dynamic active energy harvesting method has been proposed as a way to widen the bandwidth of resonant piezoelectric energy harvesters; however, the bandwidth extension is dependent on power electronic efficiency. In this dissertation a new energy harvesting system is proposed that includes a resonant inverter topology, in conjunction with new low-power analog control circuitry, in order to produce the first wideband autonomous dynamic active energy harvesting system. Experimental results using the Mide Volture V20w piezoelectric device shows that the harvested power is up to twice that of the adaptive rectifier method. These results include previously ignored loss mechanisms such as control losses, gating losses, and phase detection losses; making this system the first autonomous energy harvesting system of its kind.

CHAPTER I

Introduction

Energy harvesting is the process of converting ambient or wasted energy into usable energy. There are many historical examples of energy harvesting that have had drastic ramifications on our society. One great example of this is the water mill, which increased the feasibility of mass-producing flour, a basic ingredient in many foods. Today energy harvesting continues to provide power to devices that have limited or no access to the electric grid. Energy harvesting is used in many different applications including biomedical, military, civil structures, Internet of Everything, advanced warning systems, distributed control, and many others [1]. Continued development of these energy harvesting systems could provide drastic improvements to critical systems in our society.

One proposed energy harvesting system that could significantly aid our society is energy harvesting for pacemakers [46, 63]. Currently pacemakers are powered by batteries, which have a finite energy storage. When the battery's energy is nearly depleted, pacemakers are surgically replaced inside the patient. This surgical procedure is an invasive procedure which can compromise the health of the patient, and is extremely costly. Placing an electrostatic energy harvester between the heart and the chest cavity [63] is able to produce enough power to the pacemaker such that it can last a lifetime. This technology helps extend the lifetime of elderly patients with pacemakers, and reduces the cost of their medical care.

In addition to biomedical applications, energy harvesting systems provide energy in many other locations that have limited electrical access. Beyond the aforementioned example, many modern energy harvesting applications seek to replace or supplement batteries. This is of particular interest to the military, which sends soldiers on missions in areas with little or no electrical access. Currently soldiers carry battery packs in order to power critical electronics such as GPS and radios. However, batteries are heavy and have a finite amount of energy storage. To circumvent this

problem the military has funded projects such as flexible photovoltaic fabrics, energy-harvesting boots, and energy-harvesting backpacks [6, 17, 21, 65]. It is important that these energy harvesting mechanisms do not significantly add to the soldiers' physical load, yet can provide power for these critical electronic devices. Energy harvesting systems can be vital for the successful completion of missions and the safe return of our soldiers.

Recent advancements in communication and low-power circuitry have increased the use of wireless sensor and identifier nodes. Some exciting applications for wireless sensors and identifier nodes include: building environmental control, home automation, smart environment, managing inventory control, drug administration, flood detection, forest-fire detection, and many more [1]. Despite their high utility, many sensor network systems require placement of nodes in remote locations characterized by limited access to electrical power sources. Currently sensor nodes are powered by batteries, which are the limiting factor in their lifetime. To increase the longevity of wireless sensor nodes, the energy density of the storage element must increase. To accomplish this [34, 49, 52, 59] suggest replacing the battery with either a micro-heat engine or a micro-fuel cell .

The high energy density of hydrocarbon fuels hint that heat engines are an attractive energy source for wireless sensor nodes. Despite the intrinsic advantages, practical difficulties have limited the development of micro-heat engines. Currently the power generated is significantly too high, and starting the heat engines has proven to be a challenge [49,52], making intermittent use difficult. The potential energy density of micro fuel cells is smaller than for micro-heat engines; however, their power levels are applicable for wireless sensor nodes. Fuel cells have been shown to provide several times the energy density as batteries and are a promising technology for the field [59]. Despite the improved energy density of micro-heat engines and fuel cells they still suffer from the same fundamental flaw as batteries: they have a finite energy storage which limits the lifetime of the wireless sensor node. For this reason, many researchers believe energy harvesting is the future of powering wireless sensor nodes [49, 52].

1.0.1 Energy Harvesting for Wireless Sensor Nodes

Harvesting energy from ambient sources such as acoustic noise, solar radiation, thermal gradients, wind, or mechanical vibrations have been shown to be an effective means for powering wireless sensor and identifier nodes [8, 33, 44, 45, 49, 52, 66]. The most effective energy source is dependent on both the available energy in the location

of the sensor node and the effectiveness of the energy harvesting system . For example, in direct sunlight photovoltaic energy harvesting systems have the greatest power density; however, for indoor applications the power density of photovoltaics is greatly reduced. A list of power sources for wireless sensor nodes and their power density is shown in Table 1.1.

Table 1.1: Power Density of Energy Sources for Wireless Sensor Nodes [52]

Energy Source	**Power Density $\frac{\mu W}{cm^3}$ after 1 year**	**Power Density $\frac{\mu W}{cm^3}$ after 10 years**
Solar outdoor/indoor	15,000/6	15,000/6
Vibrations - Piezoelectric [49]	300	300
Acoustic Noise	.96	.96
Temperature Gradients	15	15
Primary Batteries	45	3.5
Secondary Batteries	70	0
Hydrocarbon Fuel	333	33
Fuel Cells	280	28

The relatively high power density of mechanical vibrations makes them the most accessible ambient energy source in many applications. The viability of a vibration energy source is determined by the frequency and magnitude of the base acceleration [49]. To harvest energy from mechanical vibrations, an electromechanical device is typically inserted into a high-Q resonant structure, such as the one depicted in Fig. 1.1. The resonant structure is typically a mass-spring system, where the resonant frequency of the mechanical system is tuned to the frequency of the vibration source. If the resonant frequency and the vibration source frequency are close, then the mass will oscillate with a large amplitude. An electromechanical device is inserted into the system which extracts electrical energy, and provides damping to the mechanical system. The electrical energy extracted can then be stored in an electrical storage element [7, 8, 49, 52, 62].

Three electromechanical devices that are typically considered for low-power vibration energy harvesting are piezoelectric devices, variable-capacitance devices, and magnetic field-based generators [42, 49, 52, 65]. Each harvesting mechanism has advantages and disadvantages which dictate the applications in which they should be used.

Limited examples of low-power magnetic field-based energy harvesting apparatus exist because of their relatively large size and small output voltages [49]. Examples of

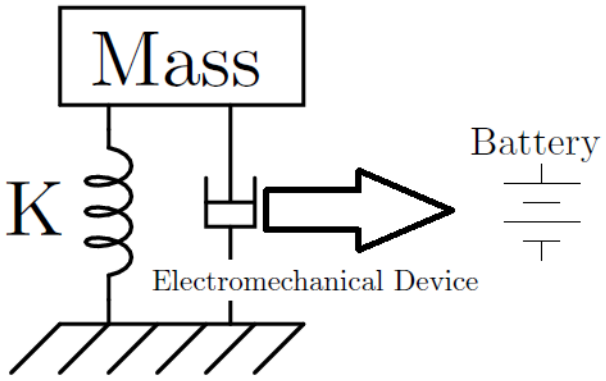

Figure 1.1: High-Q resonant mass-spring-damper system used to harvest energy from mechanical vibrations.

magnetic energy harvesting are shown in [2,67]; however, [52] claims that to reduce the size to $1cm^3$ would reduce the harvesting device's voltage to about 100mV. The power generated is AC power, which makes the small output voltage problematic. Typical methods for converting AC to DC requires diode rectification, which is not possible at such small voltage levels. Low-power magnetic energy harvesting therefore has many technological difficulties, while providing no inherent advantages, for milliwatt-level energy harvesting.

In low-power applications, piezoelectric devices have the largest energy density of the three devices [50]. Beyond their energy density, piezoelectric devices have a lot of practical properties which make energy harvesting from them easier. For example, piezoelectric devices do not need an electrical energy source to initiate the harvesting process, and have a relatively large output voltage. One challenge that faces these devices is that they are difficult to integrate into a microsystem [52].

Conversely, variable-capacitance devices are micro-electromechanical devices, which can be easily integrated into microsystems. This makes them well suited for harvesting energy for low-power sensor nodes; however, practical difficulties have limited their use [52]. Challenges such as achieving a large capacitance ratio and a large maximum voltage are compounded by an incomplete understanding of the harvesting methods. These challenges cause them to have the lowest energy density of the discussed energy harvesting devices [50].

Electromechanical devices provide a way to extract usable energy from the mechanical system so that it can be used to power a wireless sensor node. The method by which energy is extracted from the mechanical system greatly affects the energy harvesting capabilities of the system. There are two classes of energy harvesting

methods: passive and active. Passive energy harvesting methods have unidirectional power flow from the mechanical system to the electrical energy storage element. Conversely, active energy harvesting methods have bi-directional power flow between the mechanical system and the electrical energy storage element.

Active energy harvesting techniques are necessary for electret-free variable capacitance devices, and provide increased energy harvesting for piezoelectric devices. Demonstrations of the active harvesting methods are shown in [5, 9, 27, 30, 31, 36, 69].

1.0.1.1 Active Energy Harvesting for Variable-Capacitance Devices

In order to use passive methods of energy harvesting with a variable-capacitance device, an electret material must be used to bias the device. The benefit of an electret-based energy harvesting system is that it does not require an initial precharge; however, the electret material has a finite lifetime [37]. Successful electret-based energy harvesting systems have been made using different processes, including a single-layer silicon-on-insulator process [15], and deep reactive-ion etching process [14].

Active energy harvesting methods are typically implemented on electret-free variable-capacitance devices. These devices require charge to be inserted onto the device in order to initiate energy harvesting; however, they can be fabricated in a silicon process which is compatible with CMOS, allowing for close integration with CMOS electronics [5, 9, 57] and are not limited by the lifetime issues associated with the electret. Due these considerations, electret-free variable-capacitance devices are considered a good solution for energy harvesting for wireless sensor nodes.

1.0.1.2 Active Energy Harvesting for Piezoelectric Devices

Unlike electret-free variable capacitance devices, the literature provides both active and passive energy harvesting methods for piezoelectric devices [4,11,27,30,40,41]. For a well designed piezoelectric electric energy harvesting system, the resonant frequency of the mechanical mass-spring system matches the vibration source frequency. In this case [31] demonstrates that active harvesting methods harvest significantly more power than the passive methods.

Due to the small bandwidth of the high-Q resonant mechanical structure, there are many harvesting scenarios in which the vibration source frequency deviates from the mechanical resonant frequency. In this scenario, the power harvested using a passive method is drastically reduced. However, an active energy harvesting method called the Dynamic Active Energy Harvesting (DAEH) method derives an optimal

load impedance to maximize the power extracted from the device. The optimal load impedance is a function of system parameters and the excitation frequency. Theoretically, applying the optimal load impedance to the piezoelectric device allows 100% of the available energy to be harvested over an infinite bandwidth; however, energy loss in the power electronics limit the practical bandwidth [31].

1.0.2 Academic Contributions

While advantageous, active energy harvesting techniques are marred by a significant amount of power which flows between the energy harvesting device and the electrical energy storage, yet is not part of the net harvested power. This apparent power, which is present in active harvesting methods, makes the efficiency of the power electronic circuitry which interfaces the mechanical device and the electrical energy storage device extremely important.

The goal of this dissertation is to investigate the impact of power electronic efficiency on energy harvesting from mechanical vibrations, and to use the developed framework to guide the design of piezoelectric and variable-capacitance energy harvesting systems. Due to the current state of the art, the presented work for each of the harvesting devices has a slightly different focus.

1.0.2.1 Electrostatic Energy Harvesting

Four active methods of variable-capacitance energy harvesting are known: the Constant Voltage Method, the Constant Charge Method, the Charge-Pump Method, and the Constant Charge With Parallel Capacitance (CCPC) Method [36,51,52]. All four methods have been reported; however, the literature is lacking a formal comparison of these methods. Chapter III evaluates these four methods while considering power electronic circuit efficiency as a key parameter. By including efficiency as a parameter, new fundamental properties of these devices are derived: a threshold efficiency necessary for energy harvesting, analytical solutions for optimal harvesting conditions, and a comparison of the methods at practical power electronic efficiencies. A case study demonstrates the advantage of using the Charge Pump method for MEMs applications, and illustrates the use of the new fundamental properties in the design of two circuit topologies that are practical for MEMs-based vibration energy harvesters.

Two classes of variable-capacitance device architecture are currently presented in the literature: area-overlap devices and gap-closing devices [49]. In most variable-

capacitance energy harvesting systems, the maximum voltage on the device is constrained by the voltage limitation of the CMOS process and the pull-in effected created by the electrostatic force in the device [10, 36, 64]. However, with the development of high-voltage processes such as silicon on insulator, some devices are constrained solely by the pull-in effect. For gap-closing devices, this means the the maximum charge on the device should be constrained instead of the maximum voltage [10, 64]. In Chapter IV, energy harvesting methods are compared for charge-constrained gap-closing devices, and voltage-constrained area-overlap devices. The CCPC Method is not beneficial for gap-closing devices, so a new energy harvesting method is proposed for gap-closing devices: the Constant Voltage With Series Capacitance (CVSC) Method. Including power electronic efficiency in the comparison, it is shown that, assuming efficient power electronics, these devices harvest a similar amount of power; however, at practical power electronic efficiencies the gap-closing device is capable of harvesting up to 1.6 times as much power. A case study compares two devices with the same energy density. It is shown that the Constant Charge Method on a gap-closing device can harvest the most power of any method; however, the large voltages associated with the method remain a complication. This leads to the proposal of a new energy harvesting method where both the maximum voltage and charge are constrained. This method allows for some of the energy harvesting benefits of implementing the Constant Charge Method on a gap-closing device, while providing the ability to limit maximum voltage in the system.

1.0.2.2 Piezoelectric Energy Harvesting

Unlike variable capacitance energy harvesting, extensive research has gone into understanding impacts of power electronics on active harvesting methods for piezoelectric energy harvesting [27, 31]. In [31], it has been shown that dynamic active energy harvesting can theoretically harvest up to 100% of the available energy, and that deviations from this are due to power electronic efficiency. The benefits of the dynamic active energy harvesting (DAEH) method were experimentally validated by [31]. However, their implementation is not an autonomous system because the MOSFET gate drive, control circuitry, microcontroller, and phase detection power consumption exceeded that of the energy harvested, questioning the practical viability of the method. To overcome this, Chapter V develops a resonant full bridge inverter topology which, in combination with low-power analog control circuitry and low frequency digital control, reduces the loss mechanisms such that the practical benefits of the method are realized. For the first time, experimental results of the

dynamic active energy harvesting approach include all of the associated loss mechanisms, making it a wideband autonomous energy harvesting system [61].

CHAPTER II

Background: Vibration Energy Harvesting Methods

2.1 Variable-Capacitance Energy Harvesting

A variable-capacitance energy harvesting device is a micro-electromechanical system in which a mass, M, is sprung between two conductive materials (electrodes) [43]. The capacitance of the device, C, is approximately determined by the area of overlap of the conductive materials and the distance between them.

$$C = \varepsilon \frac{Area}{Distance} \tag{2.1}$$

There are two common types of variable capacitance devices. The first is an area-overlap device, in which the mechanical vibrations cause the fingers on the mass to overlap with the fingers on the wall of the device (changing the area), as shown in Fig. 2.1 [49]. The second type of device is a gap-closing device, in which the mechanical vibrations cause the sprung mass to get closer to the fingers on the wall of the device (changing the distance) as shown in Fig. 2.2 [49]. As either the area of overlap or distance between the electrodes change, so too does the capacitance of the device. Based on the frequency and magnitude of the source vibration the variable capacitance device will achieve a maximum capacitance C_{max}, and a minimum capacitance, C_{min}. The ratio of C_{max} to C_{min} is an important device parameter, hereafter denoted by R_c:

$$R_c = \frac{C_{max}}{C_{min}}. \tag{2.2}$$

The literature provides expressions for the ideal energy harvested per mechanical cycle for each of the four methods of energy harvesting. These equations are derived after making a quasi-static assumption, meaning here that the electrical energy harvest-

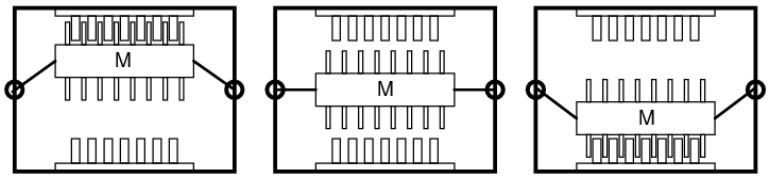

Figure 2.1: Physical model of a area-overlap variable-capacitance energy harvesting device.

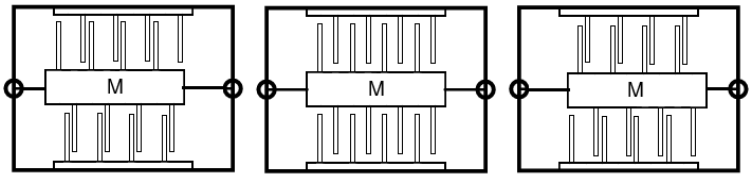

Figure 2.2: Physical model of a gap-closing variable-capacitance energy harvesting device.

ing does not affect the mechanical displacement. This assumption does not prohibit dynamic analysis: redefining C_{max} and C_{min} to values achieved by the dynamic excitation will maintain the validity of this theory.

The energy harvesting capabilities of variable-capacitance devices are limited by the physical strength of the electrodes. Stored energy in the variable-capacitance device causes an electrostatic pressure between the electrodes, and this pressure can cause the pull-in effect, which results in the device short-circuiting [38, 49]. In order to avoid the pull-in effect constraints are placed on the devices. For an area-overlap device, such as the one depicted in Fig. 2.1, the maximum allowable voltage across the device is an important device parameter. The pressure on the electrodes in an area-overlap device is dependent on the distance between electrodes (D), the permittivity of air (ϵ_0), and the voltage on the device (V):

$$P = \frac{F_{es}}{A} = \frac{\epsilon_0 V^2}{2D^2}. \tag{2.3}$$

Therefore, to limit the pressure, the maximum voltage applied to the device should be constrained [10, 35, 36, 52, 64]. In a gap-closing device, such as the one depicted in Fig. 2.2, the pressure on the electrodes is dependent on the area of overlap of the electrodes (A) and the charge on the device (Q):

$$P = \frac{F_{es}}{A} = \frac{Q^2}{2A^2\epsilon_0}. \tag{2.4}$$

Therefore, to mitigate the pull-in effect on a gap-closing device, the maximum charge should be constrained [10, 49, 64].

In order to maximize the energy that can be extracted from these devices [18, 22, 49] have compared many different types of variable-capacitance devices including out-of-plane gap-closing devices, in-plane gap closing devices, and in-plane overlap converters . These works seek to maximize the capacitance ratio while considering system stability and other practical issues facing these devices. In [22] they conclude that the in-plane gap closing device can harvest approximately 1.6-1.8 times as much power per unit volume as the other devices; however [49] claim the out-of-plane gap closing converter can harvest the most power. These conclusions were drawn while considering the mechanical system parameters.

2.1.1 Energy Harvesting Methods

There are four energy harvesting methods for variable-capacitance devices that are currently considered in the literature. For each method a voltage-versus-charge (VQ) plot is shown. The net area enclosed by the VQ plot represents the theoretical maximum energy that can be harvested using that method, and is denoted by E_{ideal}. The expression for the ideal energy harvested is given by:

$$E_{ideal} = \oint V(q)dq = E_{out} - E_{in}. \tag{2.5}$$

The ideal energy harvested assumes 100%-efficient power electronics. It accounts for the electrical energy supplied to the harvesting device, E_{in}, to initiate harvesting and the electrical energy extracted from the device, E_{out}. Due to the electro-mechanical energy conversion of the energy harvesting device, E_{out} is larger than E_{in}.

The literature provides a discussion of the ideal energy harvested using each of the four methods of energy harvesting for voltage-constrained variable capacitance devices [36, 52].

2.1.1.1 Constant Voltage

The Constant Voltage Method charges the capacitive device to a voltage V_{max} when the capacitance is at its maximum value so that the charge on the device is given by:

$$Q_{max} = C_{max}V_{max}. \tag{2.6}$$

As the device's capacitance is reduced to its minimum value, the voltage across it is held constant at V_{max}. Charge is extracted from the device, until the remaining charge is

$$Q_{min} = C_{min} V_{max}. \tag{2.7}$$

Finally, once the device reaches its minimum capacitance, the voltage on the device is reduced to zero [36, 52, 64, 64]. The voltage and charge fluctuations of this process are illustrated in Fig. 2.3. Using (2.5), the energy into and out of the device can be

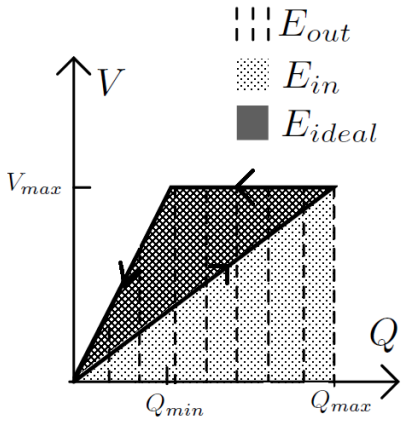

Figure 2.3: Voltage versus charge plot for the Constant Voltage Method.

derived directly from the shaded areas shown in Fig. 2.3:

$$E_{in} = \frac{1}{2} Q_{max} V_{max} = \frac{1}{2} C_{max} V_{max}^2, \tag{2.8}$$

$$E_{out} = (Q_{max} - Q_{min}) V_{max} + \frac{1}{2} Q_{min} V_{max} = (C_{max} - \frac{1}{2} C_{min}) V_{max}^2, \tag{2.9}$$

Using the Constant Voltage Method on an voltage constrained device, [36] show that the ideal energy that can be harvested, E_{ideal}, is

$$E_{ideal} = E_{out} - E_{in} = \frac{1}{2} (C_{max} - C_{min}) V_{max}^2. \tag{2.10}$$

An experimental implementation of the Constant Voltage Method on a voltage-constrained variable capacitance device is demonstrated in [64]. Assuming ideal power electronics, the Constant Voltage Method is shown to harvest the most amount of energy of any method [36, 64]. Some challenges facing this methods are:

- the changing voltage on the device requires magnetics-based power electronics,

which are difficult to integrate into a microsystem

- might require two voltage rails in the system (depending on battery and circuitry voltage) [36]
- the harvesting method requires sensing of the state of the variable capacitor [64].

2.1.1.2 Constant Charge

The Constant Charge Method of energy harvesting charges the device to a voltage V_{init} while the device is at C_{max}. The device is then left in an open-circuit configuration such that charge on the device is constant. Once the device capacitance reaches C_{min}, the voltage across the device reaches V_{max}, and the energy is harvested from the device by discharging the capacitor [36, 49]. Fig. 2.4 helps explain the Constant Charge Method by showing the variations of both the voltage and the charge on the device during the harvesting process.

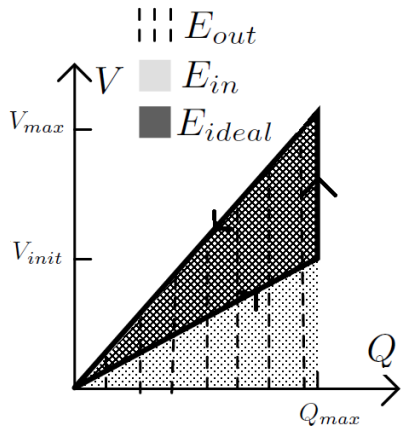

Figure 2.4: Voltage versus charge plot for the Constant Charge Method.

The voltage on the device is inversely proportional to the capacitance during the constant charge part of the cycle. The maximum voltage experienced by the device is derived in (2.11).

$$\begin{aligned} Q_{max} = C_{max}V_{init} &= C_{min}V_{max} \\ \Rightarrow V_{max} &= \frac{C_{max}}{C_{min}}V_{init} \end{aligned} \tag{2.11}$$

In order to prevent the voltage from exceeding the device ratings, V_{init} must be selected according to (2.11). Using the V-Q plot shown in Fig. 2.4, E_{in}, E_{out}, and

E_{ideal} are derived:

$$E_{in} = \frac{1}{2} Q_{max} V_{init} = \frac{1}{2} \frac{C_{min}^2}{C_{max}} V_{max}^2, \tag{2.12}$$

$$E_{out} = \frac{1}{2} Q_{max} V_{max} = \frac{1}{2} C_{min} V_{max}^2, \tag{2.13}$$

Using the Constant Charge Method on an area-overlap device, the ideal energy that can be harvested, E_{ideal}, is

$$\Rightarrow E_{ideal} = \frac{1}{2} C_{min} V_{max}^2 - \frac{1}{2} \frac{C_{min}^2}{C_{max}} V_{max}^2. \tag{2.14}$$

The Constant Charge Method harvests less energy than the Constant Voltage Method by a factor of V_{init}/V_{max} when used on a voltage-constrained variable capacitance device [36]. This method also suffers from some of the same challenges facing the Constant Voltage Method including:

- requires magnetics-based power electronics
- the harvesting method requires sensing of the state of the variable capacitor.

However, unlike the Constant Voltage Method, [35] claim that only one voltage rail is required for the Constant Charge Method.

2.1.2 Constant Charge with Parallel Capacitance

The Constant Charge with Parallel Capacitance Method, or CCPC Method, is very similar to that of the Constant Charge Method, with the exception that a capacitor is placed in parallel with the device. The parallel capacitor aids in energy harvesting because it allows the variable-capacitance device to undergo a change in both voltage and charge [23]. For the CCPC Method, the device and the parallel capacitor are charged to V_{init} when the device is at C_{max}. Then the device and the parallel capacitor are open-circuited. As the capacitance changes from C_{max} to C_{min}, charge flows out of the device and into the parallel capacitance, simultaneously raising the voltage of both the device and the parallel capacitance. The voltage across the device reaches V_{max} when the device's capacitance is at C_{min}. At this point the energy is harvested from the device and the parallel capacitance [36]. The device varies from C_{min} back to C_{max} with no charge, allowing the cycle to restart. The

variations of both the voltage and the charge on the harvesting device are portrayed in Fig. 2.5. When C_p is zero, the cycle is identical to the Constant Charge cycle. However, as C_p gets arbitrarily large the cycle mimics the Constant Voltage Method.

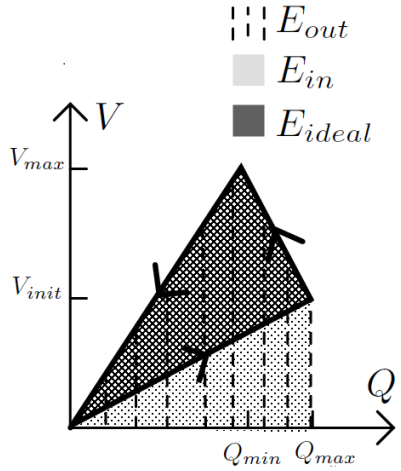

Figure 2.5: Voltage versus charge plot for the Constant Charge with Parallel Capacitance Method.

E_{ideal} is derived from the shaded areas in Fig. 2.5.

$$E_{in} = \frac{1}{2}(C_{max} + C_p)V_{init}^2, \tag{2.15}$$

and

$$E_{out} = \frac{1}{2}(C_p + C_{min})V_{max}^2, \tag{2.16}$$

where

$$\frac{V_{max}}{V_{init}} = \frac{C_{max} + C_p}{C_{min} + C_p}. \tag{2.17}$$

In [35], it is shown that the ideal energy extracted is given by:

$$E_{ideal} = \frac{1}{2}(C_p + C_{min})V_{max}^2 - \frac{1}{2}\frac{(C_{min} + C_p)^2}{C_{max} + C_p}V_{max}^2. \tag{2.18}$$

The CCPC Method can harvest up to the same amount of energy as the Constant Voltage Method. At practical power electronic efficiencies, an optimal parallel capacitance is chosen based on the losses in the circuitry which implement this method [36]. Some of the challenges associated with this method include:

- it is difficult to implement in a microsystem because the power electronics re-

quire a magnetic component.

- circuitry must track the state of the variable capacitance device.

However, [35,36] argue that the CCPC Method preserves the single voltage rail benefit of the constant charge method while approaching the energy harvesting capabilities of the Constant Voltage Method.

2.1.3 Charge Pump Method

The Charge Pump Method energy harvesting cycle is a combination of the Constant Charge Method and the Constant Voltage Method. This method starts with the device at an initial voltage V_{min} when the capacitance is at a maximum such that:

$$Q_{max} = C_{max}V_{min}. \tag{2.19}$$

The device is then open-circuited, undergoing a constant charge phase until the voltage on the device reaches V_{max}. Once the voltage on the device has reached V_{max}, it is held there such that the device undergoes a constant voltage phase until the device's capacitance reaches C_{min}.

$$Q_{min} = C_{min}V_{max} \tag{2.20}$$

Once the device has reached C_{min}, its voltage drops during another constant charge phase as the capacitance increases to C_{max}. Charge is returned to the device during another constant voltage phase in order to get the device back to its original state [52, 69]. The resulting voltage and charge variations on the device from this method are illustrated in Fig. 2.6. The circuit shown in Fig. 2.7 implements the desired behavior of the Charge Pump Method, and is useful for gaining an intuitive understanding of the approach. The terms E_{in}, E_{out}, E_{ideal} are derived from the shaded areas in Fig. 2.6:

$$E_{in} = V_{min}(Q_{max} - Q_{min}) = V_{min}(V_{min}C_{max} - V_{max}C_{min}), \tag{2.21}$$

$$E_{out} = V_{max}(Q_{max} - Q_{min}) = V_{max}(V_{min}C_{max} - V_{max}C_{min}), \tag{2.22}$$

In [52], the net energy harvested using this method is shown to be

$$\Rightarrow E_{ideal} = (V_{max} - V_{min})(V_{min}C_{max} - V_{max}C_{min}). \tag{2.23}$$

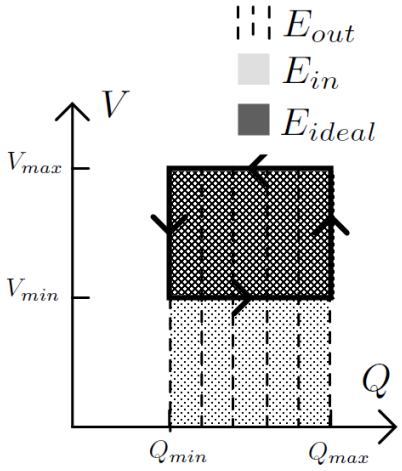

Figure 2.6: Voltage versus charge plot for the Charge Pump Method.

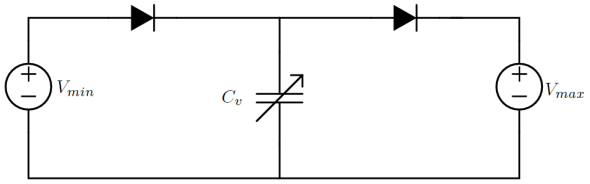

Figure 2.7: Diode-based Charge Pump Method Energy Harvesting Circuit.

The Charge Pump Method does not suffer from the same challenges as the other three methods:

- the fixed voltage conversion allows the use of switch-capacitor topologies and can therefore be implemented entirely on a chip [69]
- it does not require circuitry to monitor the state of the variable-capacitance device [52].

For these reasons it is an attractive energy harvesting method.

2.1.4 Incorporating Power Electronic Efficiency

The ideal energy harvested derived assumes 100% efficient power electronics. In Chapters III and IV, power electronic efficiency is incorporated into the existing analysis of energy harvesting methods. In order to incorporate circuit efficiency as a parameter, it is assumed that the input and output energy of the device is penalized by a constant efficiency η. Using efficiency, as opposed to specific loss models, allows the analysis to be generalized for different power electronic architectures. It is understood that typically efficiency is a function of operating conditions, however using

a single efficiency parameter yields more tractable mathematical expressions without significantly altering the intuition developed by the analysis. Using the power electronic efficiency, η, the net energy harvested, E_{net}, for each method is derived by penalizing the E_{in} and E_{out}:

$$E_{net} = E_{final} - E_{initial} = \eta E_{out} - \frac{1}{\eta} E_{in}. \tag{2.24}$$

The net energy equation is normalized by the maximum energy that can be stored on the harvesting device, which represents the maximum possible energy that can be harvested, as will be seen. For voltage-constrained area-overlap the maximum energy that can be stored on the device is

$$\frac{1}{2} C_{max} V_{max}^2; \tag{2.25}$$

therefore, the normalized net energy, N_{Enet}, is

$$N_{Enet} = \frac{E_{net}}{E_{max}} = \frac{\eta E_{out} - \frac{1}{\eta} E_{in}}{\frac{1}{2} C_{max} V_{max}^2}. \tag{2.26}$$

For charge constrained gap-closing devices the maximum energy that could be stored on the device is

$$\frac{Q_{max}^2}{2C_{min}}; \tag{2.27}$$

therefore, the N_{Enet} is given by

$$N_{Enet} = \frac{E_{net}}{E_{max}} = \frac{\eta E_{out} - \frac{1}{\eta} E_{in}}{\frac{Q_{max}^2}{2C_{min}}}. \tag{2.28}$$

As will be shown, each method has a threshold power electronic efficiency, η_{thresh}, which must be exceeded in order to harvest energy. To solve for η_{thresh}, E_{net} is set to zero in (2.24) and solved for η:

$$\eta_{thresh} = \sqrt{\frac{E_{in}}{E_{out}}}. \tag{2.29}$$

2.2 Piezoelectric Energy Harvesting Methods

A simple model of a piezoelectric device is developed in [40]. Here it is shown that the piezoelectric devices can be modeled as a current source in parallel with a

capacitor, as illustrated in Fig. 2.8. From this model of the piezoelectric device, it can be shown that the device current is proportional to the time derivative of the applied force. Therefore, the output of a piezoelectric device will AC in nature.

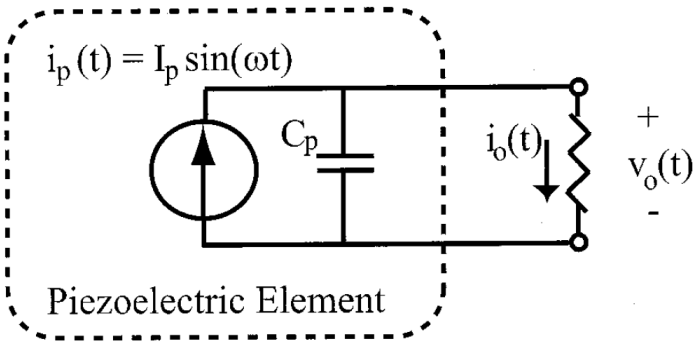

Figure 2.8: An electric circuit model of a piezoelectric device connected to a resistive load [40].

The simplest energy harvesting method is to connect a resistive load directly to the device, as shown in [16]. The size of the load resistance impacts the amount of power that can be harvested from the device. In [4], it is shown that the optimal load resistance, R_{opt}, is

$$R_{opt} = \frac{1}{C_p \omega}. \tag{2.30}$$

R_{opt} maximizes the energy harvested using this method; however, this method is not suitable for wireless sensor nodes. Wireless sensor nodes are powered with DC power and can not be modeled as a resistance. The following methods convert the AC power from the piezoelectric device into DC power which can be used by a wireless sensor node.

2.2.1 Rectifier Methods

To provide the DC power required by wireless sensor nodes a rectifier and filter capacitance can be used to convert the AC voltage of the device to DC. The energy harvested from the device per cycle is the shaded region in the V-Q plot, which is illustrated in Fig. 2.9 Several harvesting methods are based on this architecture as discussed in [40, 47, 49, 56]. In this section the most promising of these methods are discussed.

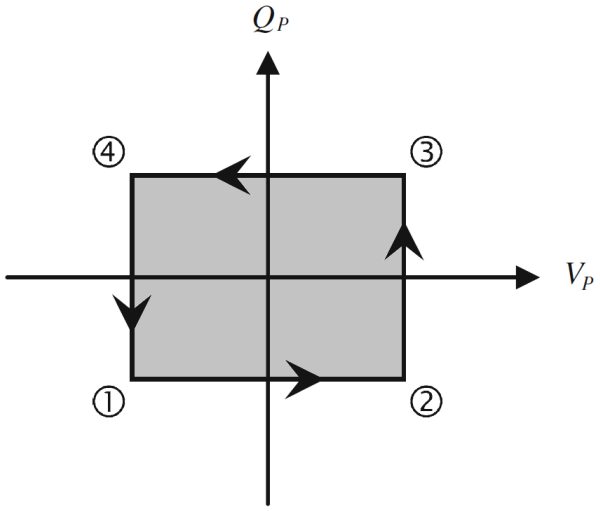

Figure 2.9: Voltage versus charge in a piezoelectric device during a harvesting cycle using the rectifier approach [27]. The shaded region represents the harvested energy during the cycle.

In [40], it is shown that the power harvested from the device is

$$\langle P(t) \rangle = \frac{2V_{rect}}{\pi}(I_p - V_{rect}\omega C_p). \tag{2.31}$$

Therefore, in order to maximize the power extracted from the device the DC voltage on the output of the rectifier should be held constant at

$$V_{rect} = \frac{I_p}{2\omega C_p}. \tag{2.32}$$

The optimal V_{rect} is one half of the open-circuit voltage of the device,V_{oc}, generated by the mechanical excitation. As discussed in [31], under these conditions the harvested energy is

$$E_{rect} = \frac{1}{4}C_p V_{oc}^2. \tag{2.33}$$

V_{rect} is dependent on the magnitude and frequency of the vibration, so [40] proposes an adaptive energy harvesting method. A peak power tracking algorithm measures the harvested power and adapts V_{rect} towards its optimum value. This method was implemented using a circuit architecture shown in Fig. 2.10 and the resulting waveforms are shown in Fig. 2.11.

The adaptive rectifier technique requires a microcontroller to implement the control scheme. The power consumption of such a controller could prohibit the use of

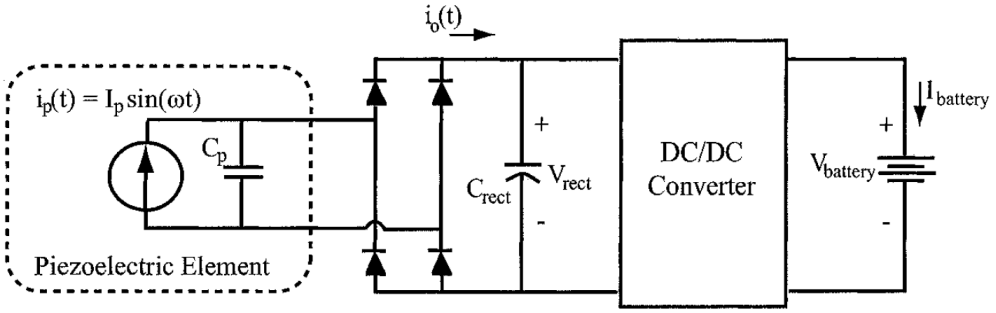

Figure 2.10: A circuit model of the adaptive rectifier energy harvesting method discussed in [40].

the adaptive rectifier in low-power applications. To mitigate this issue [41] use a step-down converter in discontinuous mode. It is shown that, if a DCM step-down converter is operated with a switching frequency of f_s and an inductance L, then the optimal duty ratio, D_{opt} is

$$D_{opt} = \sqrt{\frac{4V_{rect}\omega LC_p f_s}{\pi(V_{rect} - V_{battery})}}. \tag{2.34}$$

For large excitation values, where V_{rect} is much larger then $V_{battery}$ then the optimal duty cycle is

$$D_{opt} \approx \sqrt{\frac{4\omega LC_p f_s}{\pi}}. \tag{2.35}$$

For large excitation values the duty cycle for the converter is approximately constant. This removes the need for an adaptive controller, greatly reducing the power consumption of the control circuitry. In [41] an autonomous energy harvesting system using this technique was designed, and was able to harvest demonstrate a significant increase in energy harvesting.

In [24], a discontinuous mode buck-boost converter is used to interface the the rectifier and the battery. The DCM buck-boost converter has a resistive input impedance, so the rectifier has a linear voltage/current relationship despite power being extracted to the battery. Solving for the optimal input impedance [24] presents an open-loop energy harvesting system that reduces control losses while effectively harvesting power over an large excitation range.

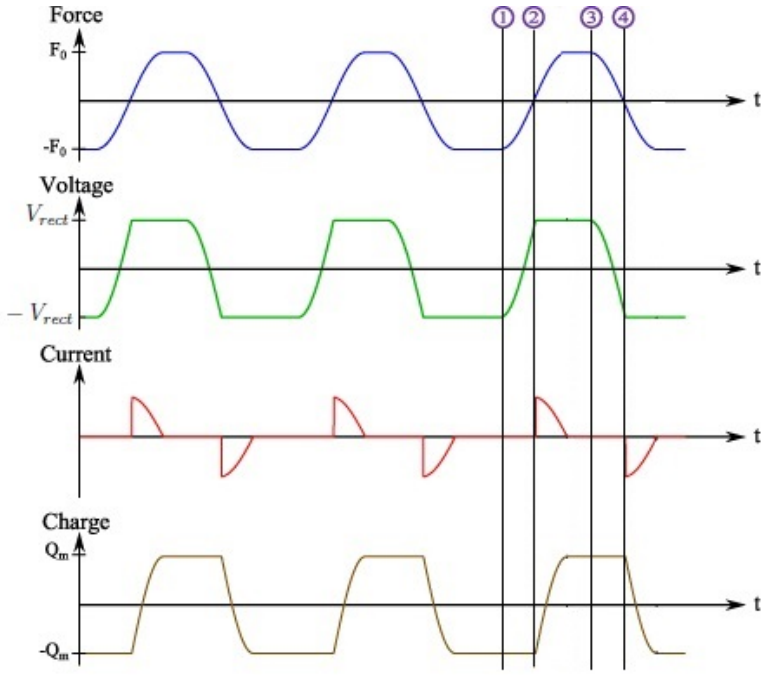

Figure 2.11: The piezoelectric device waveforms for the adaptive rectifier energy harvesting method [11].

2.2.2 Semi-active Harvesting Methods

Conventional rectifier-based approaches were enhanced by the introduction of the synchronized switch harvesting on inductor (SSHI) electronic interface depicted in Fig. 2.13a. The parallel SSHI method utilizes a resonant transition to invert the voltage on the piezoelectric device [3, 4]. The resulting V-Q plot for this method is illustrated in Fig. 2.12. The resonant transition causes the voltage on the device to be inverted quickly with respect to the time frame of the mechanical excitation. This limits the impact of piezoelectric capacitance because the piezoelectric current is not used to charge and discharge the entire piezoelectric capacitance; instead, an inductor resonantly aids with this transition.

In [58], it is illuminated that the parallel SSHI circuit significantly outperforms the standard rectifier approach for weakly-coupled systems; however, for strongly coupled systems, the standard rectifier approach and the parallel SSHI topology harvest similar amounts of energy. Furthermore, [58] claims that the power harvesting capabilities of the SSHI method on weakly-coupled systems are highly dependent on circuit efficiency.

At low excitation levels, the SSHI methods are inherently inefficient. Switch "S" is a bidirectional switch which is implemented with two MOSFETs and two diodes

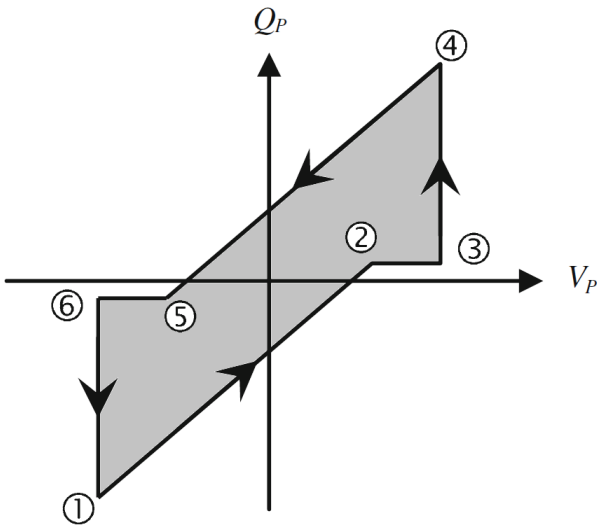

Figure 2.12: Voltage versus charge in a piezoelectric device during a harvesting cycle using the SSHI approach [27]. The shaded region represents the harvested energy during the cycle.

as shown in Fig 2.14 [3, 29]. The diode voltage drop associated with the rectifier bridge and the switch S is detrimental to circuit efficiency, especially in low-power applications where the piezoelectric voltage is small. In [32] a new circuit topology is presented which reduces the number of diodes allowing the SSHI circuit to be used in lower power applications; however, until all diodes are removed from the conduction path, the power harvested at low excitation levels will be limited.

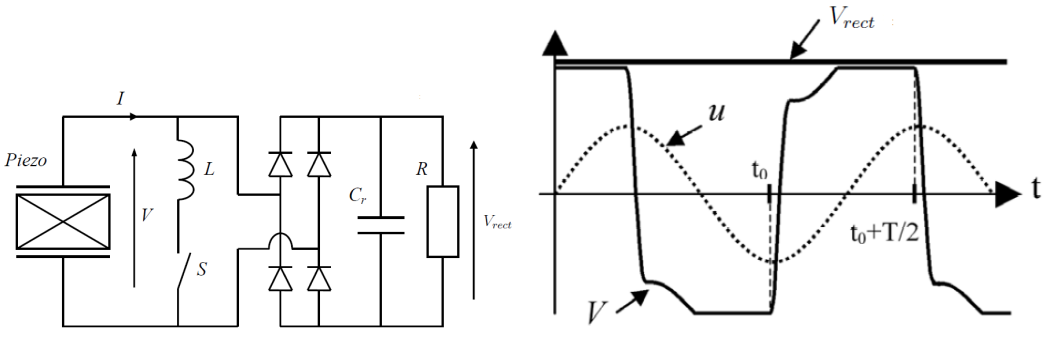

(a) Circuit Toplogy (b) SSHI Waveforms

Figure 2.13: Circuit schematic of the parallel SSHI energy harvesting method and the resulting device waveforms [26].

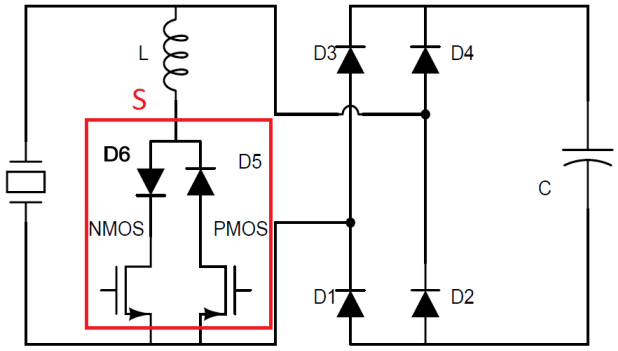

Figure 2.14: A Circuit topology for an implementation of the parallel SSHI energy harvesting technique [3, 29]. Multiple diodes along the conduction path reduce performance at low voltage levels.

2.2.3 Active Energy Harvesting Methods

2.2.3.1 Phase-Locked Active Energy Harvesting

The Phase-Locked Active Energy Harvesting (PLAEH) method utilizes bi-directional power flow between the energy harvesting device and the energy storage element. A pulse-width-modulated full bridge inverter is used to apply a square wave voltage with a magnitude of V_{bus} to the piezoelectric device in phase with the maximum and minimum of the applied force [27,30]. The resulting V-Q plot for the PLAEH method of energy harvesting is shown in Fig. 2.15. In [30], it is shown that the maximum energy that can be extracted is

$$E_{active} = C_p V_{oc} V_{bus}. \tag{2.36}$$

The energy harvested using the PLAEH method is a function of the excitation and the magnitude of the applied square wave. This is in contrast to the rectifier methods, where the harvested power is a function of only the excitation. Increasing the magnitude of the applied square wave, the harvested energy is increased. In practice, the harvested energy is limited by the efficiency of the power electronics that implement the method, the dynamics of the high-Q resonant structure, and the mechanical limitations of the device such as depoling and breakdown fields [30]. Demonstrations of the PLAEH energy harvesting method in [11, 27, 30] demonstrate the significant energy harvesting improvement of the PLAEH method over rectifier techniques. It is also shown in [27] that the PLAEH method outperforms SSHI technique. It should

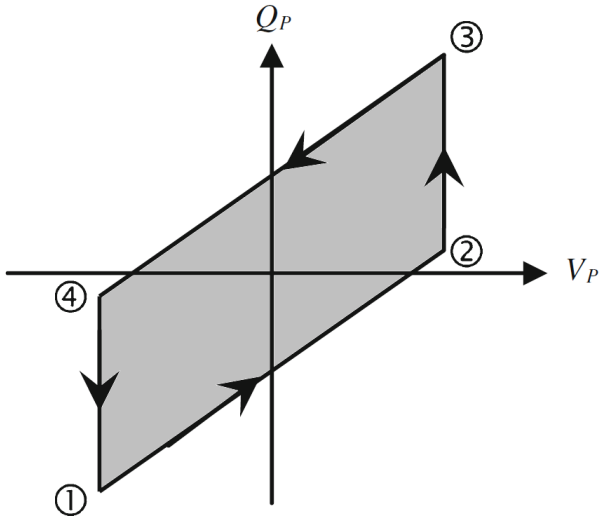

Figure 2.15: Voltage versus charge in a piezoelectric device during a harvesting cycle using the active approach [27]. The shaded region represents the harvested energy during the cycle.

be noted that none of the active energy harvesting examples are autonomous systems, meaning the harvested power is less then the power requirement of the circuit which implements the method. The circuit topology used to implement the method is shown in Fig. 2.16, and the resulting waveforms are shown in Fig. 2.17.

The phase-locked active energy harvesting method is effective at harvesting energy when the mechanical resonant frequency and source frequency are extremely close. However, the small bandwidth of the high-Q resonant mechanical structure means that deviations in the resonant frequency from the excitation frequency, for example due to mechanical parameter tolerances, can result in dramatically reduced harvesting levels. To mitigate this issue, researchers [13, 28, 48, 68] have proposed various mechanical techniques to increase the energy harvesting bandwidth. One such solution is proposed in [53, 54], here a Duffing oscillator is used to extend the bandwidth. The problem is many of the mechanical solutions lower the quality factor of the mechanical system, which reduces the power harvesting capabilities at the resonant frequency.

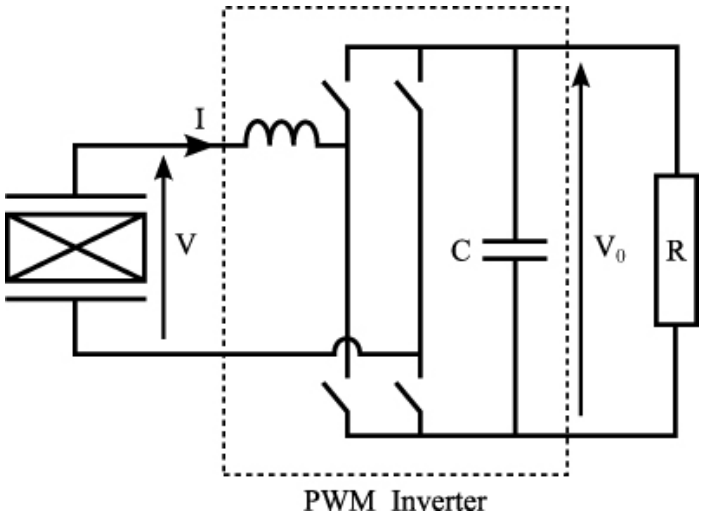

Figure 2.16: A pulse-width-modulated inverter is used to implement the phase-locked active energy harvesting method [11].

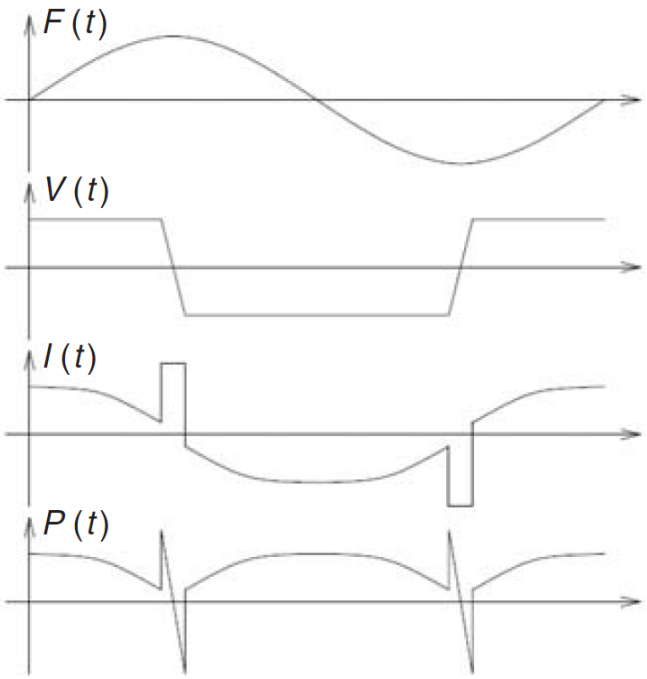

Figure 2.17: The piezoelectric device waveforms for the phase-locked active energy harvesting method [11].

2.2.4 Dynamic Active Energy Harvesting (DAEH) Method

An electrical strategy for increasing the bandwidth is presented in [31], and is called the dynamic active energy harvesting (DAEH) method. Similar to the active energy harvesting method, a pulse-width-modulated full bridge inverter is used to apply a square-wave voltage with a magnitude of V_{bus} to the piezoelectric device; however, unlike the active energy harvesting method , the DAEH method does not restrict the phase of the applied square wave. The independent phase control leads to an increased energy harvesting bandwidth, as explained in this section. The high-Q mechanical system is modeled as a mass-spring-damper system, as illustrated in Fig. 2.19. Using this model for the energy harvesting system, [31] derives an optimal load impedance to maximize the power extracted from the device,

$$\tilde{Z}_{opt} = \frac{\omega^2 m - k + j\omega b}{\omega^2 C' b - j\omega(\omega^2 C' m - (C' + d^2 k)k)}. \tag{2.37}$$

Equation (2.37) is a function of system parameters including the mechanical resonant frequency and the excitation frequency. Assuming a sinusoidal excitation force, this impedance can be emulated by applying a sinusoid whose magnitude is

$$V_{mag} = \sqrt{\omega^2 b^2 + (k - \omega^2 m)^2}\frac{F_m}{2kd\omega b}, \tag{2.38}$$

and phase relative to the input force is

$$\phi = 180^\circ - \tan^{-1}\left(\frac{k - \omega^2 m}{\omega b}\right). \tag{2.39}$$

It is important to note that the efficiency of the power path of the electronics that applies such an impedance is crucial in maximizing the energy harvested over a wide frequency range. Using the device parameters in [31], the effects of the power electronic's power-path efficiency on the DAEH method are shown in Fig. 2.20. The resulting device wave forms are shown in Fig. 5.1.

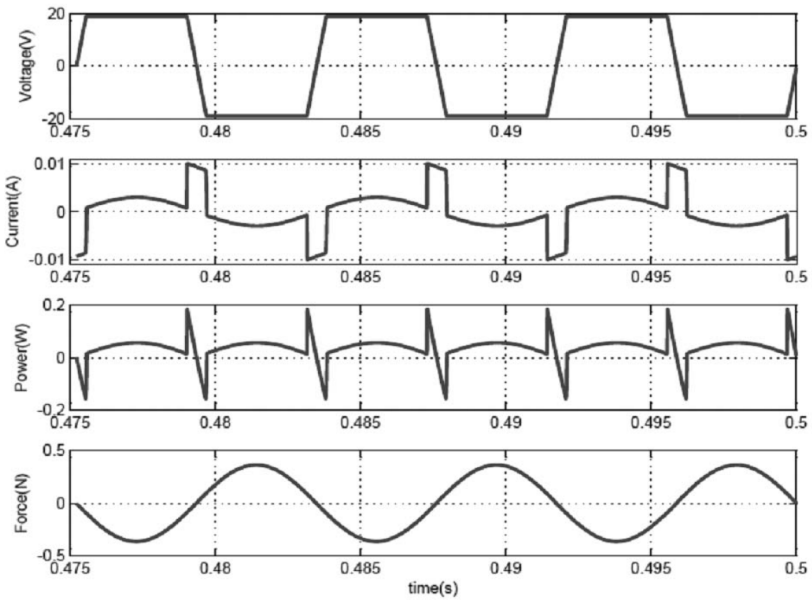

Figure 2.18: The device waveforms for an implementation of the dynamic active energy harvesting method [31]

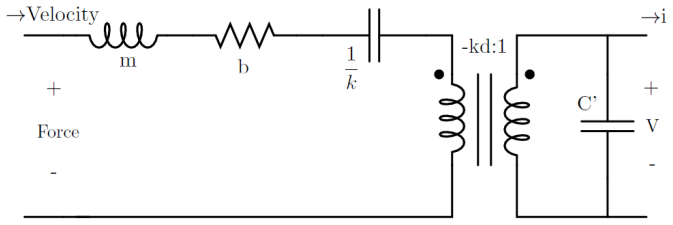

Figure 2.19: Electric circuit model of a resonant mass-spring piezoelectric energy harvesting system.

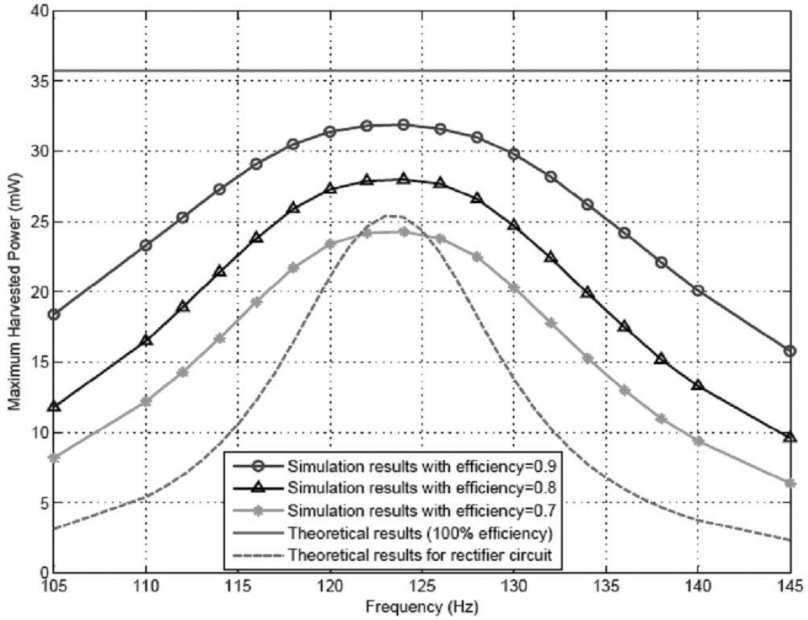

Figure 2.20: The theoretical power harvested using the adaptive rectifier and the DAEH method is plotted as a function of excitation frequency for various power electronic efficiencies. As the excitation frequency deviates from the mechanical resonant frequency, the impact of power-path circuit efficiency on energy harvesting increases. [31]

CHAPTER III

Voltage-Constrained Variable-Capacitance Energy Harvesting

3.1 Introduction

The purpose of this chapter is to determine how power electronic circuit efficiency affects the existing four methods of energy harvesting for an overlap-type (i.e., voltage-constrained) variable-capacitance device. Each of the methods will be compared by how much energy they harvest as a function of power electronic circuit efficiency, providing a more complete understanding of each method. This is accomplished by applying the efficiency-based analysis presented in Section 2.1.4 to the current derivations of the energy harvesting methods. Using this analysis it will be shown that, over some efficiency ranges, the Constant Voltage Method does not harvest more energy than the Constant Charge Method. Furthermore, from this work it is revealed that each method has a threshold efficiency required for energy harvesting. This analysis contributes to the field by producing additional guidelines for designing an energy harvesting circuit. This is accomplished by providing analytical solutions for computing both the optimal parallel capacitance for the CCPC Method, and the optimal input and output voltages for the Charge Pump Method as a function of power electronic efficiency. Finally, an energy harvesting system is proposed based on the Charge Pump Method which advances the system in [69] by providing a design which can be easily synthesized on a chip and incorporates the optimal harvesting conditions derived in this chapter.

3.2 Voltage-Limited Variable Capacitance Theory

3.2.1 Constant Voltage Method

The Constant Voltage Method charges the capacitive device to a voltage V_{max} when the capacitance is at C_{max}, and clamps the voltage as the device capacitance decreases to C_{min}. In Section 2.1.1.1 it is shown that the ideal energy harvested for a voltage-limited device using the Constant Voltage Method is

$$E_{ideal} = E_{in} - E_{out} = \frac{1}{2}(C_{max} - C_{min})V_{max}^2. \tag{3.1}$$

Penalizing the input energy and output energy by an efficiency, η, the net energy harvested is

$$E_{net} = \eta E_{out} - \frac{1}{\eta}E_{in} = \eta(C_{max} - \frac{1}{2}C_{min})V_{max}^2 - \frac{1}{2\eta}C_{max}V_{max}^2. \tag{3.2}$$

Using (2.26), the normalized net energy harvested is derived:

$$N_{Enet} = 2\eta - \frac{\eta}{R_c} - \frac{1}{\eta}. \tag{3.3}$$

The normalized net energy is plotted in Fig. 3.1 and illustrates how efficiency affects energy harvesting for the Constant Voltage Method. Given highly-efficient power electronics and a device with a large R_c, the Constant Voltage Method's harvests the maximum available energy, $\frac{1}{2}C_{max}V_{max}^2$. The harvested power decreases as a strong function of efficiency, making power electronic efficiency particularly important for this method.

Fig. 3.1 shows the normalized net energy harvested falls below zero between 70% and 85%. The threshold efficiency for the Constant Voltage Method is given by:

$$\eta_{thresh} = \sqrt{\frac{E_{in}}{E_{out}}} = \sqrt{\frac{R_c}{2R_c - 1}}. \tag{3.4}$$

A good variable-capacitance harvesting device has a C_{max} that is much larger than C_{min}. Setting R_c to infinity shows the behavior of the best possible device, which results in the lowest possible threshold efficiency.

$$\lim_{R_c \to \infty} \eta_{thresh} = \lim_{R_c \to \infty} \sqrt{\frac{R_c}{2R_c - 1}} = \sqrt{\frac{1}{2}} = 70.71\% \tag{3.5}$$

A capacitance ratio of 25 or higher is sufficiently large for (3.5) to be a good approx-

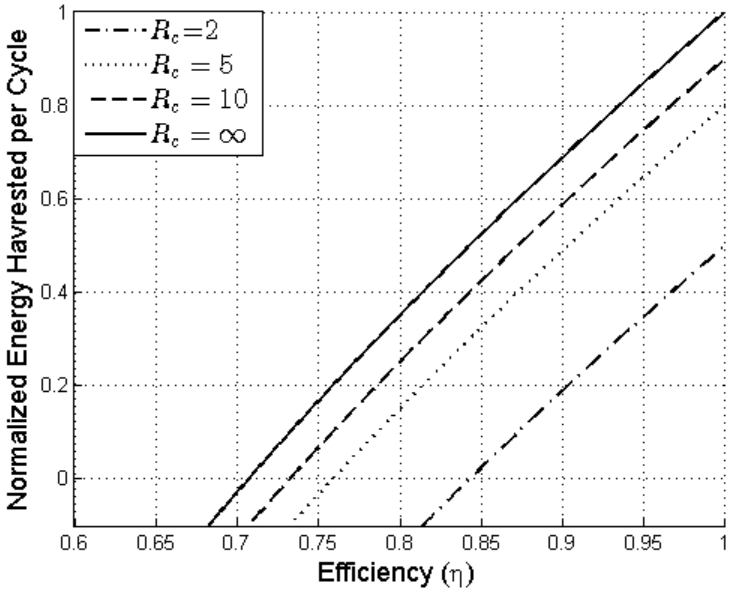

Figure 3.1: Normalized net energy harvested, N_{Enet}, using the Constant Voltage Method as a function of efficiency, η, for various values of capacitance ratio, R_c.

imation of the threshold efficiency.

3.2.2 Constant Charge Method

As discussed in Section 2.1.1.2, the Constant Charge Method of energy harvesting charges the device to a voltage V_{init} while the device is at C_{max}. The device is then left in an open-circuit configuration so that the charge on the device is kept constant. Once the device capacitance reaches C_{min}, the voltage across the device reaches V_{max}, and energy is harvested from the device by discharging the capacitance.

$$E_{ideal} = \frac{1}{2} C_{min} V_{max}^2 - \frac{1}{2} \frac{C_{min}^2}{C_{max}} V_{max}^2 \tag{3.6}$$

Using (2.24) and (3.6) to solve for the net energy harvested yields:

$$E_{net} = \eta \left[\frac{1}{2} C_{min} V_{max}^2 \right] - \frac{1}{2\eta} \left[\frac{C_{min}^2}{C_{max}} V_{max}^2 \right]. \tag{3.7}$$

Using (2.26), the normalized net energy harvested is shown to be:

$$N_{Enet} \;=\; \frac{\eta}{R_c} - \frac{1}{\eta R_c^2}. \tag{3.8}$$

Equation (4.15) is illustrated in Fig. 3.2 to elucidate harvesting characteristics of

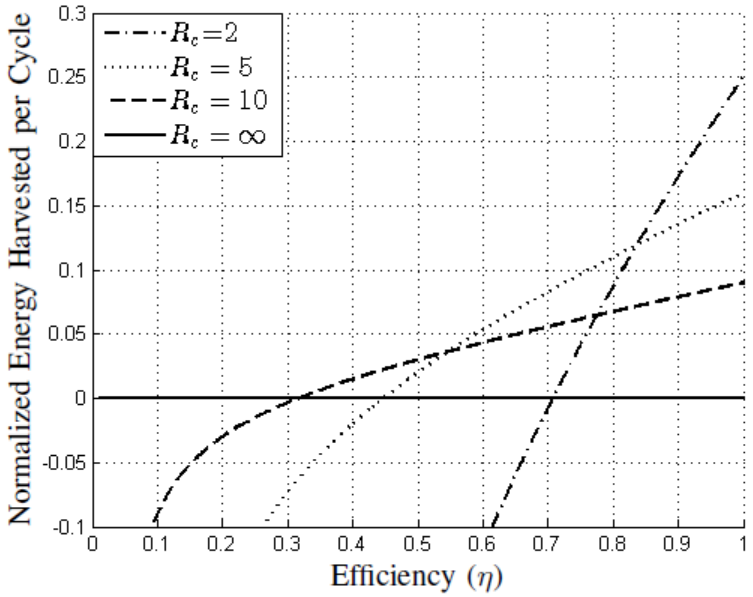

Figure 3.2: Normalized energy harvested, N_{Enet}, using the Constant Charge Method as a function of efficiency, η, for various values of the capacitance ratio, R_c.

this method. It can be shown that the highest ratio of harvested energy to available energy occurs when the power electronic efficiency is high and the capacitance ratio has a value of 2. This can be shown by optimizing the normalized energy harvested with respect to R_c. In this case, the Constant Charge method harvests a quarter of the maximum available energy. As R_c becomes large, the Constant Charge Method harvests very little energy relative to the maximum available energy. The mechanical energy in the system that can be harvested is determined by the electrostatic force and the distance of travel. In this system the electrostatic force is proportional to the square of the voltage on the device. As the capacitance ratio increases, a smaller V_{init} must be applied to the device in order meet the maximum voltage constraint. The additional energy harvesting capability of the system is small because the majority of the energy harvesting occurs when the voltage on the device is large. On the other hand, power electronic efficiency has a very small impact on the large R_c device when using the Constant Charge method. The N_{Enet} does not fall below zero until very low efficiencies. This trend is elucidated by solving for the threshold efficiency:

$$\eta_{thresh} = \sqrt{\frac{E_{in}}{E_{out}}} = \sqrt{\frac{1}{R_c}}. \tag{3.9}$$

The minimum threshold efficiency that is achieved by the Constant Charge Method is

$$\lim_{R_c \to \infty} \eta_{thresh} = 0. \tag{3.10}$$

3.2.3 Charge Pump Method

The Charge Pump Method Method has two distinct segments to its harvesting cycle: a constant charge segment and a constant voltage segment. By combining these portions the power harvested using the Charge Pump Method can be optimized for a given power electronic efficiency. In Section 2.1.3, it is shown that the ideal energy that can be harvested is

$$E_{ideal} = (V_{max} - V_{min})(V_{min}C_{max} - V_{max}C_{min}). \tag{3.11}$$

Including efficiency as a parameter, as demonstrated in (2.24), the net harvested energy is given by:

$$E_{net} = (\eta V_{max} - \frac{V_{min}}{\eta})(V_{min}C_{max} - V_{max}C_{min}). \tag{3.12}$$

Fig. 3.3 and 3.4 depict the net energy harvested using the Charge Pump method under two different operating conditions. The net energy equation for the Charge Pump Method is a function of two controllable design criteria: V_{max} and V_{min}. In Fig. 3.3, the voltage V_{min} is held constant and the net energy harvested is plotted at several power electronic efficiencies as a function of V_{max}. Conversely, in Fig. 3.4 V_{max} is held constant and the net energy harvested at many power electronic efficiencies is plotted as a function of V_{min}. In both Fig. 3.3 and 3.4 the ideal energy harvested ($\eta = 1$) is plotted as function of voltage, unveiling conditions on V_{max} and V_{min} which must be met in order to harvest energy. The constraints on V_{max} and V_{min} are:

$$V_{min} < V_{max} < R_c V_{min}. \tag{3.13}$$

The conditions noted in (3.13) are developed from fundamental circuit principles. First, V_{max} must be larger than V_{min} so that the diodes of Fig. 2.7 do not continuously conduct, effectively shorting V_{max} and V_{min}. Secondly, if V_{max} is larger than $R_c V_{min}$, then the voltage across the device will never be large enough to forward bias the output diode, and so electrical power is never extracted.

Fig. 3.3 and Fig. 3.4 reveal the existence of optimum harvesting conditions. For

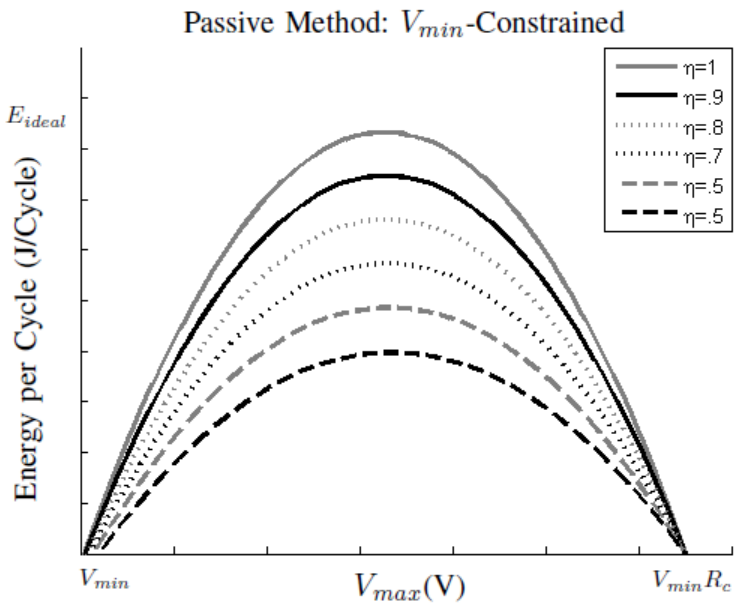

Figure 3.3: Net energy harvested using the V_{min}-constrained Charge-Pump Method.

example, in Fig. 3.3, given a constrained V_{max}, there exists an optimum V_{min} that maximizes the energy harvested. Likewise in Fig. 3.6, given a constrained V_{min} an optimal V_{max} can be found that maximizes the energy harvested.

The optimal harvesting condition for both the V_{max}-constrained case and the V_{min}-constrained case are derived from (3.12). To find the optimum V_{min}, denoted as $V_{min_{opt}}$, the derivative of the net energy equation is taken with respect to V_{min} and set to zero as shown in (3.14).

$$\frac{dE_{net}}{dV_{min}} = 0 = \eta C_{max} V_{max} - \frac{1}{\eta}(2V_{min}C_{max} - V_{max}C_{min}) \tag{3.14}$$

The resulting value of V_{min} is therefore:

$$V_{min_{opt}} = V_{max}\left[\frac{\eta^2}{2} + \frac{1}{R_c 2}\right]. \tag{3.15}$$

A visual representation of (3.15) portrayed in Fig. 3.5 illuminates the large influence of power electronic efficiency on optimal harvesting conditions for a V_{max}-constrained harvesting application.

To derive the optimal V_{max}, denoted as $V_{max_{opt}}$, for the V_{min}-constrained case, the

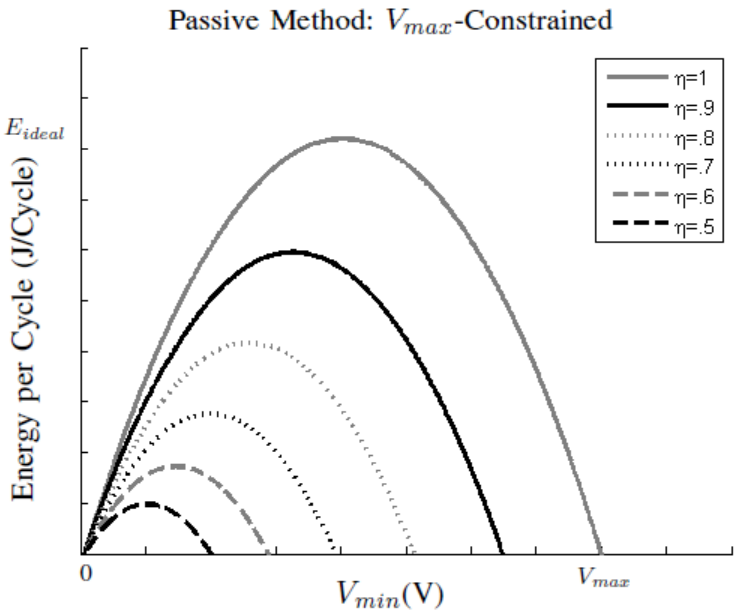

Figure 3.4: Net energy harvested using the V_{max}-constrained Charge-Pump Method.

derivative of the net energy equation is taken with respect to V_{max} as shown in (3.16).

$$\frac{dE_{net}}{dV_{max}} = \eta C_{max} V_{min} - 2\eta V_{max} C_{min} + \frac{1}{\eta} V_{min} C_{min} \tag{3.16}$$

To obtain $V_{max_{opt}}$, (3.16) is set to zero and solved for V_{max};

$$V_{max_{opt}} = V_{min}\left[\frac{1}{2\eta^2} + \frac{R_c}{2}\right]. \tag{3.17}$$

Finally, a plot of (3.17) is shown in Fig. 3.6, which reveals a relatively weak relationship between $V_{max_{opt}}$ and power electronic efficiency for the V_{min}-constrained harvesting application with large values of R_c.

Using $V_{min_{opt}}$, the normalized net energy harvested is derived as a function of efficiency and shown in Fig. 3.7.

$$N_{Enet} = 2\eta\left[\frac{\eta^2}{2} + \frac{1}{2R_c}\right] - \frac{2\eta}{R_c} - \frac{2[\frac{\eta^2}{2} + \frac{1}{2R_c}]^2}{\eta} + \frac{2[\frac{\eta^2}{2} + \frac{1}{2R_c}]}{\eta R_c} \tag{3.18}$$

It is illustrated that, for large values of R_c and high efficiency power electronics, at most half of the maximum available energy can be harvested; however, as efficiency declines, the harvested energy does not decline as rapidly as that of the Constant Voltage Method.

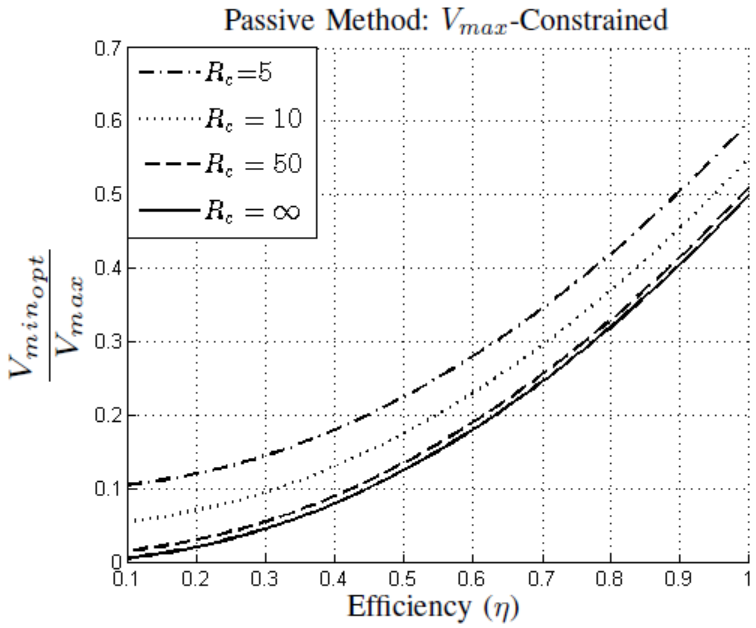

Figure 3.5: The optimal V_{min} to V_{max} ratio is shown for the V_{max}-constrained case. This plot is a function of power electronic efficiency and capacitance ratio.

The trends discussed in this section help guide the design of a Charge Pump Method energy harvesting circuit by clarifying the relationship between V_{max} and V_{min}. For a typical electret-free variable-capacitance device, the allowable V_{max} is small, hence V_{max}-constrained theory will provide an optimal V_{min} from (3.15). However, for high voltage devices where the allowable V_{max} of the device cannot be reached within the constraints of the design, the V_{min}-constrained theory will provide an optimal V_{max} from (3.17). Finally, to ensure a positive net energy harvested, the threshold efficiency is given by:

$$\eta_{thresh} = \sqrt{\frac{E_{in}}{E_{out}}} = \sqrt{\frac{V_{min}}{V_{max}}}. \tag{3.19}$$

The threshold efficiency for the Charge Pump Method is therefore independent of device parameters and instead dependent on design variables V_{max} and V_{min}.

3.2.4 Constant Charge with Parallel Capacitance Method

The Constant Charge with Parallel Capacitance Method, or CCPC Method, adds a parallel capacitance to the Constant Charge Method in order to shape the harvesting cycle. A discussion of the CCPC method is in Section 2.1.2. Here it is shown that

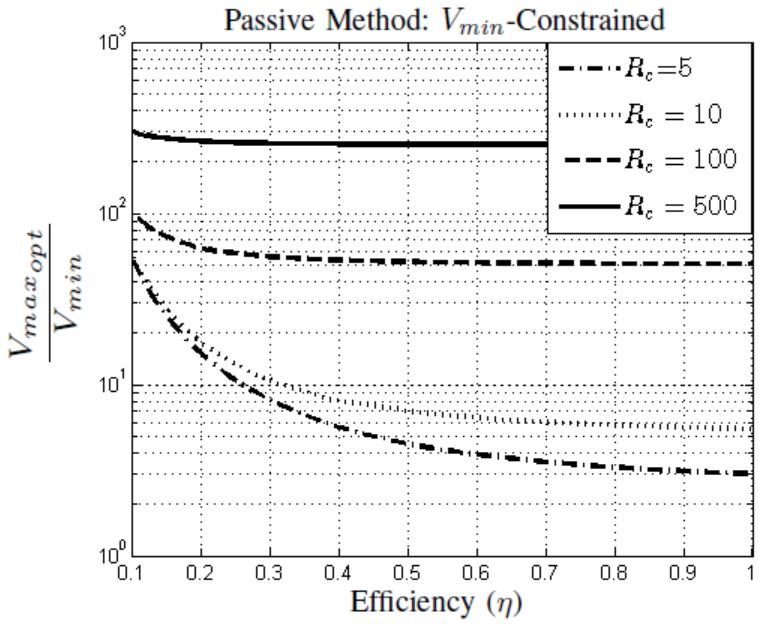

Figure 3.6: The optimal V_{max} to V_{min} ratio is shown for the V_{min}-constrained case. This plot is a function of power electronic efficiency and capacitance ratio.

the ideal energy extracted by this method is

$$E_{ideal} = \frac{1}{2}(C_p + C_{min})V_{max}^2 - \frac{1}{2}\frac{(C_{min} + C_p)^2}{C_{max} + C_p}V_{max}^2. \tag{3.20}$$

To include efficiency as a parameter, the energy inserted and removed by the power electronic circuitry is penalized; however, energy transfer between the two capacitors when they are in the open-circuit configuration is considered to occur without loss. Using (2.24) an equation for E_{net} is derived:

$$E_{net} = \frac{\eta}{2}(C_p + C_{min})V_{max}^2 - \frac{1}{2\eta}\frac{(C_{min} + C_p)^2}{C_{max} + C_p}V_{max}^2. \tag{3.21}$$

In [36] it was shown through simulation that there exists an optimal C_p; however, by including efficiency as a parameter, a value can be derived analytically for the optimal C_p. Conversely, the ideal C_p can be chosen for a given efficiency in order to maximize the amount of energy harvested per cycle. To calculate the optimal C_p the derivative of the net energy equation is taken with respect to optimal C_p and set to

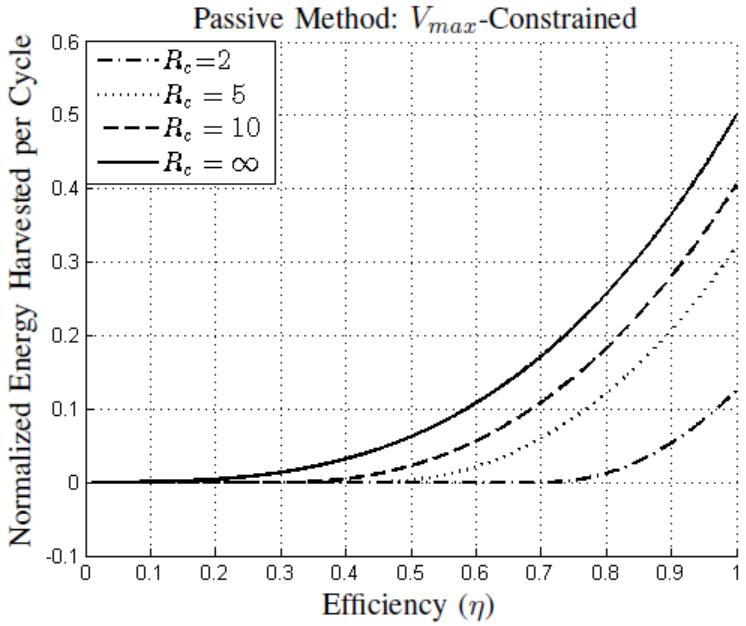

Figure 3.7: The normalized net energy harvested using the Charge Pump method while V_{max} is constrained and V_{min} is optimized.

zero. The optimal C_p denoted as $C_{p_{opt}}$ is

$$C_{p_{opt}} = C_{max} \frac{1 + \sqrt{1 - \frac{\eta+1}{\eta-1}\left(\eta^2 + \frac{1}{R_c^2} - \frac{2}{R_c}\right)}}{\eta + 1}; \tag{3.22}$$

The relationship between $C_{p_{opt}}$ and power electronic efficiency is illustrated in Fig. 3.8. A highly-efficient converter will have a large C_p, which will make the cycle look mostly like a constant voltage cycle; however, an inefficient converter's ideal C_p will be small, so the cycle is similar to the constant charge cycle.

Using $C_{p_{opt}}$, the normalized net energy harvested is derived as a function of efficiency and plotted in Fig. 3.9.

$$N_{Enet} = \frac{\eta(C_p + C_{min})}{C_{max}} - \frac{(C_{min} + C_p)^2}{\eta C_{max}(C_{max} + C_p)} \tag{3.23}$$

Given highly-efficient power electronics and a device with a large R_c the CCPC Method harvests the maximum available energy; however, the energy harvested declines rapidly as efficiency decreases.

The threshold efficiency for the CCPC Method is given by:

$$\eta_{thresh} = \sqrt{\frac{E_{in}}{E_{out}}} = \sqrt{\frac{C_{min}+C_p}{C_{max}+C_p}}. \tag{3.24}$$

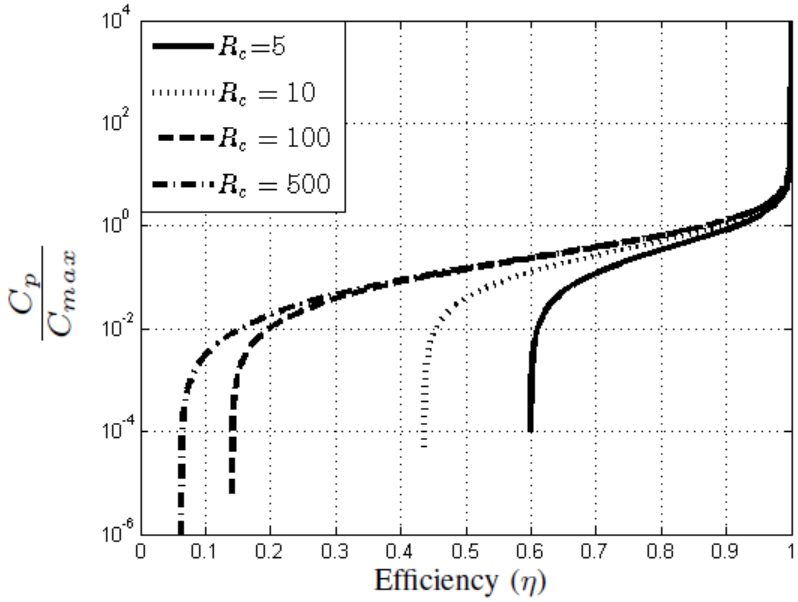

Figure 3.8: Optimal C_p for a given power electronic efficiency and capacitance ratio.

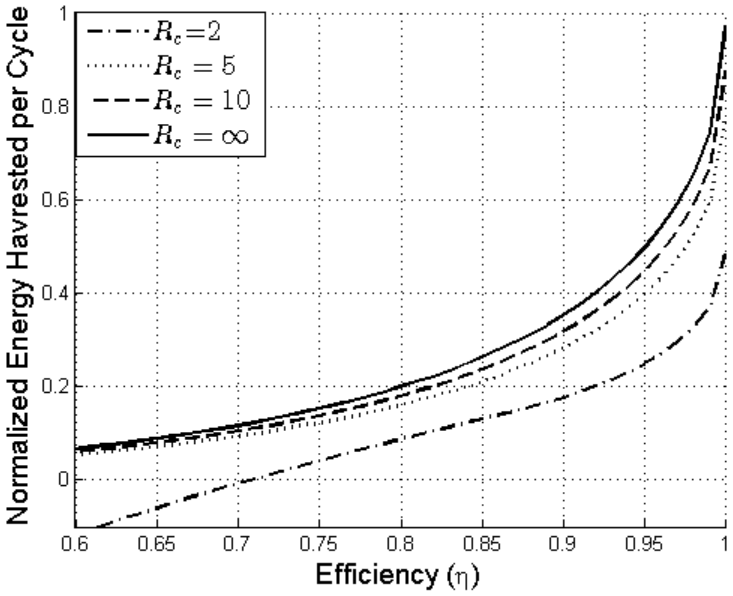

Figure 3.9: The normalized net energy harvested plotted as function of efficiency while using the optimal C_p for the CCPC Method.

Similar to the Constant Charge Method, as the capacitance ratio becomes arbitrarily large,

$$\lim_{R_c \to \infty} \eta_{thresh} = 0. \tag{3.25}$$

3.3 Discussion

Using efficiency as a parameter, a comparison of the four methods of energy harvesting on a specific device demonstrates the advantages and disadvantages of each method. Investigating a specific device will provide an application of the fundamental principles shown in the theory section and examine more practical issues, including estimated power levels. The chosen device is referred to as the large R_c device and is similar to the device used in [36]. The device properties are shown in Table 3.1. It is a comb-type variable-capacitance device with an excitation frequency of 2520 Hz, meaning the device varies from C_{max} to C_{min} at a frequency of 5040 Hz. In order to harvest energy, a battery must be used to both supply energy to the harvesting cycle and provide energy storage for the harvested energy. The nominal voltage of the battery is referred to as V_{bat}, and is assumed to be 4 Volts.

Table 3.1: Large R_c Area-overlap-Device Properties

Parameter	**Value**
Allowable V_{max}	8 Volts
C_{max}	260pF
C_{min}	2pF

3.3.1 Case Study: Selecting a Harvesting Method

In order to select the best harvesting method a number of factors must be considered: power harvested, practicality of implementation, and ease of integration into a micro-sized energy harvester. Fig. 3.10 highlights the Constant Voltage Method, the CCPC Method, and the Charge Pump Method because they each harvest a significant amount of power over a wide efficiency range. However, the Constant Voltage Method and CCPC Method are practically difficult to implement. These methods require the device to be charged and discharged when the oscillating mass of the device is at a certain position. This requires the controller to have knowledge of the position of the energy harvester. Such a control strategy was developed by [36]; however, 34% of their harvested power was dedicated to their controller implementation. Even if a

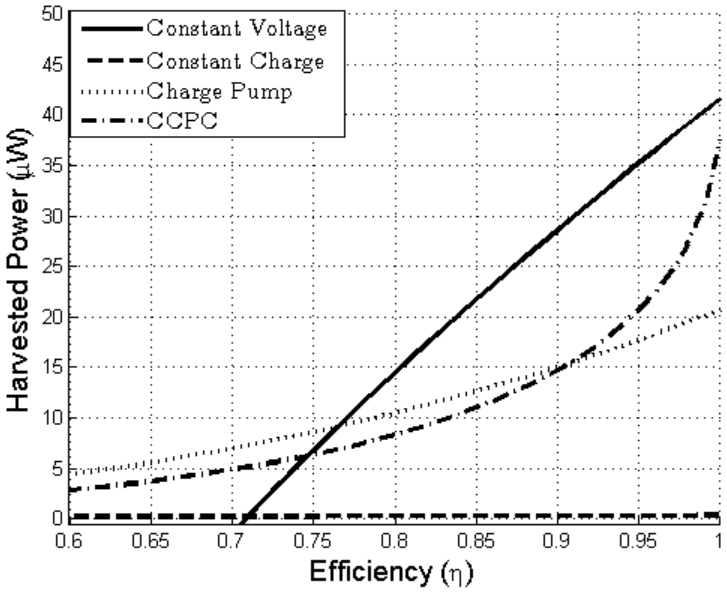

Figure 3.10: Comparison of power harvested for each harvesting methods using the Large R_c device assuming optimized conditions for the Charge Pump and CCPC methods. The Constant Charge Method harvests $.32\mu W$ at $\eta = 1$ and $.19\mu W$ at $\eta = .6$.

highly-efficient control circuit and power electronic converter was developed for these methods, the varying nature of the voltage on the device as energy is transferred back to the battery would require a magnetic-component based power electronic circuit. This can be difficult to implement in a microsystem, as it requires a micro-sized magnetic core on a chip. In [36] an estimated 5.6μW could be harvested from the Large R_c Device using the CCPC Method. If the Charge Pump Method was used in combination with the optimal minimum voltage shown in (3.15), then based on (3.12) we expect to harvest 10.8μW from the same device given an assumed efficiency estimate of 80% (η=.80).

The Charge Pump Method has many advantages: it can be easily implemented on an integrated circuit, does not require active control, and it harvests significant energy over a wide efficiency range. The Constant Voltage Method harvests approximately the same power at 80% efficiency as the Charge Pump Method does at 90% efficiency; however, it is probable that the circuitry implementing the Charge Pump Method will be more efficient due to a lack of switching losses. The optimum ratio of V_{max} to V_{min} for the Charge Pump Method is fixed for a given efficiency, so transferring energy between these sources corresponds to a fixed voltage conversion ratio. This allows for the design of highly-efficient power electronic circuitry. Switched-capacitor converter

topologies can accomplish a fixed voltage gain without a magnetic component (i.e. inductor or transformer). The control of the Charge Pump Method does not require knowledge of the state of the variable-capacitance device, which simplifies the design and saves energy. The theoretical energy harvested using this method is shown in Fig. 3.10. The Charge Pump Method harvests a comparable amount of energy as the CCPC Method and the Constant Voltage Method over typical power electronic efficiency ranges, but was chosen because of the other advantages highlighted in this paragraph.

3.3.2 Case Study: Design of an Energy Harvesting System

In order to maximize the power harvested, it is important that the design of the energy harvesting system is closely tied to the optimal harvesting conditions derived in (3.15). Due to the area-overlap device architecture the allowable V_{max} is small, so this design is based on the V_{max}-constrained theory. Assuming 100% efficiency and a V_{max} of 8 Volts, the optimum V_{min} is 4.03 Volts, so if the converter is efficient then a 2:1 switched-capacitor circuit can be used to transfer energy from V_{max} back to V_{min}, and the ratio of these voltages will be very close to optimal. Fig. 3.11 depicts the discrepancy between using $V_{min_{opt}}$ and the 2:1 converter as a function of efficiency. Using a 2:1 switched-capacitor converter is effective as long as the overall circuit efficiency is high (i.e.,$> 85\%$). The proposed circuit topology is shown in Fig. 3.12.

As the device capacitance oscillates between C_{max} and C_{min}, energy is harvested and stored in the output capacitor, which causes V_{max} to rise. A hysteresis controller dictates when the switched-capacitor converter is enabled. The switched-capacitor converter operates by turning "on" S1 and S3 for the first half of the switching period, and S2 and S4 for the second half of the switching period. The switching frequency of the switched-capacitor converter is much higher than the excitation frequency of the device, and thus is able to transfer energy back to V_{min} on a faster time scale than it is harvested. In order to minimize switching losses, a hysteresis controller, implemented by a single comparator, only turns the switched-capacitor converter on for short bursts and allows a tiny voltage swing across V_{max}. The hysteresis band is set to keep V_{max} between 8.012 Volts and 8.004 Volts. By keeping the ratio of V_{min} to V_{max} greater than but close to 2:1, the efficiency of this topology can be high.

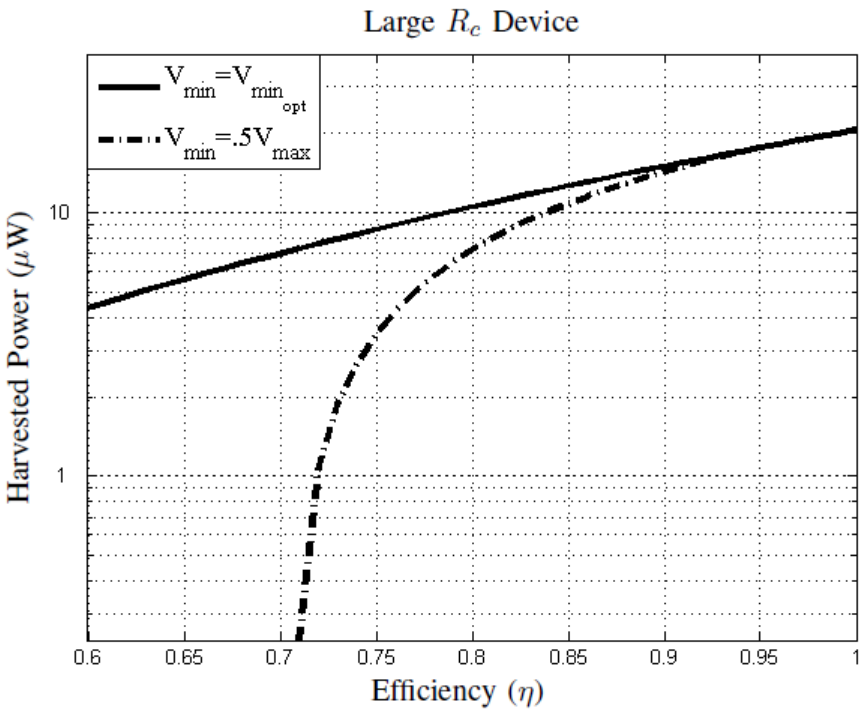

Figure 3.11: Comparison of power harvested using the V_{max}-constrained Charge Pump Method when V_{min} is optimal versus $\frac{1}{2}V_{max}$.

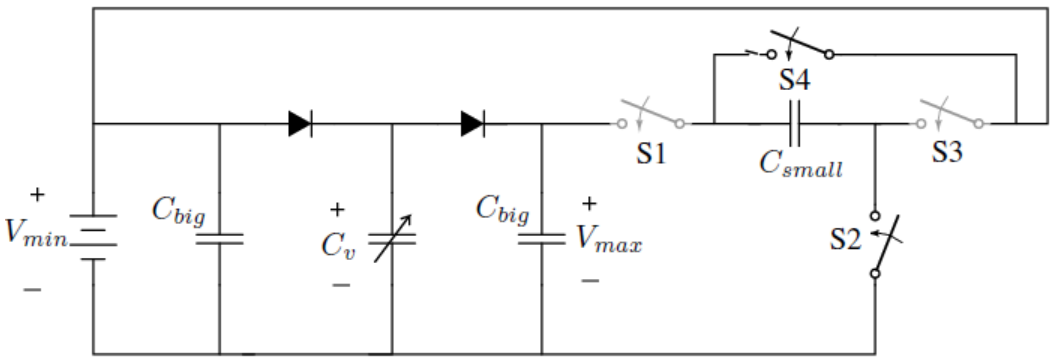

Figure 3.12: Charge Pump Method energy harvesting circuit topology with switched-capacitor energy return.

3.3.3 Case Study: Simulation Results

The energy harvesting system portrayed in Fig. 3.12 was simulated in LTSPICE. The simulation included many realistic loss mechanisms in order to provide a conservative estimate of power harvested. An appropriate loss model was created based on loss mechanisms associated with implementing this design on an integrated circuit. The switches required in this design are bi-directional switches which must be able to hold 10 Volts and carry 20 mA. In order to withstand the required voltage range a 12 Volt process was used for the design. Using models of this process, parameter values for the transistors were extracted. These transistors have an on-resistance of 257 mΩ (when V_{gs} is 3.3 Volts), a leakage current of 1μA, a drain-to-source capacitance of 0.16 pF, and a gate to source capacitance of 1.6 pF. The absolute maximum ratings for drain to source voltage (12 Volts) and current (6 A) are not exceeded in the simulation. The gating losses are calculated by assuming the energy sourced to the gate capacitance is lost during each switching cycle. The diode characteristics are modeled based on the Fairchild Semiconductor BAX16. This diode has a forward voltage drop of 0.65 Volts and a leakage current of 25nA. Finally, an ESR of 1mΩ is used for the capacitors. The control losses are derived from the operating power of a comparator. An Intersel-ISL7819 comparator's losses (1.65 μW) are used to represent control losses.

The results of this simulation are summarized in Table 3.2 and Fig. 3.13, which shows the output voltage rising as energy is harvested from the device. Once the voltage reaches the top of the hysteresis band, the switched-capacitor converter is turned on and energy is returned to the source. Using the theory developed in this paper, an energy harvesting system was developed that harvests 12.09 μW, more than twice the amount of energy as predicted in [36] while using the same device properties.

Table 3.2: LTSPICE simulation results for the large R_c device, using the Charge Pump Method with a switched-capacitor topology

Simulation Results	
Switched-Capacitor Efficiency	86.9%
Energy Harvested	12.09μW

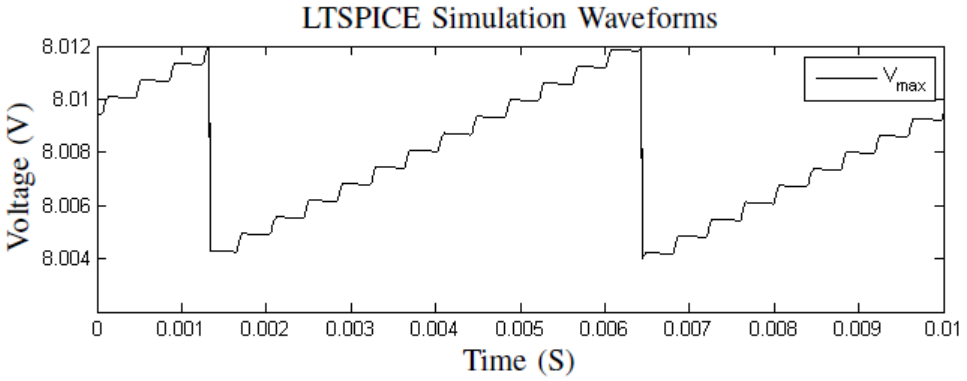

Figure 3.13: V_{max} voltage variations from the LTSPICE simulation of the charge pump energy harvesting system.

3.3.4 Application of Theory to Future Devices

A device with a large allowable V_{max} has not yet been physically realized due to difficulties in manufacturing, but it has been proposed that large gains in energy harvesting could be made if such a device existed [36]. By applying the theory presented in this paper, the ceiling of energy harvesting from these devices can be raised even further. The Charge Pump Method is perceived to be the best option for the same reasons it was optimal for the Large R_c device: it can be implemented on an integrated circuit, it has simple control, and it harvests energy over a large efficiency range. An example device, described in Table 3.3, is used to illustrate important trends. Fig. 3.14 demonstrates that, for the given device parameters, the V_{max}-constrained Charge Pump Method harvests nearly an order of magnitude more energy per cycle than the V_{min}-constrained Charge Pump Method whose V_{min} is constrained by V_{bat} .

Table 3.3: Large V_{max} Device Properties

Parameter	**Value**
Allowable V_{max}	80 Volts
C_{max}	35pF
C_{min}	1.75pF

The difficulty of the V_{max}-constrained method is that $V_{min_{opt}}$ is not close to V_{bat}. This motivates the design of a two-converter topology. The first converter generates $V_{min_{opt}}$ from V_{bat}, and the second converter returns harvested energy from V_{max} to $V_{min_{opt}}$. A ladder converter, as shown in [55], can be used to generate a large fixed voltage gain as required to generate $V_{min_{opt}}$ from V_{bat}. Similar to the Large R_c device, the same 2:1 switched-capacitor converter can be used for the second converter.

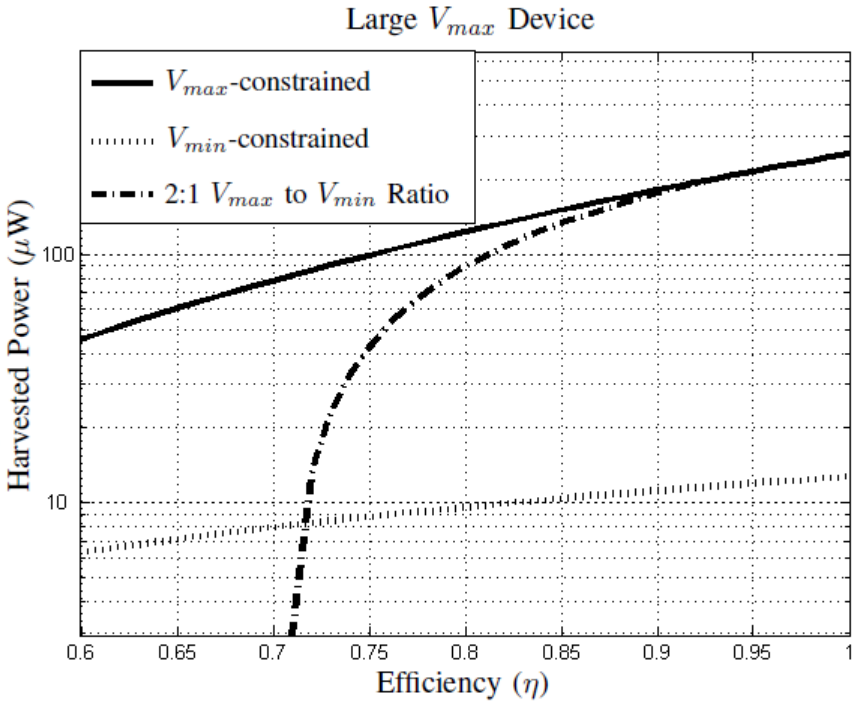

Figure 3.14: Comparison of power harvested when using the V_{min}-constrained Charge Pump Method when V_{max} is optimized, and the V_{max}-constrained Charge Pump Method when V_{min} is optimal and $\frac{1}{2}V_{max}$. The constrained V_{min} is the battery voltage (4 V) and the constrained V_{max} is the allowable V_{max} (80 V).

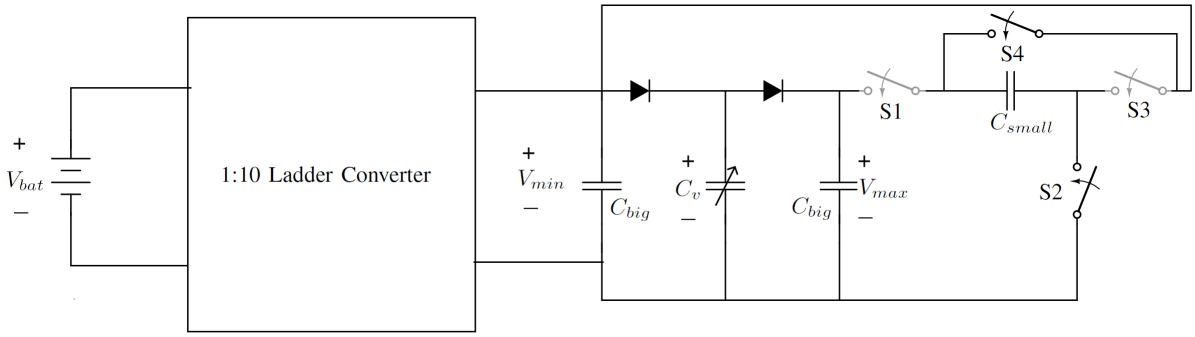

Figure 3.15: Proposed two converter circuit topology for a device with a large V_{max}.

Assuming an ideal efficiency (η=1) and V_{max}=80 Volts, then V_{min} becomes 40 Volts which is very close to $V_{min_{opt}}$ (42 Volts). In order to create V_{min} from V_{bat}, a 10:1 ladder converter is required. The proposed circuit topology is shown in Fig. 3.15. Together, these converters create near optimal harvesting conditions for the Charge Pump Method.

3.4 Summary and Conclusion

This chapter seeks to increase the viability of electret-free variable-capacitance energy harvesters by maximizing the power harvested from these devices. This was accomplished by incorporating power electronic efficiency into the existing analysis of harvesting methods. Including power electronic efficiency as a parameter led to: the derivation of a threshold efficiency for each of the energy harvesting methods, a comparison of the net energy harvested using different harvesting methods over a wide efficiency range, and analytical solutions for the optimal harvesting conditions for applicable methods. The new theoretical background developed in this chapter motivates the design of a energy harvesting system based on the Charge Pump Method. Analytical solutions for optimal energy harvesting conditions inspired the use of a 2:1 switched capacitor converter topology as the basis of said harvesting system. An LTSPICE simulation verified the advantages of the proposed Charge-Pump Method harvesting system by revealing that $12.09\mu W$ could be harvested from this system, which is more than twice the power previously asserted for the same device. To improve the power harvested from these devices, many have proposed a high-voltage variable-capacitance device. To maximize the power harvested from such a device, a two-converter harvesting topology is proposed to implement the V_{max}-constrained Charge Pump Method near its optimal harvesting conditions.

CHAPTER IV

Charge-Constrained Variable-Capacitance Energy Harvesting

4.1 Introduction

This chapter seeks to compare the energy harvesting capabilities of gap-closing and area-overlap variable-capacitance devices by investigating the impact of power electronic efficiency on their harvesting methods. Four energy harvesting methods (Constant Voltage Method, Constant Charge Method, Charge Pump Method, and the new Constant Voltage Series Capacitance (CVSC) Method) are derived for gap-closing devices when the maximum charge on the device is constrained. The energy harvesting capability of charge-constrained gap-closing devices is then compared to the energy harvesting capability of voltage-constrained area-overlap devices derived in Chapter III. This comparison illustrates that at practical power electronic efficiencies the gap-closing device can harvest significantly more power. Finally, a case study demonstrates the energy harvesting benefits of using a charge-constrained device, elucidates some of the practical difficulties, and leads to the proposal of a new energy harvesting method that accommodates both a voltage and charge constraint.

4.2 Charge-Constrained Variable Capacitance Theory

4.2.1 Charge-Constrained Constant Voltage Theory

The Constant Voltage method holds the voltage constant on the the variable-capacitance device as the capacitance reduces its value from C_{max} to C_{min}. This process is described thoroughly in Section 2.1.1.1 and the VQ plot is shown in Fig. 2.3.

When the device capacitance is at its maximum value the charge on the device is,

$$Q_{max} = C_{max}V_{max}. \tag{4.1}$$

Therefore, the energy injected into the device is

$$E_{in} = \frac{1}{2}Q_{max}V_{max} = \frac{Q_{max}^2}{2C_{max}}. \tag{4.2}$$

As the capacitance of the device is reduced, so to does the charge on the device. Once the device capacitance reaches C_{min} the charge on the device is

$$Q_{min} = C_{min}V_{max}. \tag{4.3}$$

The energy extracted from the device is

$$E_{out} = (Q_{max} - Q_{min})V_{max} + \frac{1}{2}Q_{min}V_{max} = Q_{max}V_{max} - \frac{1}{2}Q_{min}V_{max}. \tag{4.4}$$

Using (2.5) the ideal energy harvested from a charge constrained device using the Constant Voltage Method is

$$E_{ideal} = \frac{1}{2}(Q_{max} - Q_{min})V_{max} = \frac{1}{2C_{max}}(1 - R_c)Q_{max}^2. \tag{4.5}$$

Including the efficiency of the power electronics as shown in (2.24), the net energy harvested is

$$E_{net} = \frac{Q_{max}^2}{C_{max}}(\eta - \frac{\eta}{2R_c} - \frac{1}{2\eta}). \tag{4.6}$$

The normalized net energy N_{Enet} is derived from (2.28) and is

$$N_{Enet} = \frac{2\eta}{R_c} - \frac{\eta}{R_c^2} - \frac{2}{R_c\eta}. \tag{4.7}$$

The normalized net energy is plotted in Fig. 4.1 and illustrates how efficiency effects energy harvesting for the Constant Voltage Method on a gap-closing device. As the capacitance ratio increases, the Constant Voltage Method harvests only a small fraction of the available energy independent of power electronic efficiency. At smaller capacitance ratios, the Constant Voltage Method harvests a larger proportion of the available energy; however, the harvested power is extremely dependent on power electronic efficiency. In fact, as the efficiency decreases, the harvested power becomes negative. The minimum efficiency required for energy harvesting is independent of

the type of constraint applied to the device; therefore, the 71% threshold efficiency derived in Chapter III still applies.

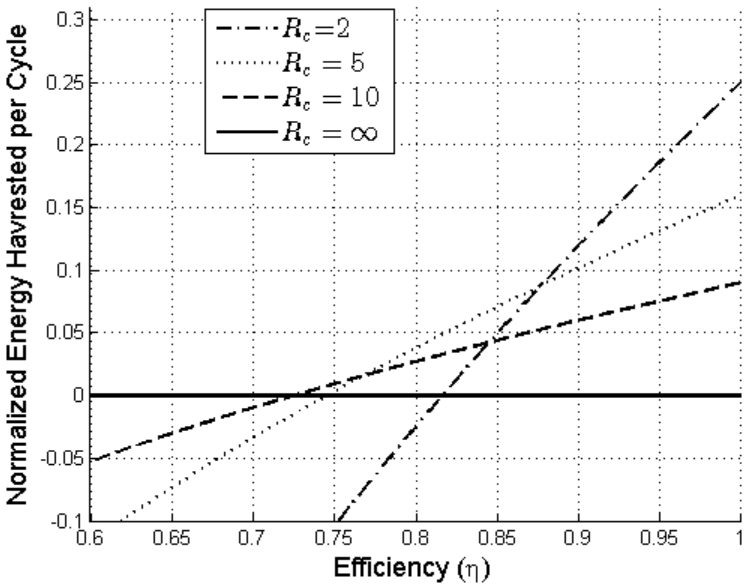

Figure 4.1: Normalized energy harvested, N_{Enet}, using the Constant Voltage Method as a function of efficiency, η, for various values of capacitance ratio, R_c.

4.2.2 Charge-Constrained Constant Charge Theory

The Constant Charge method holds the charge on the variable-capacitance device constant as the device capacitance reduces from C_{max} to C_{min}. This method is described thoroughly in Section 2.1.1.2, and the VQ plot is shown in Fig. 2.4.

To begin the Constant Charge Method of energy harvesting, the variable-capacitance device is charged to V_{init} when the device reaches C_{max}. The charge on the device is

$$Q_{max} = C_{max}V_{init} = C_{min}V_{max}. \tag{4.8}$$

To constrain the charge in the device the maximum initial voltage is

$$V_{init} = \frac{Q_{max}}{C_{max}}. \tag{4.9}$$

Therefore, the energy put into the device to initiate energy harvesting when the device reaches C_{max} is

$$E_{in} = \frac{Q_{max}^2}{2C_{max}} \tag{4.10}$$

When the device capacitances is C_{min} the voltage reaches a maximum of

$$V_{max} = \frac{Q_{max}}{C_{min}}, \tag{4.11}$$

and the energy is extracted from the device

$$E_{out} = \frac{Q_{max}^2}{2C_{min}}. \tag{4.12}$$

A charge-constrained device using the Constant Charge method can harvest up to

$$E_{ideal} = E_{out} - E_{in} = \frac{1}{2}Q_{max}^2 \left[\frac{1}{C_{min}} - \frac{1}{C_{max}}\right]. \tag{4.13}$$

Including power electronic efficiency the net energy harvested is derived:

$$E_{net} = \frac{1}{2}Q_{max}^2 \left[\frac{\eta}{C_{min}} - \frac{1}{\eta C_{max}}\right]. \tag{4.14}$$

Using (2.28), the normalized net energy harvested is shown to be

$$N_{Enet} = \eta - \frac{1}{\eta R_c}. \tag{4.15}$$

Fig. 4.2 illustrates the normalized net energy harvested as a function of power electronic efficiency. Several important trends for the Constant Charge Method are illuminated. First, for large capacitance ratios the normalized net energy is

$$\lim_{R_c \to \infty} N_{Enet} = \eta. \tag{4.16}$$

For the large R_c case, the power electronic efficiency essentially only impacts the energy extracted from the system. Therefore, power electronic efficiency has a minimal impact on the harvesting performance. At high efficiencies and large capacitance ratios, this method can harvest up to 100% of the available energy. For devices with smaller capacitance ratios, the Constant Charge method can still harvest an appreciable amount of power; however, as R_c is reduced, the impact of power electronic efficiency increases.

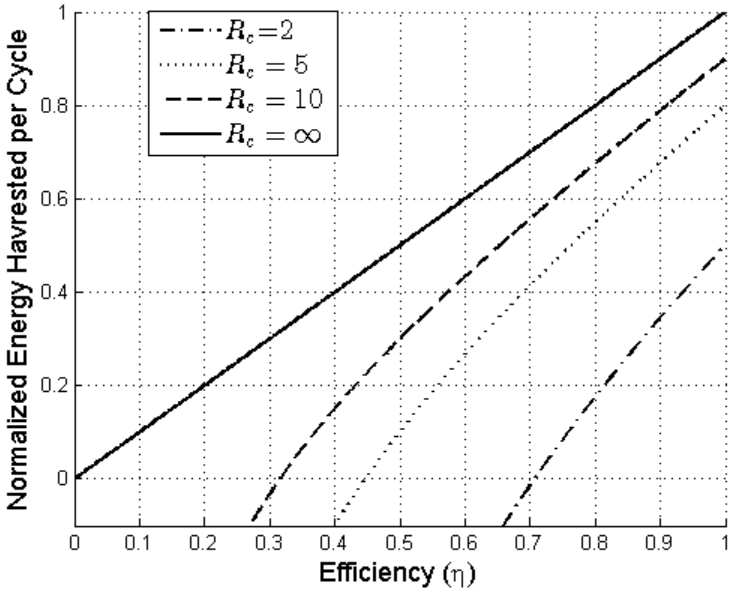

Figure 4.2: Normalized energy harvested, N_{Enet}, using the Constant Charge Method as a function of efficiency, η, for various values of capacitance ratio, R_c.

4.2.3 Charge-Constrained Charge-Pump Theory

The Charge Pump method has both a constant charge and a constant voltage portion as part of its harvesting cycle. The background for this method is presented in Section 2.1.3, and the VQ plot is shown in Fig. 2.6.

The harvesting cycle begins when the device capacitance is at C_{max}, which is concurrent with the maximum charge on the device

$$Q_{max} = C_{max}V_{min}, \tag{4.17}$$

so the energy injected into the device is

$$E_{in} = V_{min}[Q_{max} - Q_{min}]. \tag{4.18}$$

When the device capacitance is C_{min} the charge on the device is minimized

$$Q_{min} = C_{min}V_{max}, \tag{4.19}$$

and the energy extracted from the device is

$$E_{out} = V_{max}[Q_{max} - Q_{min}]. \tag{4.20}$$

Therefore, assuming 100% power electronic efficiency the ideal energy that can be extracted is

$$E_{ideal} = (V_{max} - V_{min})(Q_{max} - Q_{min}). \tag{4.21}$$

As the power electronic efficiency decreases the net energy harvested decreases. To understand this relationship, power electronic efficiency is included in the ideal energy equation to derive the net energy harvested:

$$E_{net} = (Q_{max} - Q_{min}) \left(\frac{\eta Q_{min}}{C_{min}} - \frac{Q_{max}}{\eta C_{max}} \right). \tag{4.22}$$

The net energy equation can be maximized through careful selection of Q_{min}. To derive the optimal Q_{min}:

$$\frac{dE_{net}}{dQ_{min}} = 0, \tag{4.23}$$

and it can be shown that,

$$Q_{min_{opt}} = \frac{Q_{max}}{2\eta} \left[\eta + \frac{1}{\eta R_c} \right]. \tag{4.24}$$

The optimal Q_{min} is a function of power electronic efficiency, and is illustrated in Fig. 4.3 Combining the optimal Q_{min} into the net energy equation and normalizing by the maximum available energy derives the normalized net energy harvested as

$$N_{Enet} = \frac{1}{2} \left[1 - \frac{1}{\eta^2 R_c} \right] \left[\eta - \frac{1}{\eta R_c} \right]. \tag{4.25}$$

The normalized net energy harvested is plotted as a function of power electronic efficiency in Fig. 4.4. At high efficiencies, the Charge-Pump method used on a charge-constrained variable-capacitance devices with large capacitance ratios can harvest up to 50% of the available energy. As long as the power electronic efficiency is high, the capacitance ratio of the device does not significantly alter the normalized net power harvested. However, as the power electronic efficiency is reduced, the impact of the capacitance ratio is much more significant.

The threshold efficiency for the Charge Pump Method is presented in Section 3.2.3. Here it is shown that the threshold efficiency is the square root of the ratio of the maximum voltage to the minimum voltage. This relationship holds for a voltage-

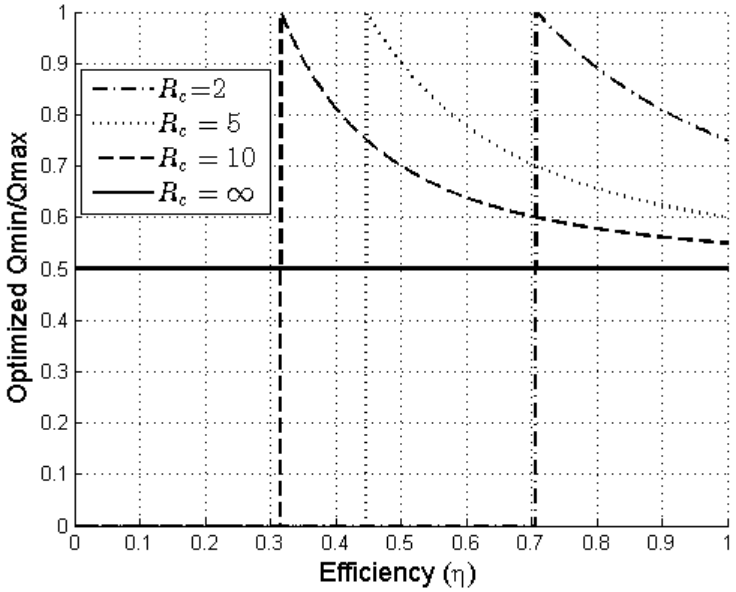

Figure 4.3: The Optimal Q_{min} is plotted as a function of power electronic efficiency for the Charge Pump Method on a charge-constrained device.

constrained implementation; however, it is redefined based on charge:

$$\eta_{thresh} = \sqrt{\frac{V_{min}}{V_{max}}} = \sqrt{\frac{Q_{max}}{Q_{min}R_c}} \tag{4.26}$$

4.2.4 Charge-Constrained Constant Charge with Parallel Capacitance Theory

The CCPC method was developed as a compromise between the Constant Voltage Method and Constant Charge Method of energy harvesting. Including a parallel capacitance allows both the voltage and charge to change on the device as the capacitance declines from C_{max} to C_{min}. This energy harvesting method is described in Section 2.1.2.

When the device is at C_{max}, energy is inserted into both device capacitance and parallel capacitance.

$$E_{in} = \frac{1}{2}(C_{max} + C_p)\frac{Q_{max}^2}{C_{max}^2} \tag{4.27}$$

Once the device reaches C_{min}, energy is extracted from the device:

$$E_{out} = \frac{Q_{max}^2}{2C_{max}^2}\frac{(C_p + C_{max})^2}{(C_p + C_{min})}. \tag{4.28}$$

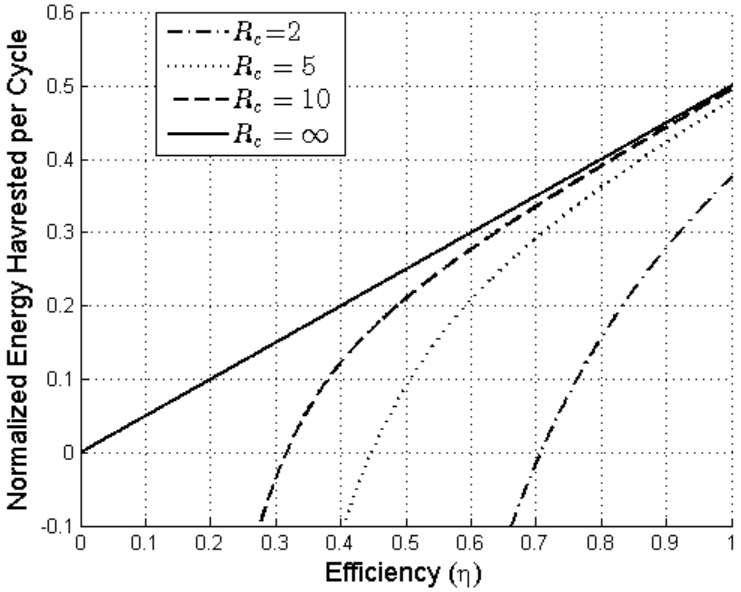

Figure 4.4: Normalized energy harvested, N_{Enet}, using the Charge Pump Method as a function of efficiency, η, for various values of capacitance ratio, R_c.

The net energy harvested is

$$E_{net} = \frac{\eta Q_{max}^2}{2C_{max}^2}\frac{(C_p + C_{max})^2}{(C_p + C_{min})} - \frac{Q_{max}^2}{2\eta C_{max}^2}(C_{max} + C_p). \tag{4.29}$$

To maximize the net energy harvested, C_p should be zero. The CCPC method is therefore not an effective method of energy harvesting for a charge-constrained device. The parallel capacitance increases the input energy into the device, and does not increase the energy harvesting during the cycle. Therefore, this method should not be considered for a charge constrained variable-capacitance device.

4.2.5 Charge-Constrained Constant Voltage with Series Capacitance Theory

A new energy harvesting method is proposed in this section, the Constant Voltage with Series Capacitance (CVSC) Method. The CVSC Method is inspired by the CCPC Method, but modified for charge-constrained devices. A capacitor C_s is connected in series with the variable capacitance device, and the voltage across the series combination is held constant during the harvesting cycle. The resulting voltage versus charge plot is shown in Fig. 4.5. In the analysis of this method it is helpful to

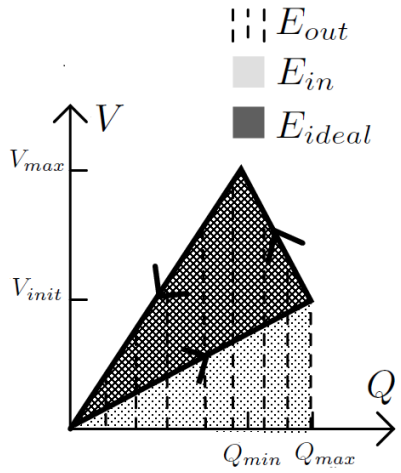

Figure 4.5: Voltage versus charge plot for the Constant Voltage with Series Capacitance Method.

define C^*_{max} as

$$C^*_{max} = \frac{C_{max}C_s}{C_{max} + C_s}, \tag{4.30}$$

and C^*_{min} as

$$C^*_{min} = \frac{C_{min}C_s}{C_{min} + C_s}, \tag{4.31}$$

When the device capacitance is at a maximum the variable-capacitance device and a series connected capacitance C_s are charged to Q_{max}. Therefore the input energy E_{in} is

$$E_{in} = \frac{Q^2_{max}}{2C^*_{max}}. \tag{4.32}$$

As the device capacitance is decreasing, the voltage is held constant across the series combination of C_s and the device. When the device capacitance gets to a minimum energy energy is extracted from the system. The energy extracted from the system is

$$E_{out} = \frac{Q^2_{max}}{C^*_{max}} - \frac{Q^2_{max}C^*_{min}}{2(C^*_{max})^2} \tag{4.33}$$

Incorporating power electronic efficiency, the net energy harvested is

$$E_{net} = \eta\left(\frac{Q^2_{max}}{C^*_{max}} - \frac{Q^2_{max}C^*_{min}}{2(C^*_{max})^2}\right) - \frac{1}{\eta}\left(\frac{Q^2_{max}}{2C^*_{max}}\right) \tag{4.34}$$

The series capacitance C_s can be optimized to maximize the harvested power.

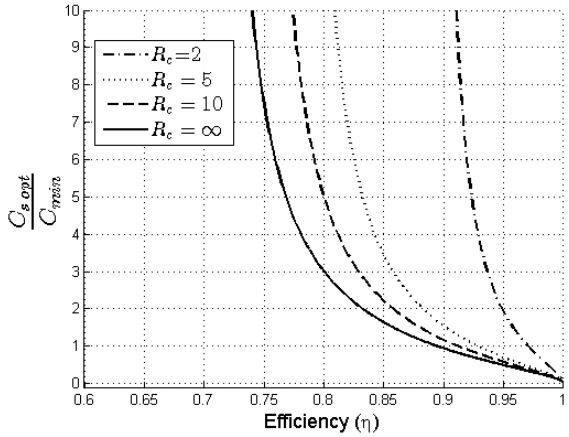

Figure 4.6: The ratio of the optimal C_s to C_{min} for the CVSC Method on gap-closing device is plotted as a function of power electronic efficiency for a variety of capacitance ratios.

The optimal $C_{s\,opt}$ is derived by solving

$$\frac{dE_{net}}{dC_S} = 0, \tag{4.35}$$

for C_s. $C_{s\,opt}$ is derived as a ratio of the maximum capacitance and plotted in Fig. 4.6. At high efficiencies the CVSC Method uses a small series capacitance and the energy harvesting method resembles the Constant Charge Method. As the efficiency declines, $C_{s\,opt}$ gets larger and the energy harvesting method resembles the Constant Voltage Method.

Substituting $C_{s\,opt}$ into (4.34) and normalizing by the maximum energy in the system, the normalized net energy is derived. The normalized net energy harvested using the CVSC Method on a gap-closing device is illustrated in Fig. 4.7.

At high efficiencies the CVSC Method can harvests up to 100% of the available energy; however, as power electronic efficiency declines, the harvested power significantly declines as well. As the efficiency declines the harvested power eventually becomes zero. The threshold efficiency for net positive energy harvesting is

$$\eta_{thresh} = \sqrt{\frac{1}{2 - \frac{C^*_{min}}{C^*_{max}}}}. \tag{4.36}$$

As the capacitance ratio gets large, the threshold efficiency approaches

$$\lim_{R_c \to \infty} \eta_{thresh} = 71\%. \tag{4.37}$$

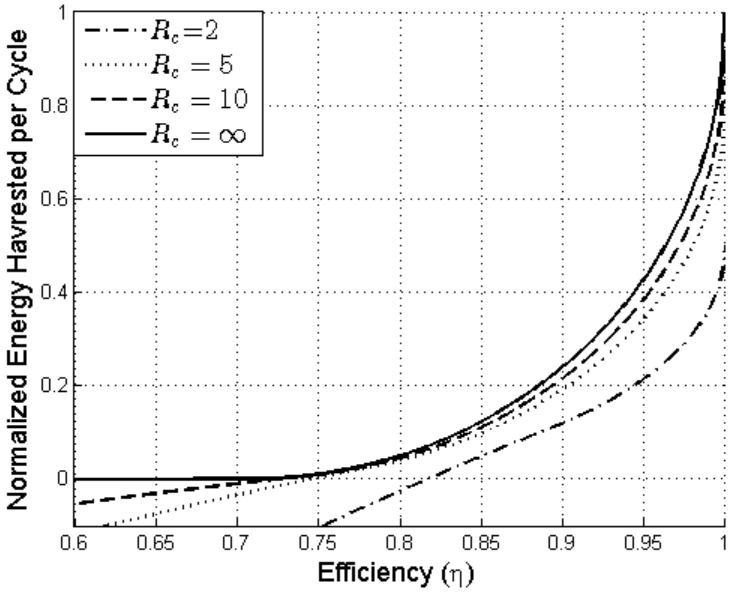

Figure 4.7: The normalized net for the CVSC Method on gap-closing device energy is plotted as a function of power electronic efficiency for a variety of capacitance ratios.

4.3 Energy Harvesting Methods for Gap-Closing Versus Area-Overlap Variable-Capacitance Devices

The energy harvesting methods for gap-closing and area-overlap type variable-capacitance devices are compared in this section. In general, the energy density of gap-closing devices and area-overlap devices are roughly the same [49], so the normalization factor used to compute N_{Enet} for both devices is the same. Harvesting methods and devices can be compared directly by the normalized net energy harvested. In Fig. 4.8 the normalized energy harvested for each method on each type of device is plotted as a function of power electronic efficiency. The plots on the left are for area-overlap devices, where the maximum voltage is constrained, and the plots on the right are for gap-closing devices, where the maximum charge is constrained.

At high power electronic efficiencies, the Constant Voltage Method has a normalized net energy of 1 for an area-overlap devices, while for gap-closing devices the Constant Charge Method has a normalized net energy of 1. Both of these systems can therefore harvest 100% of the available power. Assuming the devices have the same energy density, the Constant Voltage Method used on an area-overlap device can harvest the same amount of energy as the Constant Charge Method on a gap-closing device, independent of the capacitance ratio. However, as efficiency decreases the harvested energy using the Constant Voltage Method on an area-overlap device

decreases significantly more rapidly. The threshold efficiencies are independent of the constraint applied to the harvesting method, so, as discussed in Chapter III, the energy harvested by the Constant Charge Method is less impacted by power electronic efficiency.

The Charge-Pump method harvests up to 50% of the available power at high power electronic efficiencies independent of the constraint applied. The impact of power electronic efficiency on this method for the gap-closing devices and area-overlap devices is different. This is because the optimal harvesting conditions are affected differently by the two constraints. As the efficiency declines, the normalized power harvested using a gap-closing device is significantly more than for an area-overlap device. For example, if the efficiency of the power electronics is 85%, the gap-closing device can harvest 1.37 times more energy.

The CCPC Method should only be applied to area-overlap devices, while the CVSC Method should only be applied to gap-closing devices. The CCPC Method on an area-overlap device can harvest energy over a wider efficiency range than the CVSC Method, which can only harvest energy when the power electronic efficiency exceeds 71%. However, at practical power electronic efficiencies, both methods are outperformed by the Constant Charge Method on a gap-closing device and by the Constant Votlage Method on an area-overlap device.

Assuming ideal power electronics, viable harvesting methods can be selected for both the gap-closing devices and the area-overlap devices. However, when considering the constraints applied to the energy harvesting methods by the different types of devices it is shown that gap-closing devices harvest more energy at practical power electronic efficiencies.

In some energy harvesting applications, embedding the power electronics and energy harvesting systems into a single chip may be important. For this case, the Charge Pump Method should be selected because it requires only requires the dc-dc converter to transfer energy between fixed voltages, so switched-capacitor topologies (which can be integrated onto a chip) can be used.

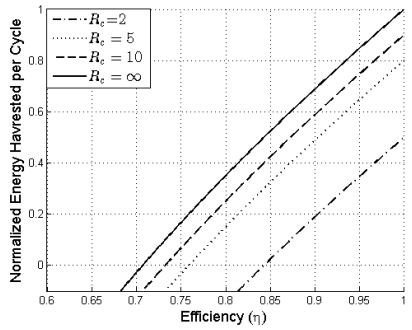

(a) CV Method - Voltage Constraint

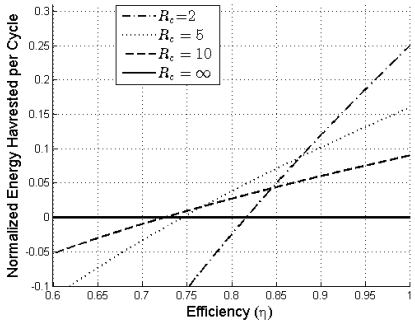

(b) CV Method - Charge Constraint

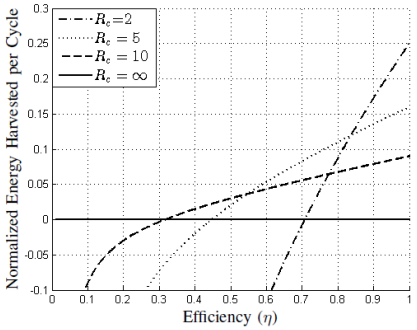

(c) CC Method - Voltage Constraint

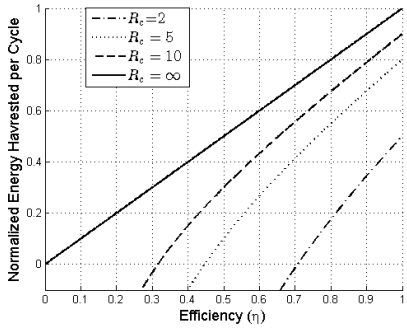

(d) CC Method - Charge Constraint

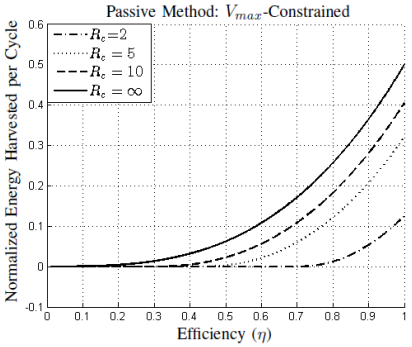

(e) Charge Pump - Voltage Constraint

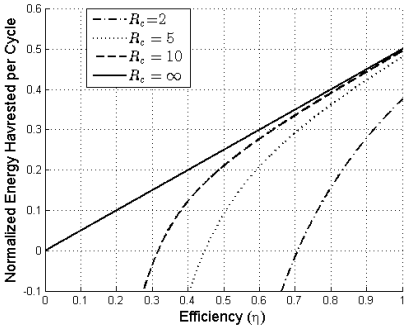

(f) Charge Pump - Charge Constraint

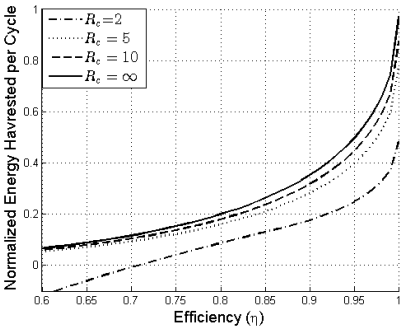

(g) CCPC Method - Voltage Constraint

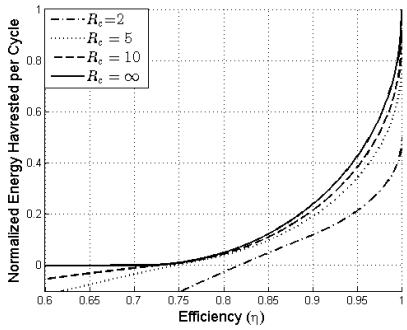

(h) CVSC Method - Charge Constraint

Figure 4.8: A comparison of the normalized energy harvested using the various methods on a area-overlap device (voltage-constrained) and a gap-closing device (charge-constrained) .

4.4 Discussion

In this section a case study is used to compare energy harvesting methods on a practical gap-closing and area-overlap device. Two energy harvesting devices are proposed based on the device parameters presented in [36]. The device presented in [36] is an area-overlap device, which is therefore voltage-constrained. Based on the assumption in [49] that area-overlap and gap-closing devices have similar energy densities, a gap-closing version of the device is proposed. Both devices, whose parameters are shown in Table 4.1, have the same maximum capacitance, minimum capacitance, and energy density as the device in [36].

4.4.1 Case Study - Large R_c Gap-closing versus Area-overlap Device

The best energy harvesting system is designed by selecting the energy harvesting device architecture and method that maximizes the harvested power at practical power electronic efficiencies. Considerations such as capabilities of the energy harvesting method, power consumption of the control circuit, and ability to integrate into microsystems are also considered. The net energy harvested for each applicable method to the large R_c gap-closing device and large R_c area-overlap device is illustrated as a function of power electronic efficiency in Fig. 4.9.

Table 4.1: Large R_c device properties for gap-closing and area-overlap devices assuming equal energy density.

Parameter	**Value**
Allowable Q_{max} (gap-closing)	183.1 pC
Allowable V_{max} (area-overlap)	8 Volts
C_{max}	260 pF
C_{min}	2 pF
Frequency	252 Hz

The net energy harvested from the gap-closing and area-overlap large R_c device elucidates similar trends as the normalized net energy plots discussed in Section 4.3. The Constant Charge Method on the gap-closing device harvests the most amount of power at practical power electronic efficiencies. Over an efficiency range of $80\% - 90\%$ the Constant Charge Method on a gap-closing device harvests at-least 1.37 times as much power as the next best device-method combination.

Despite the power gains elucidated in Fig. 4.9 some challenges must be overcome in order to make this method viable:

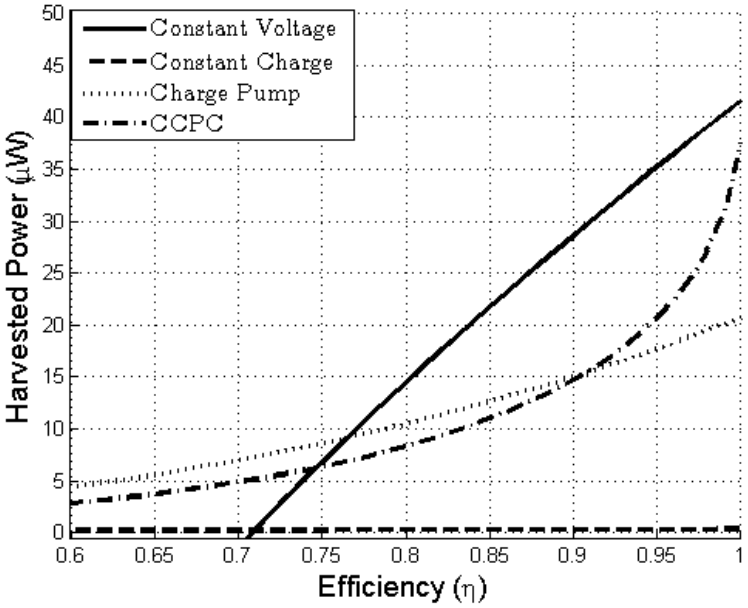

(a) Voltage Constraint

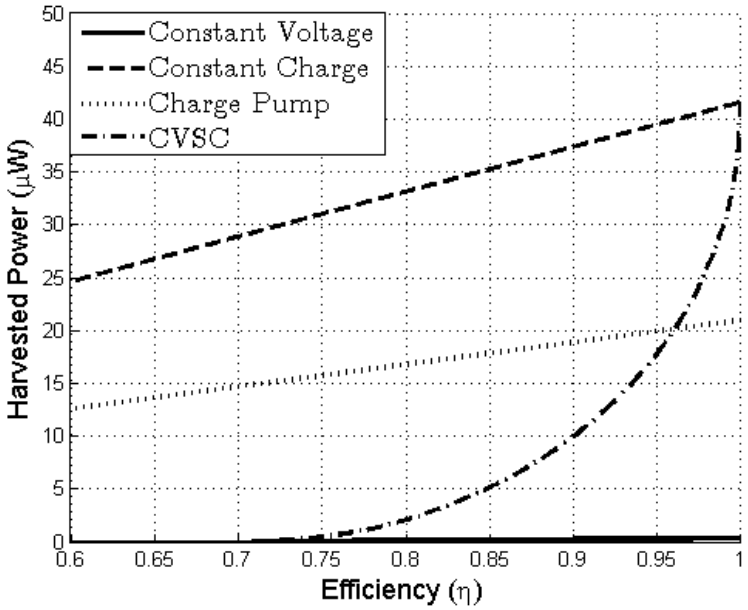

(b) Charge Constraint

Figure 4.9: The harvested power is plotted as a function of power electronic efficiency for each of the harvesting methods applied to an area-overlap device (shown on top) and a cap-closing device (shown on bottom).

- losses in the controller that implements the method must be significantly small
- efficient power electronics must be created to implement the energy harvesting method
- power electronics and variable-capacitance device must be able to withstand the resulting maximum voltage

4.4.1.1 Constant Charge Control Methodology

The Constant Charge Method on a gap-closing device requires a controller witch knowledge of the state of the variable-capacitance device. Such a controller was conceived in both [36] and [64]. The power consumption of the state detector and controller in [36] was reported to consume $3\mu W$. For the proposed energy harvesting device the power consumption of the controller does not dictate a change in energy harvesting method. However, for an energy harvesting device where the power consumption of the controller is large compared to the power harvested, the Charge Pump Method on a gap-closing device should be considered because it utilizes a passive control scheme, eliminating the need for a state detector.

4.4.1.2 Constant Charge Power Electronics

An implementation of the CCPC Method in [36] presents a circuit which could be effectively used for the Constant Charge Method as long as C_p is removed. This circuit, pictured in Fig. 4.10, uses a resonant inductor to charge and discharge the variable capacitance device, and is discussed in detail in [36].

4.4.1.3 Large Device Voltages

To implement the Constant Charge Method on a gap-closing device, the maximum allowable charge is inserted into the energy harvesting device when the device capacitance is at C_{max}. As the device capacitance is reduced, the voltage on the device increases. Once the device capacitance reaches C_{min} the voltage on the variable capacitance device is

$$\frac{Q_{max}}{C_{min}} = 91.2\ Volts. \tag{4.38}$$

Other implementations of the Constant Charge Method in [10, 39, 60] also see large maximum voltages.

Although these large maximum voltages do not cause the pull-in effect, they still posses some challenges:

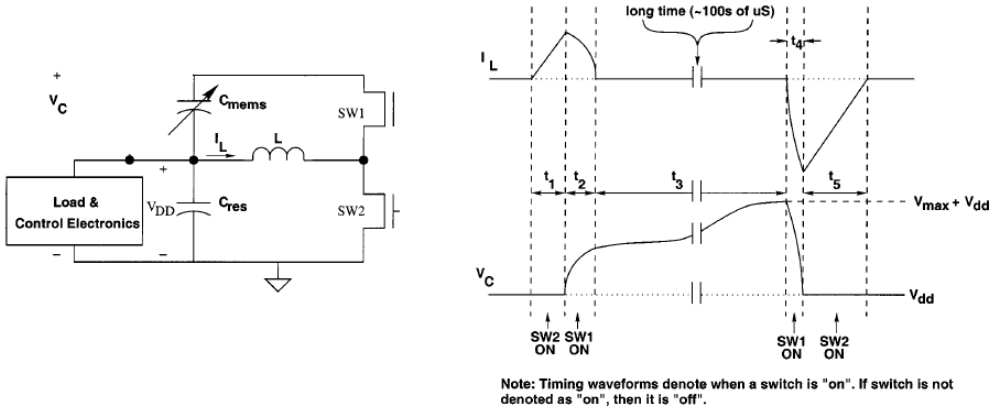

Figure 4.10: Circuit topology and theoretical waveforms for implementing the Constant Charge Method [36]

- A specialized process must be used to withstand such extreme voltages in the circuitry. For example, silicon on insulator is a process which could withstand the proposed voltage, but the cost of using such a process is significantly more than the standard CMOS process [64].
- The power electronics must be able to efficiently interface large voltage differentials between the device and the energy storage element. Typically larger voltage differentials lead to less efficient power electronics.

Despite the challenges presented by the large maximum device voltage, the benefits of the Constant Charge Method on a gap-closing device suggest the importance of continued academic pursuit of this energy harvesting system.

4.4.2 Voltage and Charge Constraints on a Gap-Closing Device

In practical applications of the Constant Charge Method on a gap-closing variable-capacitance device, it is possible that both the maximum voltage and the maximum charge should be constrained. For a gap-closing device the maximum charge on the device is constrained by the pull-in effect, and the maximum voltage on the device could be constrained by the process that creates the device or the power electronics which implement the energy harvesting method. In order to meet both constraints a new energy harvesting method is proposed, the Voltage and Charge Constrained (VCC) Method.

The VCC Method charges the gap-closing device to Q_{max} when the device capac-

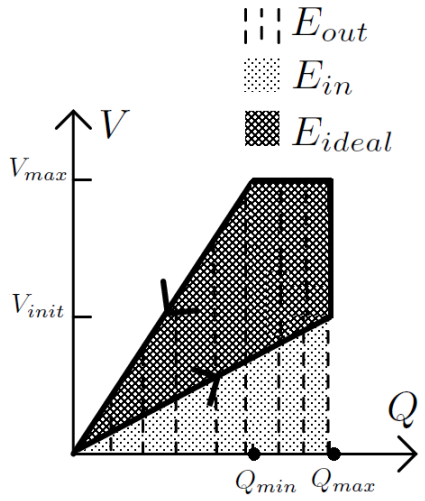

Figure 4.11: The voltage versus charge is shown for the Voltage and Charge Constrained Method of energy harvesting

itance is at a maximum. Therefore the electrical energy into the system is

$$E_{in} = \frac{Q_{max}^2}{2C_{max}}. \tag{4.39}$$

The device is then open-circuited, so as the device capacitance declines the voltage on the device increases. Once the voltage on the device reaches the maximum allowable voltage V_{max}, the device is clamped to V_{max} until the device capacitance reaches C_{min}. When the device reaches C_{min} energy is extracted from the system. The energy taken out of the device is

$$E_{out} = \frac{V_{max}^2 C_{min}}{2} + (Q_{max} - Q_{min})V_{max}. \tag{4.40}$$

The resulting voltage versus charge plot for the VCC Method is illustrated in Fig. 4.11.

A new factor K is introduced to simplify the net energy and normalized net energy equations. K is the ratio of the unconstrained maximum voltage V_{max}^* in the system to the constrained maximum voltage V_{max}.

$$K = \frac{V_{max}^*}{V_{max}} = \frac{Q_{max}}{C_{min}V_{max}} = \frac{Q_{max}R_c}{C_{max}V_{max}} \tag{4.41}$$

The constrained maximum voltage V_{max} is

$$V_{max} = \frac{Q_{max}R_c}{C_{max}K}. \tag{4.42}$$

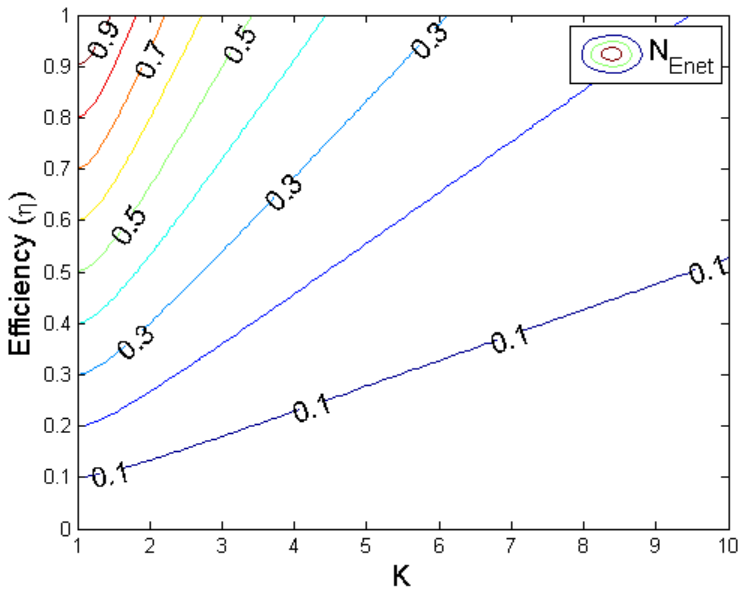

Figure 4.12: The normalized net energy harvested is plotted as a function of both power electronic efficiency and K for a variable-capacitance device with a large capacitance ratio ($R_c \to \infty$).

Therefore the net energy equation is derived in terms of K, Q_{max}, C_{max},C_{min}, and η:

$$E_{net} = \eta \left[\frac{Q_{max}^2 R_c}{C_{max} K} - \frac{Q_{max}^2 R_c^2 C_{min}}{2K^2 C_{max}^2} \right] - \frac{Q_{max}^2}{2\eta C_{max}} \tag{4.43}$$

The net energy equation is normalized by the maximum possible energy in the electrical system when K is equal to 1, which is

$$\frac{Q_{max}^2}{2C_{min}}. \tag{4.44}$$

The normalized net energy harvested is

$$N_{Enet} = \eta \left[\frac{2}{K} - \frac{1}{K^2} \right] - \frac{1}{\eta R_c} \tag{4.45}$$

The impact of constraining the maximum voltage can therefore be elucidated by plotting the normalized net energy harvested as a function power electronic efficiency and K. This is shown for devices with a large capacitance ratio in Fig. 4.12.

The threshold efficiency required for net positive energy harvesting is effected by

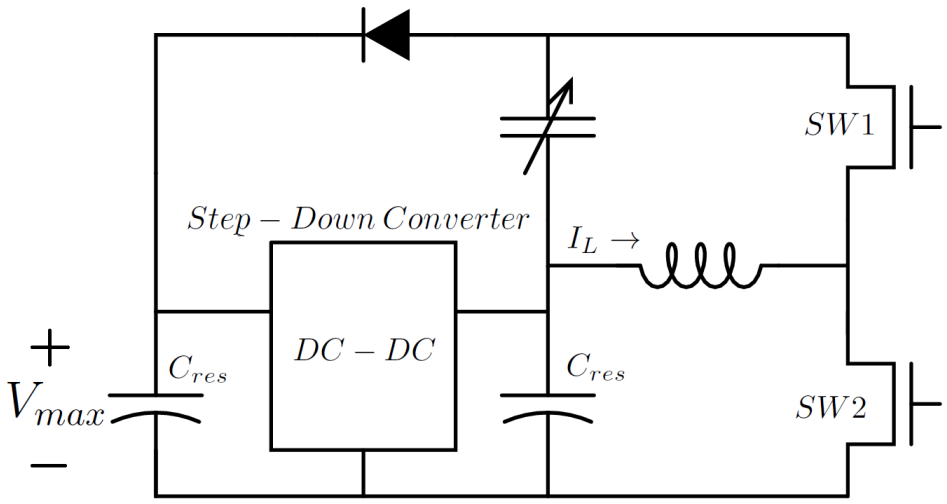

Figure 4.13: Proposed circuit topology that implements the Voltage and Charge Constrained Method.

addition of the voltage constraint. The threshold efficiency for the VCC Method is

$$\eta_{thresh} = \sqrt{\frac{1}{R_c[\frac{2}{K} - \frac{1}{K^2}]}} \tag{4.46}$$

A possible implementation of the VCC Method can be created through a modification of the circuit topology presented for the Constant Charge Method in Fig. 4.10. A diode connects a large capacitor, which is charged to V_{max}, to the variable capacitance device. When the voltage on the variable-capacitance reaches V_{max}, the diode begins to conduct and the device voltage is clamped. A hysteresis controller connected to a DC-DC converter is used to maintain the voltage at V_{max}. This circuit topology is depicted in Fig. 4.13.

4.5 Conclusion

In this chapter, gap-closing and area-overlap variable-capacitance devices are compared based on their energy harvesting capabilities. It is claimed in [49, 64] that these devices have similar energy densities despite different constraints. In order to avoid the pull-in effect on the fingers of the variable-capacitance device, the maximum charge is constrained for gap-closing devices, and the maximum voltage is constrained for area-overlap devices. The constraints placed on the energy harvesting methods by these devices affect the energy harvesting capabilities of harvesting methods.

This work elucidates the advantages of gap-closing devices by including power

electronic efficiency as a parameter in the analysis of the harvesting methods for both device architectures. It is shown, that at high power electronic efficiencies, an area-overlap device using the Constant Voltage Method or CCPC Method can harvest the same amount of energy as a gap-closing device using the Constant Charge Method or the CVSC Method. However, at practical power electronic efficiencies(80-85%) the Constant Charge Method on a gap-closing device harvests more than 1.6 times the power of any harvesting method. A case study using practical device parameters illustrates the benefits and challenges associated with implementing the Constant Charge Method on a gap-closing device. The biggest challenge to overcome is the large voltages associated with the method. To mitigate this, a new energy harvesting method is proposed that constrains both the maximum voltage on the device and the maximum charge. This new method helps engineers get the benefits associated with the Constant Charge Method on a gap-closing device, while adapting to practical constraints.

Acknowledgment

Akshay Sarin (akisarin@umich.edu) contributed to this chapter of the dissertation by assisting in: the derivation of the charge-constrained energy harvesting equations, deriving inferences, and producing graphics to illustrate key concepts.

CHAPTER V

Autonomous Wideband Piezoelectric Energy Harvesting

5.1 Introduction

The Dynamic Active Energy Harvesting (DAEH) method, discussed in Section 2.2.4, describes a method that seeks to extend the energy harvesting bandwidth of the system in order to mitigate the impact of deviations between the mechanical resonant frequency and the vibration frequency. Using the dynamic active energy harvesting (DAEH) approach, [31] harvested up to 6 times as much energy at off-resonant frequencies when compared to the adaptive rectifier technique introduced in [40].

The benefits of DAEH method were experimentally validated by [31]. However, the implementation was not an autonomous system, and the bandwidth improvements were modest due to the efficiency of the power electronics. The PWM full-bridge inverter, MOSFET gate drive, control circuitry, microcontroller, and phase detection power consumption exceeded that of the energy harvested, questioning the practical viability of the method. In this chapter, a resonant full-bridge inverter topology is presented which, in combination with low-power analog control circuitry and low frequency digital control, reduces the energy loss such that the practical benefits of the method can be realized. This work presents the first experimental implementation of the dynamic active energy harvesting method that has net positive energy harvesting, making it a wideband autonomous energy harvesting system.

5.2 The Dynamic Active Energy Harvesting Method

The DAEH method presented in [31], and discussed in Section 2.2.4, seeks to apply the optimal load impedance to the piezoelectric device. It is assumed that the vibration source applies a sinusoidal force to the piezoelectric device. The optimal load impedance would have a sinusoidal voltage across it, whose magnitude is

$$V_{mag} = \sqrt{\omega^2 b^2 + (k - \omega^2 m)^2} \frac{F_m}{2kd\omega b}, \tag{5.1}$$

and phase relative to the input force is

$$\phi = 180^\circ - \tan^{-1}\left(\frac{k - \omega^2 m}{\omega b}\right). \tag{5.2}$$

Practical implementations of this method use a square wave voltage that matches the fundamental magnitude and frequency of the optimal sinusoid [31]. The optimal load impedance has a reactive component that increases as the source excitation frequency deviates from the mechanical resonant frequency. The inverter must therefore process both reactive and real power, so as the ratio of reactive power to real power increases at off-resonant frequencies, the impact of the inverter's power path efficiency increases. It is important to note that, in practice, the efficiency of the power electronics will decrease at lower power factors. At off-resonant frequencies the power-path efficiency of the resonant inverter significantly affects the net harvested power. Using experimental device parameters from this work (shown in Table 5.1), the effects of the power electronic's power-path efficiency on the DAEH method are shown in Fig. 5.1.

Table 5.1: Volture V20w Piezoelectric Energy Harvesting System Parameters

Parameter	**Value**
Mass (m)	6.7g
Force Magnitude (F_m)	0.218N
Spring constant (k)	$3113\frac{N}{m}$
Damping coefficient (b)	$.4960\frac{N*s}{m}$
Zero-strain capacitance (C')	$.114\mu F$
Piezoelectric coupling (d)	$1.39\frac{\mu m}{v}$
Mechanical excitation period (T_m)	$8.23 \leftrightarrow 10ms$

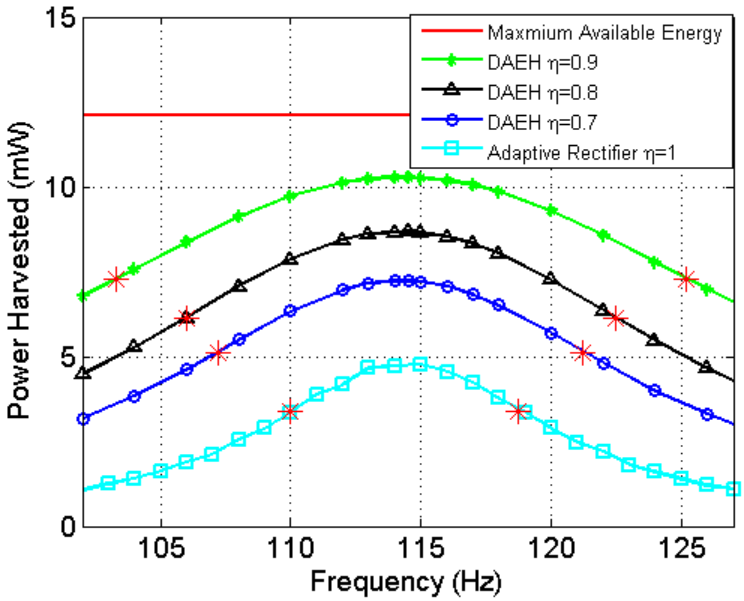

Figure 5.1: The theoretical power harvested using the adaptive rectifier and the DAEH method is plotted as a function of excitation frequency for various power electronic efficiencies. As the excitation frequency deviates from the mechanical resonant frequency, the impact of power-path circuit efficiency on energy harvesting increases. [31]

5.3 Resonant Inverter

To efficiently implement the square wave required by the DAEH method, a resonant full-bridge inverter is used as depicted in Fig. 5.2. The proposed resonant inverter creates an efficient power electronic interface between the piezoelectric device and the bus capacitance. The resonant inverter is controlled such that the magnitude and the phase of the applied square wave can be modulated while undergoing only four switching transitions per voltage inversion. Unlike previous implementations, which used pulse-width-modulation (PWM) to transition the piezoelectric device voltage between $+V_{bus}$ and $-V_{bus}$ [12, 27, 30, 31], the proposed inverter topology uses the resonance of the piezoelectric capacitance (C') in combination with the inductance (L) to achieve the voltage transition. The resonant inverter utilizes the advantage of the SSHI method, using resonance to invert the piezoelectric voltage, while still providing a bi-directional converter capable of implementing the DAEH method. By drastically reducing the number of switching events required to transition the piezoelectric voltage, the resonant inverter topology nearly eliminates switching and gating losses. The resulting improvement in efficiency is one of the major reasons the autonomous

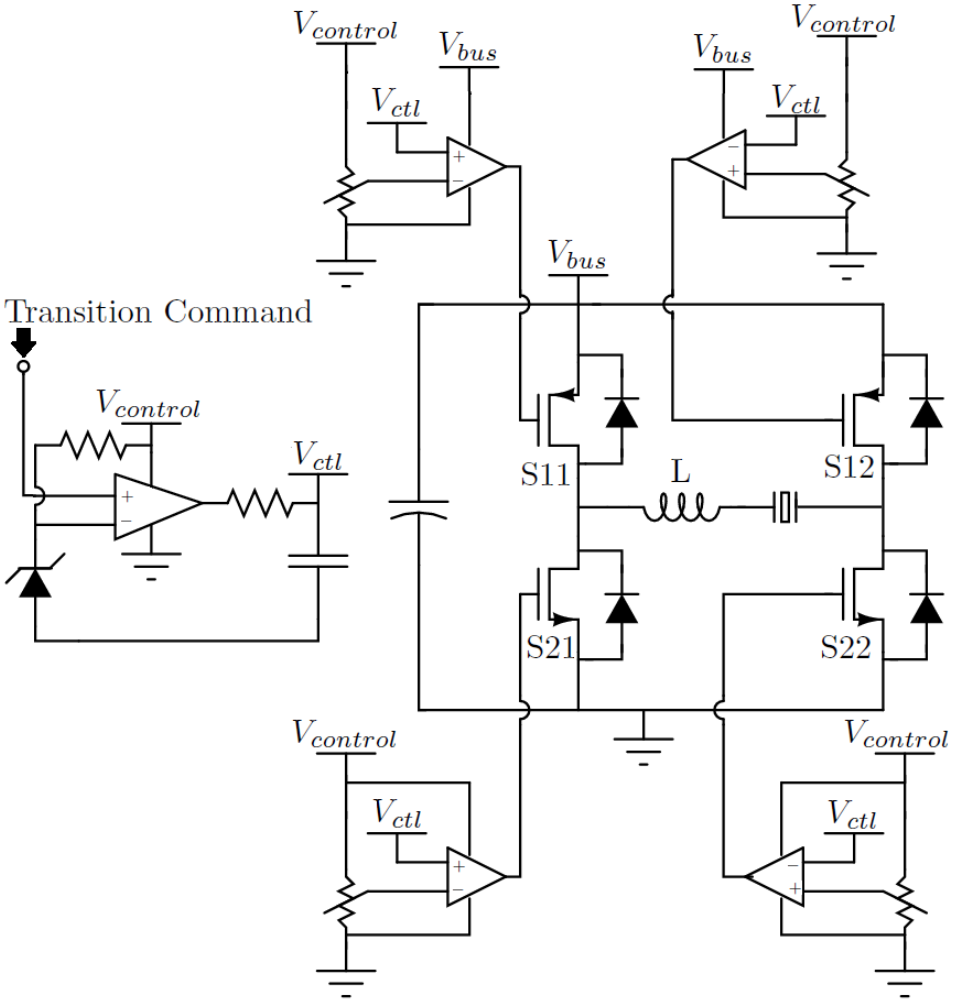

Figure 5.2: Proposed resonant full-bridge inverter for dynamic active energy harvesting.

wideband energy harvester is feasible.

5.3.1 The Resonant Transition

The proposed circuit topology inverts the piezoelectric device voltage while undergoing four switching transitions, which results in five circuit states. These states are exhibited in Fig. 5.4. To understand the resonant transition, an example voltage inversion is described.

Initially the piezoelectric device voltage is equal to V_{bus} because MOSFETs S_{11} and S_{22} are ON, while MOSFETs S_{12} and S_{21} are OFF, as portrayed in Fig 5.4a. Turning S_{11} OFF (Fig. 5.4b) and then S_{21} ON (Fig. 5.4c) initiates a resonant transition between L and C'. Once the voltage across C' reaches its minimum and the inductor current returns to zero, switch S_{22} is opened (Fig. 5.4d), ending the resonant transition. The resulting voltage and current on the piezoelectric device are shown in Fig. 5.3. At the end of the resonant transition, the resulting voltage on the device, $-V_x$, is dependent on the quality factor (Q_f) of the resonant transition:

$$V_x = V_{bus}^2 \sqrt{1 - \frac{\pi}{Q_f}}, \tag{5.3}$$

where the quality factor Q_f is determined by the energy lost energy lost during the resonant transition (E_{res}):

$$Q_f = \frac{\pi C' V_{bus}^2}{2E_{res}}. \tag{5.4}$$

Two methods of changing the device voltage from $-V_x$ to $-V_{bus}$ are proposed in Section 5.3.2.

5.3.2 Incomplete Voltage Inversion

The difference between the magnitude of the device voltage and bus voltage at the end of the resonant transition must be dealt with. Two methods for transitioning the device voltage to the bus voltage after the resonant transition are:

- clamping the device and inductor to the bus voltage (shown in Fig. 5.5)
- using the piezoelectric effect to charge the device capacitance until its voltage reaches the bus voltage (shown in Fig. 5.6).

The effectiveness of each method is determined by the amount of energy that can be harvested from the piezoelectric device. During a half-cycle of the mechanical

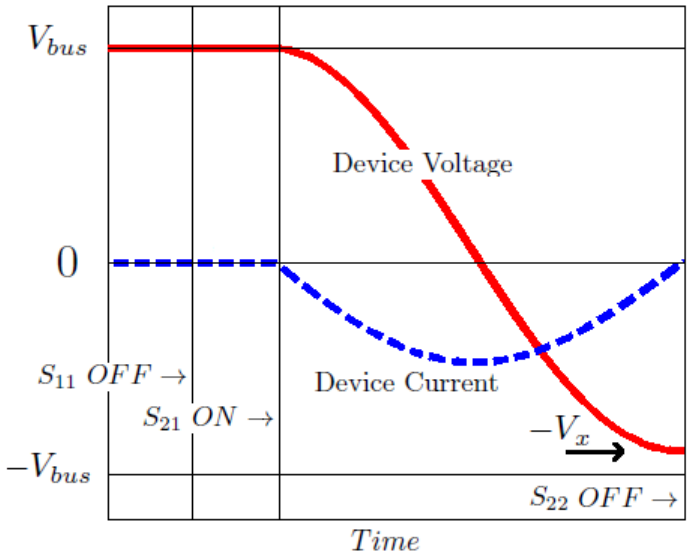

Figure 5.3: The piezoelectric device voltage and current during a resonant voltage inversion.

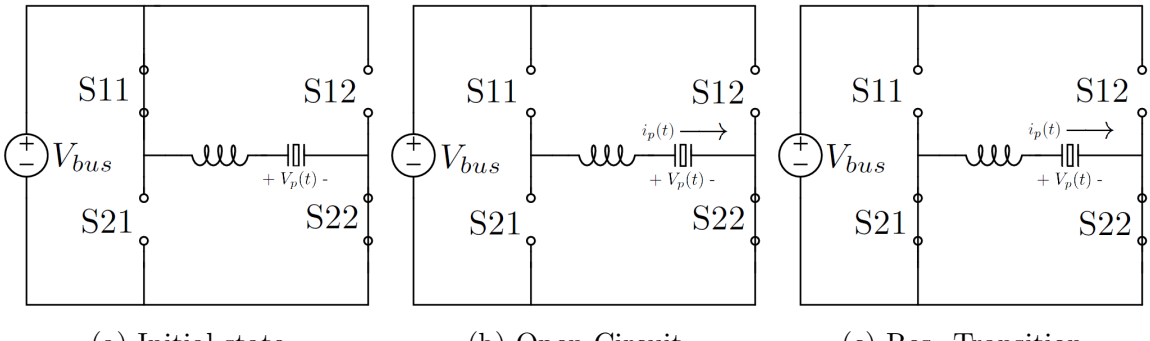

(a) Initial state (b) Open Circuit (c) Res. Transition

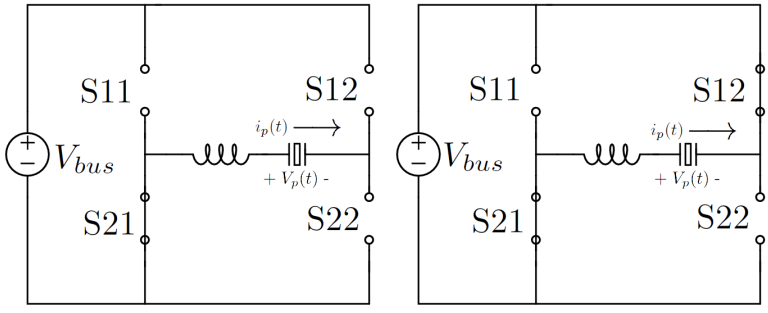

(d) Open Circuit (e) Final State

Figure 5.4: Required states for transitioning the piezoelectric device between the positive bus voltage and the negative bus voltage. To transition the device voltage between the negative bus voltage and the positive bus voltage, the states occur in reverse order.

oscillation, the maximum energy that can be harvested, E_{ideal}, is determined by V_{bus} and the device current, $i_p(t)$. The available energy is

$$E_{ideal} = V_{bus} \left\| \int_0^{\frac{Tm}{2}} i_p(t)dt \right\| = V_{bus} Q_{ideal}. \tag{5.5}$$

The energy lost by either method is dependent on the magnitude of the voltage on the piezoelectric device at the end of the resonant transition, V_x.

5.3.2.1 Clamping

Clamping the piezoelectric device and resonant inductor to the bus voltage causes the piezoelectric device voltage to be a decaying oscillation centered around V_{bus}, as shown in Fig. 5.5. The energy extracted from the bus voltage during clamping, E_{ext}, is

$$\begin{aligned} E_{ext} &= \int V_{bus} dq = V_{bus} \int_{V_x}^{V_{bus}} C' dV_p \\ &= C' V_{bus}^2 \left(1 - \sqrt{1 - \frac{\pi}{Q_f}} \right). \end{aligned} \tag{5.6}$$

After clamping the total energy (E_{ideal}) is harvested from the device. Therefore if the device is clamped to the bus capacitance, the net energy harvested to the bus, E_{clamp}, is

$$\begin{aligned} E_{clamp} &= E_{ideal} - E_{ext} \\ &= V_{bus} Q_{ideal} - C' V_{bus}^2 \left(1 - \sqrt{1 - \frac{\pi}{Q_f}} \right). \end{aligned} \tag{5.7}$$

5.3.2.2 Piezoelectric Effect

Using the piezoelectric effect to charge the piezoelectric device voltage to the bus voltage also reduces the amount of energy that can be harvested. During the charging interval (t_{pe}), the amount of charge supplied by the piezoelectric device, Q_c, to charge the device capacitance from V_x to V_{bus} is

$$Q_c = C'(V_{bus} - V_x). \tag{5.8}$$

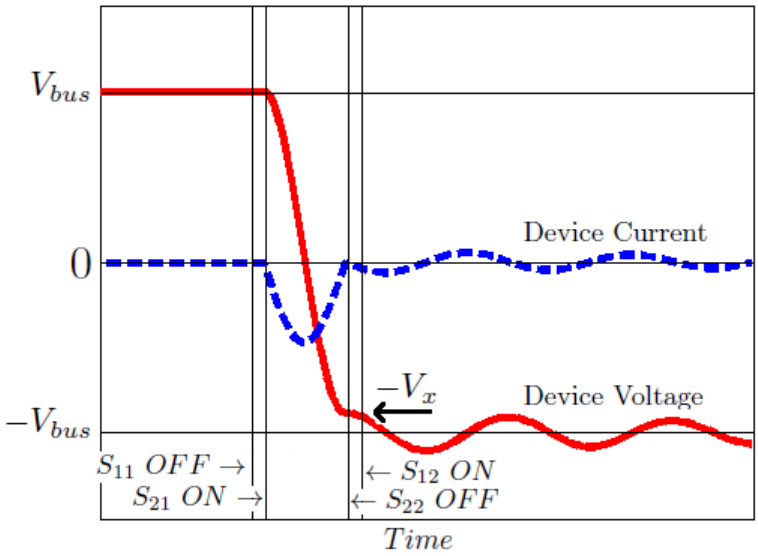

Figure 5.5: The piezoelectric device voltage and current waveforms due to clamping after the resonant transition.

This charge must be subtracted from the ideal harvested charge; therefore, the energy that can be harvested while using the piezoelectric effect for charging, E_{pe}, is

$$E_{pe} = V_{bus}(Q_{ideal} - Q_c)$$
$$= V_{bus}Q_{ideal} - C'V_{bus}^2\left(1 - \sqrt{1 - \frac{\pi}{Q_f}}\right). \tag{5.9}$$

5.3.2.3 Comparison

The energy harvested when clamping the device, E_{clamp}, is the same as when using the piezoelectric effect to charge the device, E_{pe}. Therefore, the best method for railing the device voltage after the resonant transition is based on the implementation of the method rather than the method itself. In order to reduce the complexity of the switch timing, the clamped method was used.

At low quality factors, the energy lost during clamping is larger than the energy lost during the resonant transition. However, as the quality factor becomes large, the energy lost during the resonant transition becomes equivalent to the energy lost during clamping. This relationship is illustrated in Fig. 5.7.

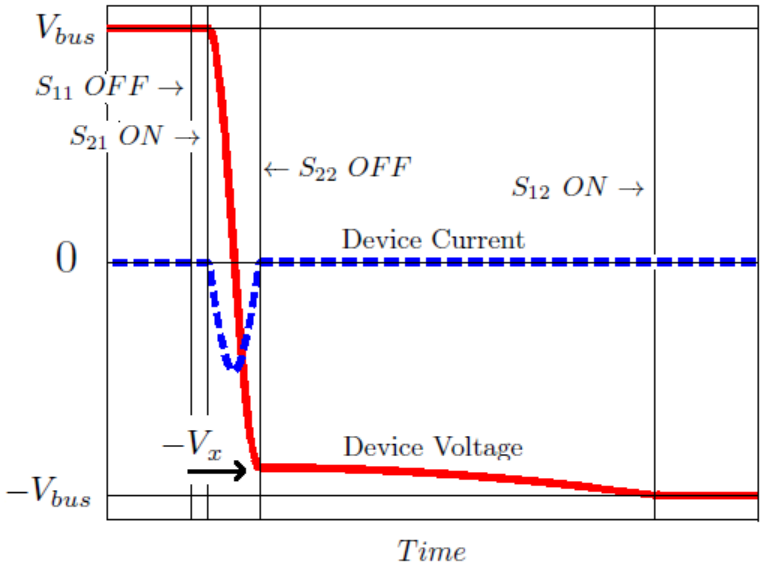

Figure 5.6: The piezoelectric device voltage and current waveforms when using the piezoelectric effect to charge the device capacitance after the resonant transition.

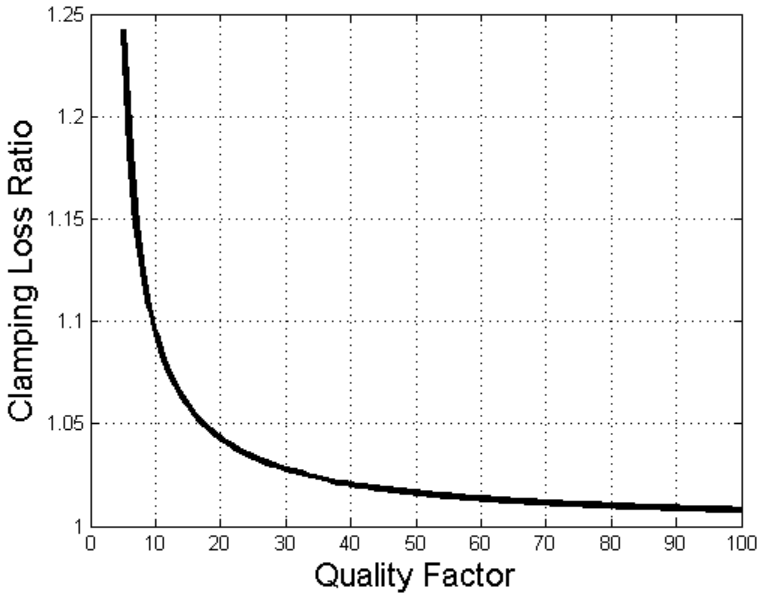

Figure 5.7: The ratio of clamping losses to resonant transition losses is plotted as a function of the quality factor of the resonant system.

5.3.3 MOSFET Timing

A practical implementation of the resonant inverter requires control over both the order of the switching and the timing associated with it. To achieve this a transition command signal is connected to a nanowatt comparator, which drives an RC circuit between 0 and $V_{control}$. As the voltage rises or declines across the capacitor in the RC circuit, it is compared to reference voltages associated with the proper switching order, as shown in Fig. 5.2. The switching order is symmetrical, so a single threshold for each switch will allow the inverter to reach both states.

The RC circuit is responsible for more than just the switch modulation order, it also must control the resonant transition. The time the circuit should be in the resonant state, shown in Fig. 5.4c, is half of the resonant period, and must be the same independent of whether the RC network is charging or discharging. In order to accomplish this, the threshold voltages for S_{21} and S_{22} are chosen symmetrically on either side of $\frac{V_{control}}{2}$:

$$V_{S21} = \frac{V_{control}}{2} - \frac{V_{control}(e^{\frac{\pi\sqrt{LC'}}{RC}} - 1)}{2(e^{\frac{\pi\sqrt{LC'}}{RC}} + 1)} \tag{5.10}$$

and

$$V_{S22} = \frac{V_{control}}{2} + \frac{V_{control}(e^{\frac{\pi\sqrt{LC'}}{RC}} - 1)}{2(e^{\frac{\pi\sqrt{LC'}}{RC}} + 1)}. \tag{5.11}$$

Unlike S_{21} and S_{22}, the timing of S_{11} and S_{12} do not effect the resonant transition; however, to minimize losses they should be switched immediately before and after the resonant transition. As discussed in section 5.3.2.3, either clamping or using the piezoelectric effect to charge the device capacitance after the resonant transition results in the same amount of harvested power. However, using the RC network to control the MOSFET timing means that, if clamping is delayed (Fig. 5.4d), then when the transition command triggers the next voltage inversion there will be a delay once the inverter is open-circuited (Fig. 5.4b). During this time the piezoelectric effect will start to discharge the piezoelectric capacitance. This reduces the effectiveness of the resonant transition and therefore should therefore be avoided.

5.4 Circuit Control

Implementing the DAEH method requires control over the phase and the magnitude of the applied square wave with respect to the applied force. Previous imple-

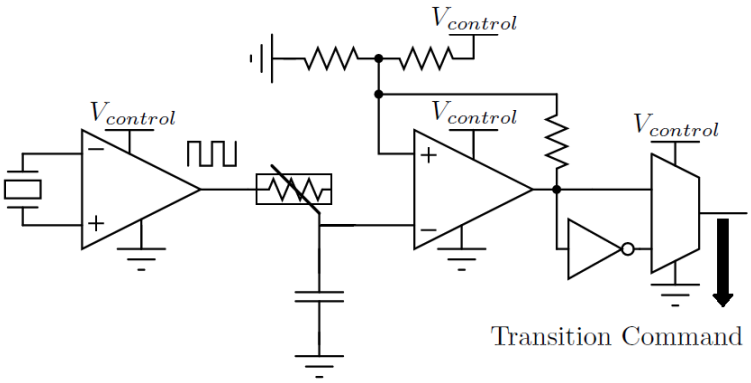

Figure 5.8: The phase control circuit detects the zero-crossings of the base acceleration and generates the transition command signal by applying the appropriate phase shift. The power consumption of this circuit is less than 15μW, while greatly reducing the computation demand of the microprocessor by accomplishing a high-frequency task.

mentations relied on high-power digital circuitry to achieve the required control. In order to achieve an autonomous energy harvesting system, a reduction of the digital computation demand was achieved by implementing high-frequency (e.g., greater than 5Hz) tasks with low-power analog circuitry.

5.4.0.1 Phase Control

In practice, the phase of the resonant inverter is adjusted relative to the zero crossing of the base mechanical acceleration. A low-power acceleration polarity detector was created using a sense-piezoelectric device. The sense-piezoelectric device is clamped in parallel with the main device, and is small so as to not interfere with the mechanical dynamics. The output voltage of the sense-piezoelectric device is proportional to the base acceleration. Using a differential comparator, a reference square wave is generated whose transitions align with the zero-crossing of the base mechanical acceleration, as shown in Fig. 5.8.

The phase-shifted signal is created by applying a time delay to the reference square wave. The time delay is generated by passing the reference square wave through an RC filter whose time constant is set by a digital potentiometer. A hysteresis comparator generates a time-delayed square wave from the first-order RC response. The maximum time delay that can be achieved by this circuit is one-half of the square wave period (180°). In order to achieve a full 360° phase shift, the time-delayed square wave is inverted using a NOT gate. A multiplexer is used to select between the inverted and the original time-delayed square wave. The phase control circuit is illustrated in Fig. 5.8. This circuit produces the transition command signal, yet in steady-state it does

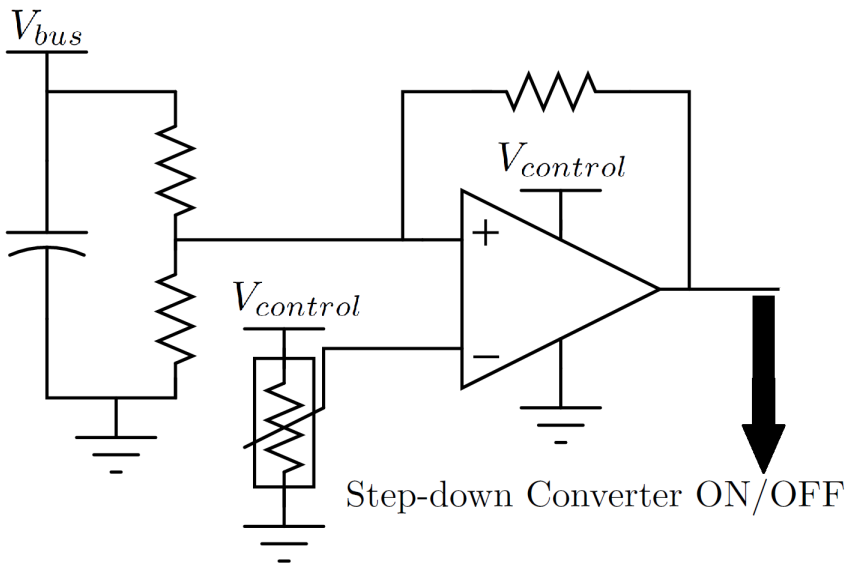

Figure 5.9: This hysteresis comparator controls the magnitude of the applied square wave by adjusting the voltage on the bus capacitance. If the voltage on the bus capacitance gets too large it activates a step-down converter to reduce the voltage.

not require microprocessor input, which greatly reduces the power consumption of the digital control.

5.4.0.2 Analog Magnitude Control

The magnitude of the square wave voltage applied to the device by the inverter is determined by the bus voltage, V_{bus}. The bus voltage is controlled using an analog hysteresis controller (as shown in Fig. 5.9), which connects a load when the bus voltage is above the upper threshold, and disconnects it when the bus voltage is below the lower threshold. This load could be a DC-DC converter whose output is connected to a battery. The hysteresis controller allows the harvested power to be measured, which is necessary for the peak power tracker. This process is discussed in Section 5.4.1.

5.4.1 Digital Control

The digital control in this work is implemented on an ATMEGA328 microcontroller with a clock frequency of 62.5KHz; however, in a practical energy harvesting system for a wireless sensor node the microcontroller used to implement the node itself could be used to control the energy harvesting system. The microcontroller is responsible for implementing the peak-power-tracking algorithm by changing the

phase and magnitude of the applied square wave, yet its power consumption must be minimal in order to achieve an autonomous design. This is accomplished by designating the high-frequency tasks to analog circuitry, as described in sections 5.4.0.1 and 5.4.0.2. The digital control interfaces with the analog circuitry through two digital potentiometers and a multiplexer. Modulation of these allows the microcontroller to change the magnitude and phase of the applied square wave; however, it does not require the micocontroller to be awake in order to maintain the phase and magnitude.

A peak-power-tracking algorithm, similar to that in [31], is used to find the optimum bus voltage and phase angle with one modification: in order to reduce power consumption, the net power harvested is computed by measuring the voltage on the bus capacitance at the beginning of the magnitude control hysteresis cycle (discussed in Section 5.4.0.2), and after a delay, t_{delay}. Therefore the average power harvested, $P_{harvest}$, is measured passively during each magnitude control hysteresis cycle.

$$P_{harvest} = \frac{\frac{1}{2}C_{bus}\left[V_{bus}(t_{delay})^2 - V_{bus}(0)^2\right]}{t_{delay}} \tag{5.12}$$

In order to minimize power consumption, the microcontroller is in a "sleep" mode except when triggered by external interrupts at the appropriate time to measure the bus voltage.The stages of the peak-power controller are shown in Table 5.2. During each hysteresis cycle either the harvested power is measured, the bus voltage magnitude is perturbed, or the phase angle is perturbed.

Table 5.2: Peak-Power-Tracking Algorithm

Hysteresis Cycle	**Execution**
1	Measure Power (P1)
2	$V_{bus} = V_{bus} + \Delta V_{bus}$
3	Measure Power (P2)
4	if (P1>P2) : $V_{bus} = V_{bus} - 2\Delta V_{bus}$
5	Measure Power (P1)
6	$\phi = \phi + \Delta\phi$
7	Measure Power (P2)
8	if (P1>P2) : $\phi = \phi - 2\Delta\phi$
REPEAT	Go to 1

The length of the magnitude control hysteresis cycle therefore determines the power consumption of the microcontroller. The longer the hysteresis cycle, the less power that is consumed by the microcontroller because the ratio of sleep to awake time increases. However, this decrease in power consumption comes at the cost of

increased time required to converge to the optimal harvesting conditions.

5.5 Results

Experimental results were obtained using a Mide Volture V20w piezoelectric device with a 6.7g tip mass. The adaptive rectifier and DAEH harvesting methods were applied to the device over a frequency range of 106-122 Hz. For consistency, the magnitude of the base acceleration was held constant at $32.5\frac{m}{s^2}$. The piezoelectric device parameters, shown in Table 5.1, were calculated based on the short-circuit and open-circuit resonant frequencies of the piezoelectric device [20, 25].

5.5.1 Resonant Inverter

To demonstrate the benefits and performance of the proposed resonant inverter, an experimental implementation of the circuit was developed. The components chosen for the resonant inverter are listed in Table 5.3, and an example of the experimental device voltage is shown in Fig. 5.10. In order to achieve the bandwidth extension goals of this work, it is important to maximize the efficiency of the resonant inverter; therefore, the losses in the circuit topology are catalogued and discussed in this section.

Table 5.3: Main Circuit Components

Component	**Part Numnber**
N-channel MOSFET	TI CSD18504Q5A
P-channel MOSFET	Alpha and Omega AOD413A
Comparator	Linear Technologies LTC1540
Inductor Core	Ferroxcube RM10/LP-3F3
Inductance	2.8 mH
Inductor Turns	77
Inductor Gap	.1 mm

The most important loss mechanisms in the resonant inverter are losses during the resonant transition. This is because, as shown in equation (5.7), losses during the resonant transition also affect the clamping losses. The voltage and current through the piezoelectric device during the resonant transition are shown in Fig. 5.11. Measurement of the device capacitance (C'), the device voltage (V_p) are used to compute the energy in the system at the beginning and end of the resonant transition, as shown in Table 5.4. The energy in the system at the beginning of the resonant transition,

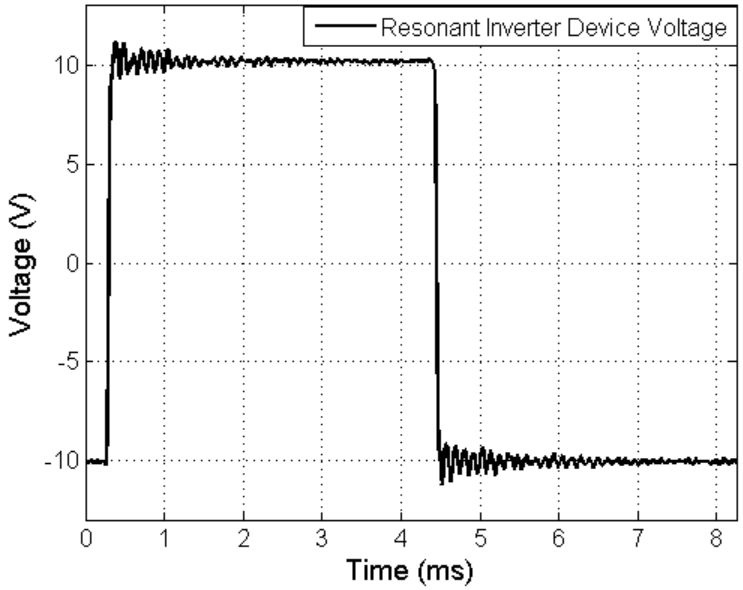

Figure 5.10: The resonant inverter emulates the optimal impedance by creating a square voltage waveform on the piezoelectric device. Experimental waveforms are shown for the case when V_{bus} is 10.

E_{init}, is stored in the piezoelectric device capacitance. During the first half of the resonant transition, energy is extracted from the piezoelectric device and is stored in the resonant inductor. In the second half of the resonant transition, energy is extracted from the inductor and is returned to the piezoelectric device capacitance (E_{final}). Assuming a constant piezoelectric device capacitance, the total energy lost during the resonant transition, E_{res}, is 700 nJ. Using the losses in the resonant transition the experimental quality factor is calculated to be 25.6.

Table 5.4: Resonant Transition Loss Breakdown at $V_{bus} = 10V$

Label	**Equation**	**Energy(μJ)**
E_{init}	$\frac{1}{2}C'V_{bus}^2$	5.68
E_{final}	$\frac{1}{2}C'V_x^2$	4.98
E_{res}	$E_{init} - E_{final}$	.7

Next, the clamping losses are computed based on the voltage at the end of the resonant transition V_x. Equation (5.3) predicts the voltage V_x to be 9.34 Volts, while experimental data found V_x to be 9.25 Volts. The resulting clamping losses are therefore approximately two times larger than predicted by equation (5.6). This is because the parasitic drain-source capacitances of the MOSFETs cause the voltage

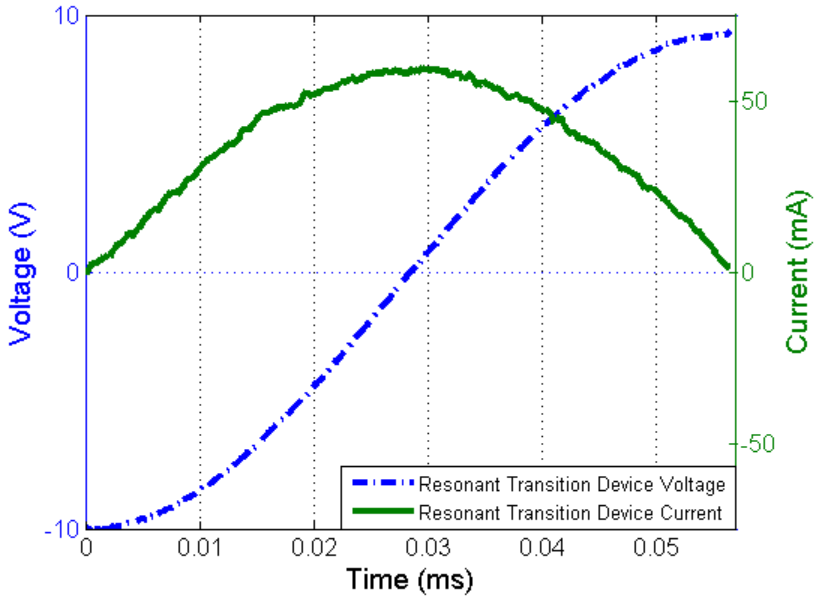

Figure 5.11: Experimental piezoelectric device voltage and current waveforms during a resonant transition when V_{bus} is 10 Volts.

on the device to decline past V_x after the resonant transition has ended. The experimental clamping losses were calculated using equation (5.6) and the voltage on the piezoelectric device at the time of clamping (as opposed to V_x).

The quiescent gating circuitry loss was calculated by removing the piezoelectric device and measuring the time it took the bus capacitance to drain from 10.1 Volts to 9.9 Volts while the transition command signal was fixed. Next, the power required to drive the gates of the MOSFETs was found by driving the resonant inverter with out a piezoelectric device, and subtracting the power consumed by the quiescent gating circuitry.

In total this implementation of the resonant inverter dissipates $946\mu W$ when driving a piezoelectric device with a 10 Volt square wave at a frequency of $114Hz$. The total losses were measured by driving the piezoelectric device with the resonant inverter while not in the presence of mechanical vibration. The bus capacitance was charged to 10.1 Volts and, because there was no mechanical excitation, the voltage on the bus capacitance declined as power was consumed by the resonant inverter. The time it took for the voltage on the bus capacitance to decay to 9.9 Volts was measured and used to determine the losses in the inverter.

The breakdown of each loss mechanism is shown in Table 5.5. The "other" category is the remaining power which is being dissipated. This is measured by taking the difference between the total measured loss and the identified loss mechanisms.

Table 5.5: Resonant Inverter Loss Breakdown at $V_{bus} = 10V$ and frequency of $114Hz$

Loss Mechanism	**Power Lost (μW)**
Resonant Transition	160
Clamping	328
Gate Drive Circuitry	
-Quiescent	94
-Switching	119
Other	245
Total	946

5.5.2 Resonant Inverter Bandwidth Extension Capabilities

Careful consideration in the design of the resonant inverter was given to minimizing losses so that the bandwidth of the dynamic active energy harvesting (DAEH) method can be improved. To demonstrate the performance of the proposed resonant inverter, two energy harvesting methods were compared on an experimental setup: the adaptive rectifier method and the DAEH method utilizing the resonant inverter.

The adaptive rectifier circuit is used as a baseline for comparison, and is operated at the harvesting conditions defined in [40]. The rectifier was made from Comchip CDBA140-G diodes, due to their low forward voltage. In order to present the adaptive rectifier method in the best possible light, all control circuitry for the adaptive rectifier was externally powered.

The resonant inverter was implemented with the elements shown in Table 5.3. To demonstrate the capabilities of the power electronics, the resonant inverter was used in a similar manner to the PWM fullbridge inverter presented in [31]. The control circuitry, including an accelerometer, were externally powered; however, the inverter loss mechanisms detailed in Table 5.5 were included. The power harvested from the resonant inverter is shown in Fig. 5.12.

The DAEH method with the resonant inverter show dramatic performance improvements over the adaptive rectifier approach, as shown in Fig.5.12. When the mechanical resonant frequency and the excitation frequency are close, the DAEH method with the resonant inverter harvests nearly twice as much power as the adaptive rectifier approach. As the excitation frequency deviates from the resonant frequency of the mechanical structure, the adaptive rectifier's harvested power falls off more quickly. The DAEH method with the resonant inverter harvests up to 2.63 times as much power at off-resonant frequencies, and increases the 3db power bandwidth by a factor of 2.84.

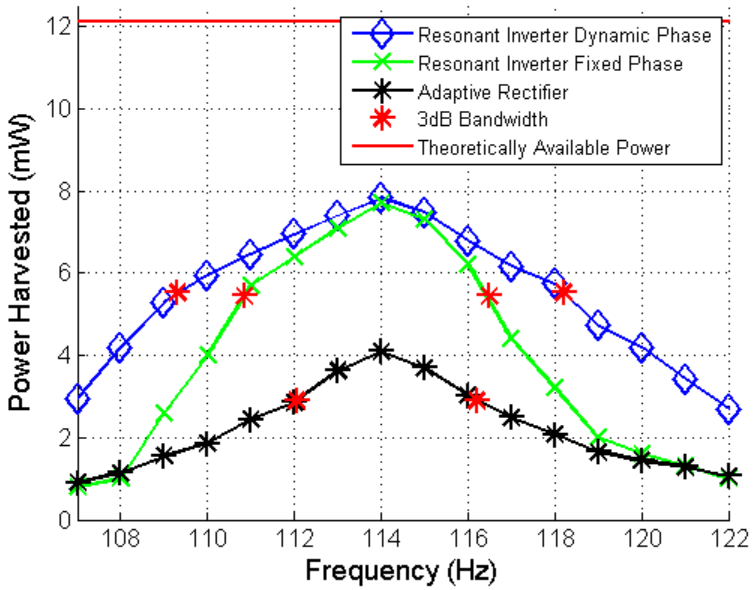

Figure 5.12: The power harvested versus excitation frequency is illustrated the DAEH method utilizing the resonant inverter, the adaptive rectifier method, and the resonant inverter with a fixed phase.

In order to demonstrate the benefit of dynamic phase modulation, the phase of the applied square wave was fixed at an angle which maximizes the power harvested when the mechanical resonant frequency and the excitation frequency are the same. As illustrated in Fig.5.12, the fixed-phase active energy harvesting method harvests a similar amount of power as the DAEH method when the excitation frequency and the mechanical resonant frequency are close; however, as the excitation frequency deviates from the mechanical resonant frequency, the DAEH method significantly outperforms the fixed-phase active energy harvesting method.

5.5.3 Autonomous System

This section demonstrates the dynamic active energy harvesting method on an autonomous system. The power extracted from the piezoelectric device is shown over an excitation frequency range of 106-122 Hz in Fig. 5.13. The total power harvested from the piezoelectric device onto the bus capacitance is shown as the harvested power. The net power harvested is the power harvested to the bus capacitance minus the control losses. The net power harvested from the DAEH method is 1.53 times more than the adaptive rectifier approach when the excitation frequency and mechanical resonant frequency are similar. As the excitation frequency deviates from

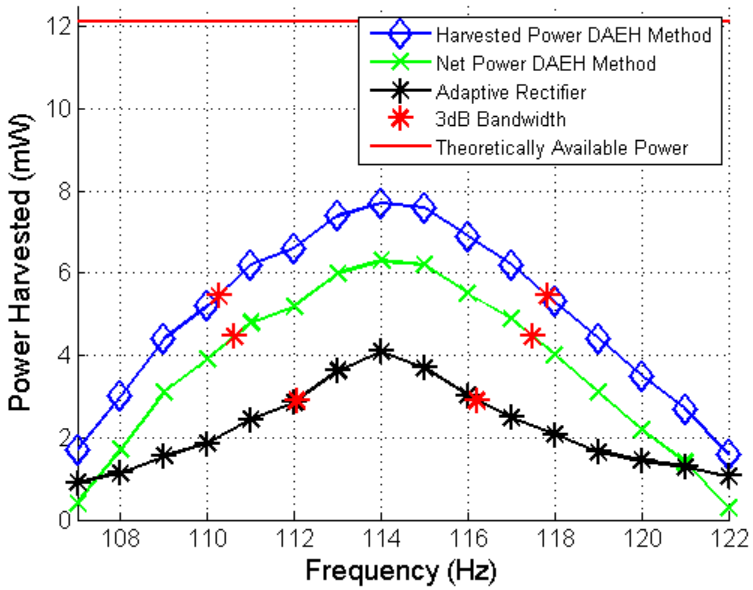

Figure 5.13: The power harvested versus excitation frequency by the autonomous energy harvesting system (shown in green) is the total power harvested (shown in blue) minus the control losses, and is compared to the baseline adaptive rectifier approach (shown in black).

the mechanical resonant frequency the net power harvested with the DAEH method is up to 2.1 times more than the adaptive rectifier approach. Furthemore, the 3dB bandwidth of the net power harvested from the DAEH method is 1.65 times larger than the adaptive rectifier approach. The comparison between the net harvested power from the DAEH method and the adaptive rectifier approach are conservative estimates of the gains of the proposed harvesting system, because no control losses were included with the adaptive rectifier approach. Given a practical implementation of the adaptive rectifier, the benefits of the proposed autonomous implementation of the DAEH method would be even more significant.

5.6 Conclusion

In this chapter a resonant inverter is presented which implements the dynamic active energy harvesting method, while reducing switching and gating losses. The resonant inverter, in conjunction with new analog circuitry that implements the high-frequency tasks required by the DAEH method, produces the first autonomous dynamic active energy harvesting system. When the excitation frequency and mechanical resonant frequency are similar this system harvests 1.5 times more power

than the adaptive rectifier approach. As the excitation frequency deviates from the mechanical resonant frequency the proposed autonomous system harvests up to 2.1 times more power than the adaptive rectifier approach. The demonstrated resonant inverter and control circuitry produce the first autonomous autonomous implementation of the dynamic active energy harvesting method for piezoelectric devices. This autonomous system increases the practical viability of using piezoelectric devices to power wireless sensor nodes.

CHAPTER VI

Conclusion

The ever-expanding role of wireless sensor and identifier nodes in our society has pushed researchers to find application appropriate energy sources to replace or supplement current battery technology. A key technology in replacing current battery technology is energy harvesting. In many applications wireless sensor nodes are in environments where mechanical vibrations are present. Typically this energy is harvested by inserting an electromechanical device (either variable-capacitance or piezoelectric device) into a mechanically resonant mass-spring system. The goal of this work is to maximize the power harvested from these systems. To achieve this goal, this dissertation explores the power electronic interface between the energy harvesting device and the electrical energy storage element. The main conclusions from this work are presented in this chapter, as well as possible future directions of the work.

6.1 Variable-Capacitance Devices

Variable-capacitance devices are proposed for energy harvesting because they can be easily integrated into a micro-system; however, the small available power from these devices has limited their use. Two classes of variable-capacitance energy harvesting devices are considered in the literature: gap-closing devices and area-overlap devices. Typically energy harvesting methods are analyzed for these devices assuming a voltage constraint; however, with the development of high-voltage MEMs processes this constraint has changed [10, 36, 64]. The increased voltage limitations from the MEMs process means that the pull-in effect is the limiting factor in device performance. To mitigate pull-in effect, area-overlap devices must limit the maximum voltage on the device, while gap-closing devices must limit the maximum charge on the device.

The existing energy harvesting methods for variable-capacitance devices are active energy harvesting methods, which means there is bidirectional power flow between

the energy harvesting device and the electrical energy storage element. Due to the energy flow in the system beyond the net harvested power, the efficiency of the power electronics which interface the device and the electrical energy storage element is crucial.

This work seeks to increase the energy harvesting capabilities of variable-capacitance devices by providing more informed energy harvesting method selection, analytical expressions for optimal harvesting conditions to guide circuit architecture selection, and a comparison of the energy harvesting capabilities of gap-closing versus area-overlap type variable-capacitance devices. In Chapter III the impact of power electronic efficiency is discussed for variable-capacitance devices whose maximum voltage is constrained. The impact of power electronic efficiency on energy harvesting methods for variable-capacitance devices whose maximum charge is constrained is derived and compared to the voltage-constrained case in Chapter IV.

6.1.1 Voltage-Constrained Variable-Capacitance Energy Harvesting

In the literature four methods of energy harvesting are proposed for variable-capacitance devices: the Constant Voltage, Constant Charge, Charge Pump, and CCPC Method [36, 52]. In [36, 49, 52] the energy harvesting capabilities of these methods on voltage-constrained devices are discussed; however, an important system parameter is neglected - power electronic efficiency. The analysis in this dissertation elucidates additional benefits and drawbacks to each method by including power electronic efficiency in the analysis of these methods.

It is shown that at high efficiencies and large capacitance ratios the Constant Voltage Method can harvest 100% of the available energy. Conversely, the Constant Charge method harvests only a small fraction of the available energy. However, as the efficiency decreases the power harvested by the Constant Voltage Method decreases significantly, whereas efficiency does not alter the harvested power as significantly for the Constant Charge Method. In fact, for large capacitance ratios, the threshold efficiency for net positive energy harvesting for the Constant Voltage is approximately 71% compared to 0% for the Constant Charge Method.

The CCPC Method described in [36] allows both the charge and voltage on the variable capacitance device to change during the harvesting cycle. At high efficiencies and capacitance ratios this harvesting method can harvest 100% of the available energy. As the power electronic efficiency declines so too does the energy harvested; however, by selecting the optimal parallel capacitance the power harvested can be maximized at given efficiency [36]. For the first time, an analytical expression for

the optimal C_p is derived as a function of system parameters and power electronic efficiency. While utilizing the optimal parallel with a large capacitance ratio, the CCPC Method can be shown to have a threshold efficiency of 0%.

The Charge Pump Method has both a constant charge and constant voltage potion to its energy harvesting cycle. At high efficiencies with a large capacitance ratio the Charge Pump Method can harvest up to 50% of the available energy. As the power electronic efficiency changes, so too does the desired ratio of constant charge to constant voltage portion of the energy harvesting cycle. This is accomplished through careful selection of the minimum and maximum voltages. By including power electronic efficiency, new analytical expressions for optimal harvesting conditions are derived that are shown to be a strong function of efficiency.

The new efficiency-based theoretical background for voltage-constrained devices motivates the design of a energy harvesting system based on the Charge Pump Method. Analytical solutions for the optimal energy harvesting conditions inspired the use of a 2:1 switched capacitor converter topology as the basis of said harvesting system. The 2:1 switch capacitor converter approximates the optimal harvesting conditions and can be implemented on a chip, which is necessary in order to achieve the benefits of variable-capacitance energy harvesting. An LTSPICE simulation verified the advantages of the proposed Charge Pump Method harvesting system by revealing that $12.09\mu W$ could be harvested from this system, which is more than twice the power previously asserted for the same device.

6.1.2 Energy Harvesting Comparison for Gap-Closing Versus Area-Overlap Devices

Chapter IV focuses on comparing energy harvesting capabilities of gap-closing (charge-constrained) and area-overlap (voltage-constrained) devices.

At 100% power electronic efficiency the Constant Voltage Method implemented on a area-overlap device and the Constant Charge Method implemented on a gap-closing device can both harvest the same amount of energy. However, at practical power electronic efficiencies (85%) the Constant Charge Method on a gap-closing device harvests approximately 1.6 times as much energy. The Constant Charge Method on a gap-closing devices is the least dependent on power electronic efficiency of any method.

At high power electronic efficiencies the Charge Pump Method can harvest up to 50% of the available energy on both area-overlap and gap-closing devices. Assuming optimal harvesting conditions, the energy harvested from a gap-closing device is much

less dependent on power electronic efficiency than an area-overlap device. At practical efficiencies the gap-closing device outperforms the area-overlap device when utilizing the Charge Pump Method.

A case study compares an area-overlap device and a gap-closing device with the same maximum energy density. This example further demonstrates the increased energy harvesting capabilities of using the Constant Charge Method on a gap-closing device, while elucidating large maximum voltages that will exist in such a device. The large maximum voltage associated with this system does not cause the pull-in effect; however, it complicates the design of the power electronic circuit which implements the method. In some practical implementations of the Constant Charge Method on a gap-closing device, the maximum voltage may need to be constrained. Hence, a new energy harvesting method is proposed which limits the maximum voltage and the maximum charge in the system.

6.1.3 Future Directions

The variable-capacitance analysis presented in this dissertation makes a quasi-static assumption: the energy extracted from the variable-capacitance device does not alter the mechanical system. This is a valid assumption when the energy extracted from the harvesting system is only a small portion of the energy of the moving mass. However, with the improved energy harvesting techniques presented in this work, the impact of the extracted energy on the mechanical system may become an important consideration. Follow-up work should consider analyzing each energy harvesting method as part of a dynamic system model. The displacement of the mass in the mass-spring-damper will determine the capacitance ratio, allowing the energy harvesting methods to be optimized for given input force as opposed to a fixed capacitance ratio.

6.2 Piezoelectric Energy Harvesting

Piezoelectric devices are proposed as a good electromechanical device for vibration energy harvesting because of their high energy density. In order to achieve large energy density, piezoelectric devices are integrated into a high-Q mechanically resonant structure. When the excitation frequency matches the resonant frequency of this structure a significant amount of power can be extracted from these systems; however, as the excitation frequency deviates from the mechanical frequency the harvested power declines significantly. The limited energy harvesting bandwidth of these

systems has restricted the practical application of dynamic piezoelectric energy harvesting. Currently energy harvesting systems require precise tolerances on parts for the mechanical resonator, and have no ability to adapt to changes in the system; for example, due to fatigue or climate.

6.2.1 Autonomous Wideband Piezoelectric Energy Harvesting

The dynamic active energy harvesting (DAEH) method is a solution for increasing the energy harvesting bandwidth of piezoelectric devices without sacrificing the peak power harvested. In [31] an optimal impedance is derived which is a function of the harvesting conditions. Using a pulse-width-modulated full-bridge inverter, the authors emulate the optimal impedance and demonstrate the improved energy harvesting abilities of their system. Despite the benefits of the proposed system, the energy harvesting capabilities of the system are reported without control, gating, and sensing losses. In fact, the control, gating, and sensing losses are significantly more than the harvested power, threatening the viability of this method.

In Chapter V the first autonomous implementation of the DAEH Method is presented. In order to create an autonomous system the system proposed in [31] was improved in three ways. First the pulse-width-modulated full-bridge inverter was replaced by a resonant inverter. The resonant inverter greatly reduces switching and gating losses, and can be easily controlled. Next, low-power analog circuitry was created to complete high-frequency controls tasks previously executed by the microcontroller. This reduces the power consumption of the microcontroller, one of the major loss mechanisms in previous implementations. Finally, a new technique for measuring the zero-crossings of the base acceleration is proposed to replace commercially available accelerometers whose power consumption is too high.

Using the new resonant inverter, low-power analog circuitry, and low-power sensing circuitry, the first autonomous wideband piezoelectric energy harvesting system is demonstrated. An experimental setup of the discussed autonomous implementation of the DAEH method was created to demonstrate the benefits of this system over the baseline adaptive rectifier approach. When the excitation frequency and mechanical resonant frequency are similar this system harvests 1.5 times more power than the adaptive rectifier method, and as the excitation frequency deviates from the mechanical resonant frequency the proposed autonomous system harvests up to 2.1 times more power than the adaptive rectifier approach. The resulting 3dB bandwidth of the system is improved by 65% over the adaptive rectifier method. These results were achieved while including all loss mechanisms associated with the circuit.

For this first time this work demonstrates the practical viability of the DAEH method. The increased energy harvesting capabilities afforded by an autonomous implementation of this method increase the practical applications of dynamic piezoelectric energy harvesting. The improved energy harvesting bandwidth allows for decreased tolerances on mechanical parameters, and can adapt to fluctuations in excitation frequency.

6.2.2 Future Work

The bandwidth extension capabilities of the DAEH Method are limited by the efficiency of the power electronic circuitry which implements the method. Using the resonant inverter to implement this impedance, a significant bandwidth extension was demonstrated; however, there is still room for improvement. Currently experimental results show that the clamping loss during the resonant transition is the dominant loss mechanism in the resonant inverter. These loss mechanism are larger than expected due to ringing after the resonant transition. To reduce the clamping losses two modifications could be made to the inverter. First, lowering parasitic drain-source capacitance through PCB layout and MOSFET selection would significantly increase the voltage on the device at the time of clamping, which ultimately reduces clamping loss. Secondly, instead of clamping at the end of the resonant transition, the inverter could be pulse-width-modulated in order to finish the transition if the voltage on the device to the bus voltage.

BIBLIOGRAPHY

BIBLIOGRAPHY

[1] Akyildiz, I. F., Su, W., Sankarasubramaniam, Y., and Cayirci, E. Wireless sensor networks: a survey. *Computer networks 38*, 4 (2002), 393–422.

[2] Amirtharajah, R., and Chandrakasan, A. P. Self-powered signal processing using vibration-based power generation. *Solid-State Circuits, IEEE Journal of 33*, 5 (1998), 687–695.

[3] Badel, A., Benayad, A., Lefeuvre, E., Lebrun, L., Richard, C., and Guyomar, D. Single crystals and nonlinear process for outstanding vibration-powered electrical generators. *Ultrasonics, Ferroelectrics and Frequency Control, IEEE Transactions on 53*, 4 (2006), 673–684.

[4] Badel, A., Guyomar, D., Lefeuvre, E., and Richard, C. Piezoelectric energy harvesting using a synchronized switch technique. *Journal of Intelligent Material Systems and Structures 17*, 8-9 (2006), 831–839.

[5] Basset, P., Galayko, D., Paracha, A. M., Marty, F., Dudka, A., and Bourouina, T. A batch-fabricated and electret-free silicon electrostatic vibration energy harvester. *Journal of Micromechanics and Microengineering 19*, 11 (2009), 115025.

[6] Bedeloglu, A. C., Demir, A., Bozkurt, Y., and Sariciftci, N. S. A photovoltaic fiber design for smart textiles. *Textile Research Journal 80*, 11 (2010), 1065–1074.

[7] Beeby, S. Energy harvesting vibration sources for microsystems applications. *Measurement Science and Technology 17*, 12 (2006), 175–195.

[8] Chalasani, S., and Conrad, J. M. A survey of energy harvesting sources for embedded systems. In *Southeastcon, 2008. IEEE* (2008), IEEE, pp. 442–447.

[9] Cowan, J. J., Rincon-Mora, G., et al. Harvesting the highest power from tiny electrostatic transducers with cmos circuits. In *Circuits and Systems (MWSCAS), 2014 IEEE 57th International Midwest Symposium on* (2014), IEEE, pp. 334–337.

[10] Despesse, G., Jager, T., Chaillout, J.-J., Leger, J.-M., and Basrour, S. Design and fabrication of a new system for vibration energy harvesting. In *Research in Microelectronics and Electronics, 2005 PhD* (2005), vol. 1, IEEE, pp. 225–228.

[11] Deterre, M., Lefeuvre, E., and Dufour-Gergam, E. An active piezoelectric energy extraction method for pressure energy harvesting. *Smart Materials and Structures 21*, 8 (2012).

[12] Deterre, M., Lefeuvre, E., and Dufour-Gergam, E. An active piezoelectric energy extraction method for pressure energy harvesting. *Smart Materials and Structures 21*, 8 (2012).

[13] Fedder, G. K., Hierold, C., Korvink, J. G., Tabata, O., Brand, O., Dufour, I., Heinrich, S., and Josse, F. *Resonant MEMS: Fundamentals, Implementation, and Application*. John Wiley & Sons, 2015.

[14] Fu, Q., and Suzuki, Y. A design method of in-plane mems electret energy harvester with comb drives. In *Journal of Physics: Conference Series* (2014), vol. 557, IOP Publishing.

[15] Fu, Q., and Suzuki, Y. Mems vibration electret energy harvester with combined electrodes. In *Micro Electro Mechanical Systems (MEMS), 2014 IEEE 27th International Conference on* (2014), IEEE, pp. 409–412.

[16] Glynne-Jones, P., Beeby, S. P., and White, N. M. Towards a piezoelectric vibration-powered microgenerator. *IEE Proceedings-Science, measurement and technology 148*, 2 (2001), 68–72.

[17] Granstrom, J., Feenstra, J., Sodano, H. A., and Farinholt, K. Energy harvesting from a backpack instrumented with piezoelectric shoulder straps. *Smart Materials and Structures 16*, 5 (2007).

[18] Hoffmann, D., Folkmer, B., and Manoli, Y. Analysis and characterization of triangular electrode structures for electrostatic energy harvesting. *Journal of Micromechanics and Microengineering 21*, 10 (2011).

[19] Holden, V. I., Lenio, S., Kuick, R., Ramakrishnan, S. K., Shah, Y. M., and Bachman, M. A. Bacterial siderophores that evade or overwhelm lipocalin 2 induce hypoxia inducible factor 1α and proinflammatory cytokine secretion in cultured respiratory epithelial cells. *Infection and immunity 82*, 9 (2014), 3826–3836.

[20] Kong, N., Ha, D. S., Erturk, A., and Inman, D. J. Resistive impedance matching circuit for piezoelectric energy harvesting. *Journal of Intelligent Material Systems and Structures* (2010).

[21] Krikke, J. Sunrise for energy harvesting products. *Pervasive Computing, IEEE 4*, 1 (2005), 4–5.

[22] Lee, C., Lim, Y. M., Yang, B., Kotlanka, R. K., Heng, C.-H., He, J. H., Tang, M., Xie, J., and Feng, H. Theoretical comparison of the energy harvesting capability among various electrostatic mechanisms from structure aspect. *Sensors and Actuators A: Physical 156*, 1 (2009), 208–216.

[23] Lee, C., Lim, Y. M., Yang, B., Kotlanka, R. K., Heng, C.-H., He, J. H., Tang, M., Xie, J., and Feng, H. Theoretical comparison of the energy harvesting capability among various electrostatic mechanisms from structure aspect. *Sensors and Actuators A: Physical 156*, 1 (2009), 208–216.

[24] Lefeuvre, E., Audigier, D., Richard, C., and Guyomar, D. Buck-boost converter for sensorless power optimization of piezoelectric energy harvester. *Power Electronics, IEEE Transactions on 22*, 5 (2007), 2018–2025.

[25] Lefeuvre, E., Badel, A., Richard, C., Petit, L., and Guyomar, D. A comparison between several vibration-powered piezoelectric generators for standalone systems. *Sensors and Actuators A: Physical 126*, 2 (2006), 405–416.

[26] Lefeuvre, E., Richard, C., Guyomar, D., and Lallart, M. *Piezoelectric Material-Based Energy Harvesting Devices: Advance of SSH Optimization Techniques (1999-2009).* INTECH Open Access Publisher, 2010.

[27] Lefeuvre, E., Sebald, G., Guyomar, D., Lallart, M., and Richard, C. Materials, structures and power interfaces for efficient piezoelectric energy harvesting. *Journal of electroceramics 22*, 1-3 (2009), 171–179.

[28] Leland, E. S., and Wright, P. K. Resonance tuning of piezoelectric vibration energy scavenging generators using compressive axial preload. *Smart Materials and Structures 15*, 5 (2006).

[29] Liu, Y. *Active Energy Harvesting.* PhD thesis, Pennsylvania State University, 2006.

[30] Liu, Y., Tian, G., Wang, Y., Lin, J., Zhang, Q., and Hofmann, H. F. Active piezoelectric energy harvesting: general principle and experimental demonstration. *Journal of Intelligent Material Systems and Structures 20*, 5 (2009), 575–585.

[31] Luo, C., and Hofmann, H. F. Wideband energy harvesting for piezoelectric devices with linear resonant behavior. *Ultrasonics, Ferroelectrics and Frequency Control, IEEE Transactions on 58*, 7 (2011), 1294–1301.

[32] Makihara, K., Onoda, J., and Miyakawa, T. Low energy dissipation electric circuit for energy harvesting. *Smart materials and structures 15*, 5 (2006).

[33] Mateu, L., and Moll, F. Review of energy harvesting techniques and applications for microelectronics (keynote address). In *Microtechnologies for the New Millennium 2005* (2005), International Society for Optics and Photonics, pp. 359–373.

[34] Mehra, A., Zhang, X., Ayon, A., Waitz, I. A., Schmidt, M., Spadaccini, C. M., et al. A six-wafer combustion system for a silicon micro gas turbine engine. *Microelectromechanical Systems, Journal of 9*, 4 (2000), 517–527.

[35] Meninger, S. *A low power controller for a MEMS based energy converter*. PhD thesis, Massachusetts Institute of Technology, 1999.

[36] Meninger, S., Mur-Miranda, J., Amirtharajah, R., Chandrakasan, A., and Lang, J. H. Vibration-to-electric energy conversion. *IEEE Transactions on Very Large Scale Integration (VLSI) Systems 9*, 1 (2001), 64–76.

[37] Mescheder, U., Müller, B., Baborie, S., and Urbanovic, P. Properties of sio2 electret films charged by ion implantation for mems-based energy harvesting systems. *Journal of Micromechanics and Microengineering 19*, 9 (2009), 094003.

[38] Mescheder, U., Nimo, A., Müller, B., and Elkeir, A. S. A. Micro harvester using isotropic charging of electrets deposited on vertical sidewalls for conversion of 3d vibrational energy. *Microsystem technologies 18*, 7-8 (2012), 931–943.

[39] Mitcheson, P. D., Miao, P., Stark, B. H., Yeatman, E., Holmes, A., and Green, T. Mems electrostatic micropower generator for low frequency operation. *Sensors and Actuators A: Physical 115*, 2 (2004), 523–529.

[40] Ottman, G. K., Hofmann, H. F., Bhatt, A. C., and Lesieutre, G. A. Adaptive piezoelectric energy harvesting circuit for wireless remote power supply. *Power Electronics, IEEE Transactions on 17*, 5 (2002), 669–676.

[41] Ottman, G. K., Hofmann, H. F., and Lesieutre, G. A. Optimized piezoelectric energy harvesting circuit using step-down converter in discontinuous conduction mode. *Power Electronics, IEEE Transactions on 18*, 2 (2003), 696–703.

[42] Paradiso, J. A., and Starner, T. Energy scavenging for mobile and wireless electronics. *Pervasive Computing, IEEE 4*, 1 (2005), 18–27.

[43] Peano, F., and Tambosso, T. Design and optimization of a mems electret-based capacitive energy scavenger. *IEEE/ASME Journal of Microelectromechanical Systems 14*, 3 (2005), 429–435.

[44] Pereyma, M. Overview of the modern state of the vibration energy harvesting devices. In *Perspective Technologies and Methods in MEMS Design, 2007. MEMSTECH 2007. International Conference on* (2007), IEEE, pp. 107–112.

[45] Raghunathan, V., Kansal, A., Hsu, J., Friedman, J., and Srivastava, M. Design considerations for solar energy harvesting wireless embedded systems.

In *Proceedings of the 4th international symposium on Information processing in sensor networks* (2005), IEEE Press, p. 64.

[46] Rajeswari, S. *Energy Harvesting Cardiac Pacemaker*. PhD thesis, California State University, Northridge, 2015.

[47] Ramsay, M. J., and Clark, W. W. Piezoelectric energy harvesting for bio-mems applications. In *SPIE's 8th Annual International Symposium on Smart Structures and Materials* (2001), International Society for Optics and Photonics, pp. 429–438.

[48] Roundy, S., Leland, E. S., Baker, J., Carleton, E., Reilly, E., Lai, E., Otis, B., Rabaey, J. M., Wright, P. K., and Sundararajan, V. Improving power output for vibration-based energy scavengers. *Pervasive Computing, IEEE 4*, 1 (2005), 28–36.

[49] Roundy, S., Wright, P., and Rabaey, J. *Energy Scavenging for Wireless Sensor Networks: With Special Focus on Vibrations*. Springer US, 2004.

[50] Roundy, S., and Wright, P. K. A piezoelectric vibration based generator for wireless electronics. *Smart Materials and structures 13*, 5 (2004), 1131.

[51] Roundy, S., Wright, P. K., and Pister, K. S. Micro-electrostatic vibration-to-electricity converters. 487–496.

[52] Roundy, S., Wright, P. K., and Rabaey, J. A study of low level vibrations as a power source for wireless sensor nodes. *Computer communications 26*, 11 (2003), 1131–1144.

[53] Sebald, G., Kuwano, H., Guyomar, D., and Ducharne, B. Experimental duffing oscillator for broadband piezoelectric energy harvesting. *Smart materials and structures 20*, 10 (2011), 102001.

[54] Sebald, G., Kuwano, H., Guyomar, D., and Ducharne, B. Simulation of a duffing oscillator for broadband piezoelectric energy harvesting. *Smart Materials and Structures 20*, 7 (2011), 075022.

[55] Seeman, M., and Sanders, S. Analysis and optimization of switched-capacitor dc dc converters. *Power Electronics, IEEE Transactions on 23*, 2 (March 2008), 841–851.

[56] Shenck, N. S., and Paradiso, J. A. Energy scavenging with shoe-mounted piezoelectrics. *IEEE micro*, 3 (2001), 30–42.

[57] Sheu, G.-J., Yang, S.-M., and Lee, T. Development of a low frequency electrostatic comb-drive energy harvester compatible to soc design by cmos process. *Sensors and Actuators A: Physical 167*, 1 (2011), 70–76.

[58] Shu, Y., Lien, I., and Wu, W. An improved analysis of the sshi interface in piezoelectric energy harvesting. *Smart Materials and Structures 16*, 6 (2007).

[59] Sim, W. Y., Kim, G. Y., and Yang, S. S. Fabrication of micro power source (mps) using a micro direct methanol fuel cell (/spl mu/dmfc) for the medical application. In *Micro Electro Mechanical Systems, 2001. MEMS 2001. The 14th IEEE International Conference on* (2001), IEEE, pp. 341–344.

[60] Stark, B. H., Mitcheson, P. D., Miao, P., Green, T. C., Yeatman, E. M., and Holmes, A. S. Converter circuit design, semiconductor device selection and analysis of parasitics for micropower electrostatic generators. *Power Electronics, IEEE Transactions on 21*, 1 (2006), 27–37.

[61] Stein, A., and Hofmann, H. Resonant inverter design for stand-alone dynamic active piezoelectric energy harvesting. In *Applied Power Electronics Conference and Exposition (APEC), 2015 IEEE* (2015), IEEE, pp. 3265–3271.

[62] Stephen, N. On energy harvesting from ambient vibration. *Journal of sound and vibration 293*, 1 (2006), 409–425.

[63] Tashiro, R., Kabei, N., Katayama, K., Tsuboi, E., and Tsuchiya, K. Development of an electrostatic generator for a cardiac pacemaker that harnesses the ventricular wall motion. *Journal of Artificial Organs 5*, 4 (2002), 0239–0245.

[64] Torres, E. O., Rincón-Mora, G., et al. Electrostatic energy-harvesting and battery-charging cmos system prototype. *Circuits and Systems I: Regular Papers, IEEE Transactions on 56*, 9 (2009), 1938–1948.

[65] Wang, G., Luo, C., Hofmann, H., and Rome, L. Power electronic circuitry for energy harvesting backpack. In *Energy Conversion Congress and Exposition, 2009. ECCE 2009. IEEE* (2009), IEEE, pp. 3544–3549.

[66] Weimer, M. A., Paing, T. S., and Zane, R. A. Remote area wind energy harvesting for low-power autonomous sensors. In *Power Electronics Specialists Conference, 2006. PESC'06. 37th IEEE* (2006), IEEE, pp. 1–5.

[67] Williams, C., and Yates, R. B. Analysis of a micro-electric generator for microsystems. *Sensors and Actuators A: Physical 52*, 1 (1996), 8–11.

[68] Yang, Z., and Yang, J. Connected vibrating piezoelectric bimorph beams as a wide-band piezoelectric power harvester. *Journal of Intelligent Material Systems and Structures 20*, 5 (2009), 569–574.

[69] Yen, B. C., and Lang, J. H. A variable-capacitance vibration-to-electric energy harvester. *Circuits and Systems I: Regular Papers, IEEE Transactions on 53*, 2 (2006), 288–295.